INTERFACIAL MOLARITIES IN IONIC SURFACTANT AGGREGATES : DETERMINING ION SPECIFIC EFFECTS BY CHEMICAL TRAPPING

By

CHANGYAO LIU

A dissertation submitted to the

Graduate School—New Brunswick

Rutgers, The State University of New Jersey

in partial fulfillment of the requirements

for the degree of

Doctor of Philosophy

Graduate Program in Department of Chemistry and Chemical Biology

written under the direction of

Professor Laurence S. Romsted

and approved by

_____

_____

_____

_____

_____

New Brunswick, New Jersey

October, 2016

ABSTRACT OF THE DISSERTATION

INTERFACIAL MOLARITIES IN IONIC SURFACTANT AGGREGATES : DETERMINING ION SPECIFIC EFFECTS BY CHEMICAL TRAPPING

By CHANGYAO LIU

Dissertation Director:

Professor Laurence S. Romsted

The striking effects of a variety of salts on protein solubility and stability was first discovered by Franz Hofmeister in 1888. For more than a century, ion-specific effects on the properties of ionic colloids, biomembranes and proteins in solution have been demonstrated thousands of times, and the ion-specific order is often called the Hofmeister series. However, a molecular level explanation for ion-specific effects has not been elucidated. Here we are trying to characterize the ion-specific effects at the molecular level by using the chemical trapping method developed by our group. The method is based on the reaction between two specifically designed probes 4-alkyl-2,6-dimethylarenediazonium ion, $z-ArN_2BF_4$ (z=16, hexadecyl, z=1, methyl), and weakly basic nucleophiles, such as water, halides, and alcohols in the interfacial region of micelles and other association colloids. This method provides estimates of interfacial molarities of water, counterions for cationic surfactants, and headgroups for anionic surfactants. Our results supports that the ion specific effects in ionic surfactant aggregates depend on a delicate balance-of-forces controlled by ion-pairing, and

that hydration interactions within the interfacial region, can be explained by the shift of the interfacial ion-pair/hydration equilibrium.

Chapter 1 is a general introduction on pertinent background information including surfactants and their aggregates, ion specific effects, and the logic of chemical trapping method. Chapter 2 describes the characterization the ion specific effects of acetate (AcO^-), mesylate (MsO^-), chloride (Cl^-), bromide (Br^-), and iodide (I^-) on micelles composed of the twin tail gemini surfactants 1,2-ethanebis(dimethyldecylammonium) (10-2-10 2X) by both the chemical trapping method and MD simulations. In chapter 3, the chemical trapping method is applied to estimate the interfacial water and counterion molarities in 10-2-10 2X (X = MsO, Cl, and Br) gemini surfactant solutions in the presence of added counterion salts NaX (X = MsO, Cl, and Br, respectively). Chapter 4 shows the specific anion effects in micelle-to-vesicle transitions in AOT/salt solutions are determined by the shift in the interfacial ion-pair/hydration equilibrium.

Acknowledgments

My most sincere thank goes to my advisor, Prof. Larry Romsted, for his support, patience, and encouragement throughout my graduate studies. Larry is someone you will instantly love and never forget once you meet him. I have been amazingly fortunate to have a mentor who is not only a serious scientist who taught me how to solve scientific problems, but also a humorous friend who helps me overcome life difficulties.

Besides my advisor, I would like to thank the rest of my thesis committee, Prof. Jeehiun Katherine Lee, Prof. John Taylor, Prof. Peter Kahn, Prof. Ralf Warmuth, and Prof. Kai Hultzsch. Their advices and comments guided me through my research towards this thesis.

I would like to thank our collaborators: Dr. Alla Malinenko, Dr. Massimiliano Porrini, Prof. Reiko Oda, Prof. Michel Laguerre, Prof. David Case, Prof. Ronald Sauers, Prof. Dario Bassani, and Prof. Sylvain Nlate. Without their help, and constant supply of samples from Alla, my work has not been possible.

I thank the past and present members of Romsted's Group. Especially, I thank Dr. Qing Gu, Yongliang Zhang, Xiang Gao, Neena Regalado, Dr. Aijaz Ahmad, Dr. Tarek Awad, and Dr. Yan Cai for their support and friendship. I benefitted a lot from the discussions with them.

Finally, I would like to thank my family: my parents for always supporting me throughout my life, and my husband Shaodong, who is also a chemist, for his continuous help along the journey of my studies both at USTC and Rutgers.

Dedication

To my daughter.

Table of Contents

List of Tables

List of Figures

Chapter 1

General Introduction

1.1 Surfactants and Their Self-assembly

1.1.1 Surfactant molecules

Surfactants, also known as amphiphilic molecules, have two basic structural components, a hydrophobic portion usually called a tail, attached to a hydrophilic portion called a headgroup.[1, 2] This unique amphiphilic character makes surfactants key components in industries that makes detergents, pharmaceuticals, petroleum, food, electronic printing, etc.[3, 4, 5, 6] Based on headgroup structures, surfactants are primarily divided into four major categories[7]: cationic, nonionic, zwitterionic, and nonionic surfactants, Figure 1.1. Furthermore, cationic, anionic, and zwitterionic surfactants are collectively called the ionic surfactants. Figure 1.2 shows some examples of both typical and "atypical" surfactant structures.

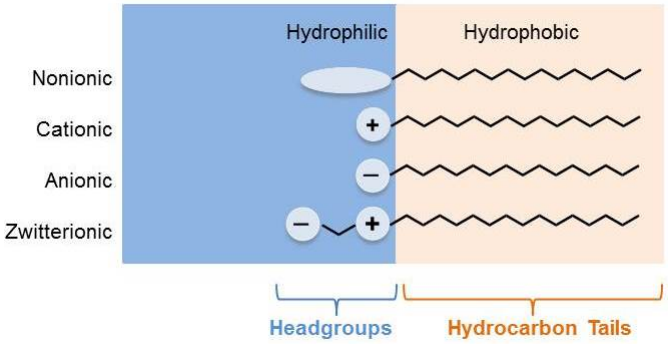

Figure 1.1: Schematic illustration of surfactant types

As shown in Figure 1.2, numerous variations are also possible in headgroup structures.

The headgroups may be attached to single chains, multiple chains, branched chains, or ring structures.[8] Many surfactants have hydrocarbon tails, but there has been increasing attention paid to fluorocarbon and silicone surfactants.[9]

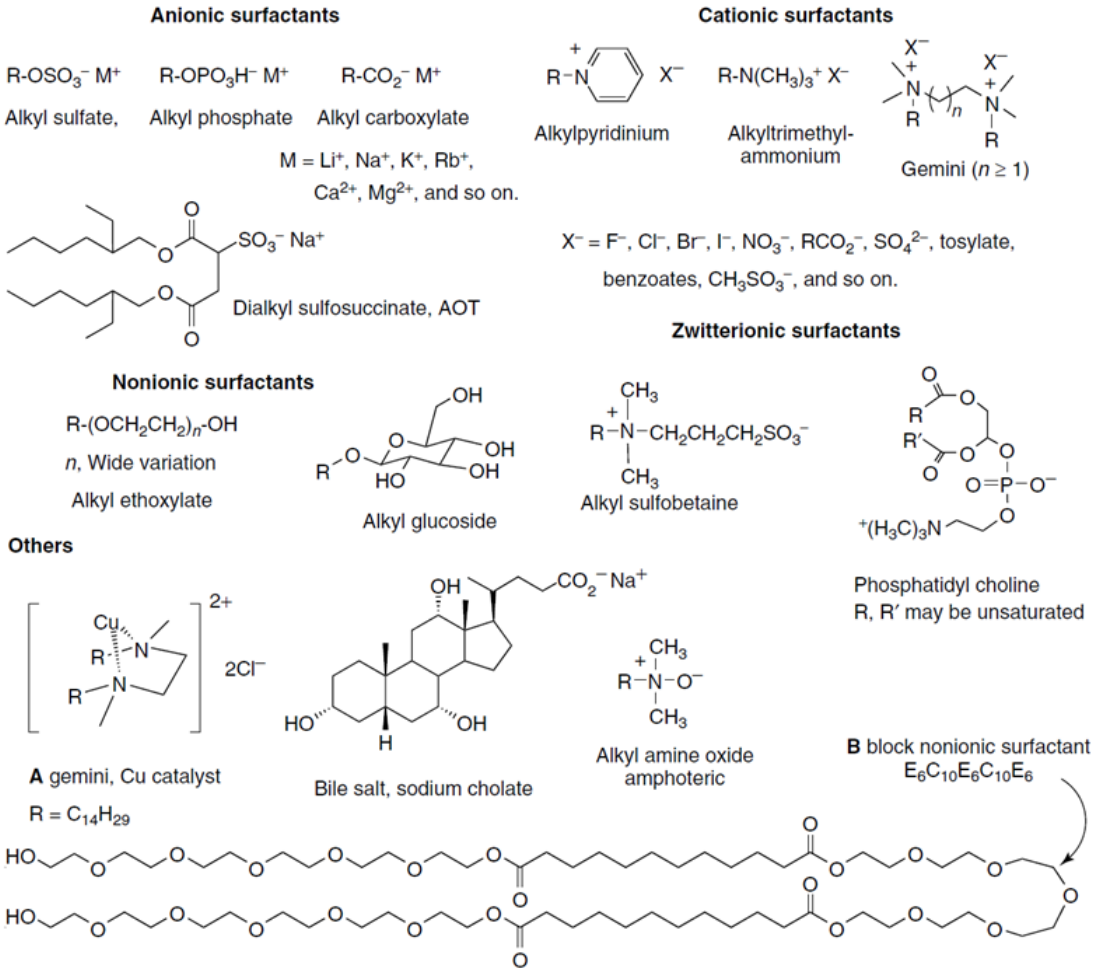

Figure 1.2: Some representative and some unconventional surfactant structures[1]

1.1.2 Micellization and surfactant self-assembly

Depending on structures and concentrations of surfactants, and sometimes other additives, surfactants self assemble into a number of aggregates of different shapes, including spherical micelles, rod-like micelles, vesicles, and bilayers, Figure 1.3.[10, 11, 12] As shown in Figure 1.3, the morphologies of surfactant aggregates may partially correlated with their "packing

parameter".[13]

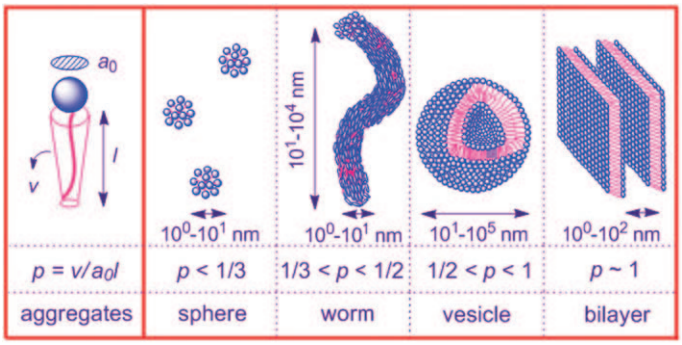

Figure 1.3: Examples of self-assembled surfactant aggregates [12]

Micelles are the most common aggregates formed by surfactants. Micelles in aqueous solution formed spontaneously by surfactants with the hydrophilic headgroups pointing out to water, while the hydrophobic tails interact with each other in the interior or core of the aggregate. Figure 1.4 illustrates the micellization process in water upon continuous addition of surfactants to their critical concentrations. The concentration, above which surfactants aggregate into micelles, is called critical micelle concentration (cmc). Micellization is a spontaneous process driven by highly cooperative noncovalent interactions. Micellar solutions are transparent thermodynamically stable solutions. At thermodynamic equilibrium, micellar solutions always contain the same concentrations of monomers and micelles with the same distribution of sizes and shapes. Figure 1.4 also shows that surfactants in micelles are constantly exchanging with their monomers in bulk solution or at the air/water interface on the microsecond timescale or faster.[14]

Table 1.1[2] lists cmc values of some selected surfactants at 25°C. The cmc is one of the most important characteristics of surfactants, and its values are sensitive to their hydrophobic chain lengths, headgroups, and counterion types.[15] For example, the cmc value decreases with increasing chain length, and the cmc values of nonionic surfactants are orders of magnitude lower than these of ionic surfactants with similar chain length. Finally, ionic surfactants with different counterion types also have different cmcs. This dependence is called an ion specific effect.

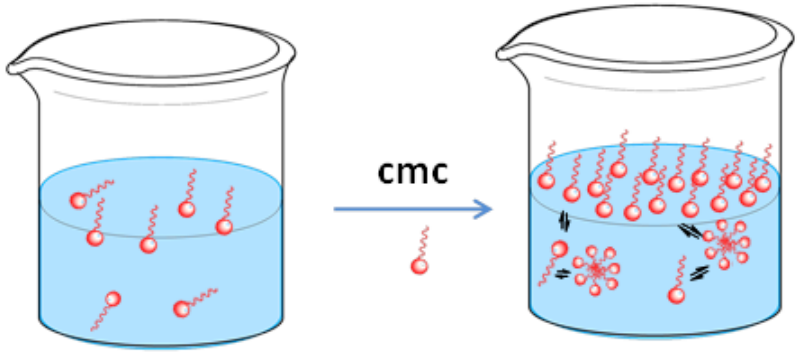

Figure 1.4: Schematic representation of micellization. The arrows show that surfactants in micelles are constantly exchanging with their monomers in bulk solution or at the air/water interface on the microsecond timescale or faster

Cmc values are also strongly affected by additives, such as, salts, alcohols, and other surfactants.[2] For nonionic surfactants, the addition of salt only has small effect on cmc values. For ionic surfactant, however, added salt lowers the cmc significantly. Salt concentration and the nature of salt are important. Addition of short-chain alcohols, MeOH to PrOH, generally increases the cmc, and micelles break up at high short-chain alcohol concentrations. However, middle-chain and long-chain length alcohols, n-butanols and longer, tend to reduce the cmc.[16] The addition of a second surfactant to a micellar solution results in mixed micelle. A mixture of cationic and anionic surfactants, often called catanionic aggregates, have very low cmc due to strong cation-anion headgroup interaction.

The values of cmc are determined by surface tension measurement or, for ionic surfactants, by conductivity.[17] Below cmc, the surface tension of a surfactant solution decreases rapidly when more surfactant is added. When the surface tension stop decreasing, micelles start to form. The concentration at the breakpoint in the surface tension plot is the cmc. Menger's recent paper[18] argue that surfactant continues to enter the interface past the cmc, but the use of this method for cmc measurement is not affected. All cmc values for ionic surfactants in this thesis work are determined by conductivity measurements performed by Alla Malinenko in France who is one of our collaborators. Figure 1.5 illustrates the equivalent conductivity decrease above the cmc for ionic surfactants because some of the

Table 1.1: List of cmc values of selected surfactants at 25°C[2]

Surfactant	cmc (mM)
Dodecylammonium chloride	14.7
Dodecyltrimethylammonium chloride	20.3
Decyltrimethylammonium bromide	65
Dodecyltrimethylammonium bromide	15.6
Hexadecyltrimethylammonium bromide	0.92
Dodecylpyridinium chloride	14.7
Sodium tetradecyl sulfate	2.1
Sodium dodecyl sulfate	8.3
Sodium octyl sulfate	133
Sodium p-octylbenzene sulfonate	14.7
Sodium p-dodecylbenzene sulfonate	1.20
Dimethyldodecylamineoxide	2.1
$CH_3(CH_2)_9(OCH_2CH)_6OH$	0.9
$CH_3(CH_2)_9(OCH_2CH)_9OH$	1.3
$CH_3(CH_2)_{11}(OCH_2CH)_6OH$	0.087
$CH_3(CH_2)_7C_6H_4(CH_2CH_2O)_6$	0.205
Potassium perfluorooctanoate	28.8

counterions are associated with micelles and do not contribute to the conductivity. Again, the cmc is the concentration at the breakpoint in the conductivity plot. Sometimes it may be very hard to define the break by naked eye when the change in slop is gradual, however, the cmc can still be estimated by fitting the conductivity data to a nonlinear function obtained by direct integration of a Boltzmann type sigmoidal function.[19]

While micelles are frequently spherical, they can also grow into rod-like, or worm-like, micelles through a sphere-to-rod transition, Figure 1.6. The critical concentrations, above which spherical micelles grow into rod-like micelles with large aggregation numbers, is sometimes called the second cmc as defined by Porte et al.[20] The first experimental evidence of the sphere-to-rod transition was also reported in the same paper for cetylpyridinium bromide (CPBr) was measured by viscosity. Below the second cmc, added surfactant increases the number of spherical micelles without transforming them into elongated aggregates.[21] Indeed, all of the additives mentioned in previous paragraphs that can lower cmc values may also induce micellar growth and the sphere-to-rod transition. Worm-like micelles exhibit a hierarchy of length scales and unusual viscoelastic behavior. [22, 23, 24, 25, 26, 27, 28]

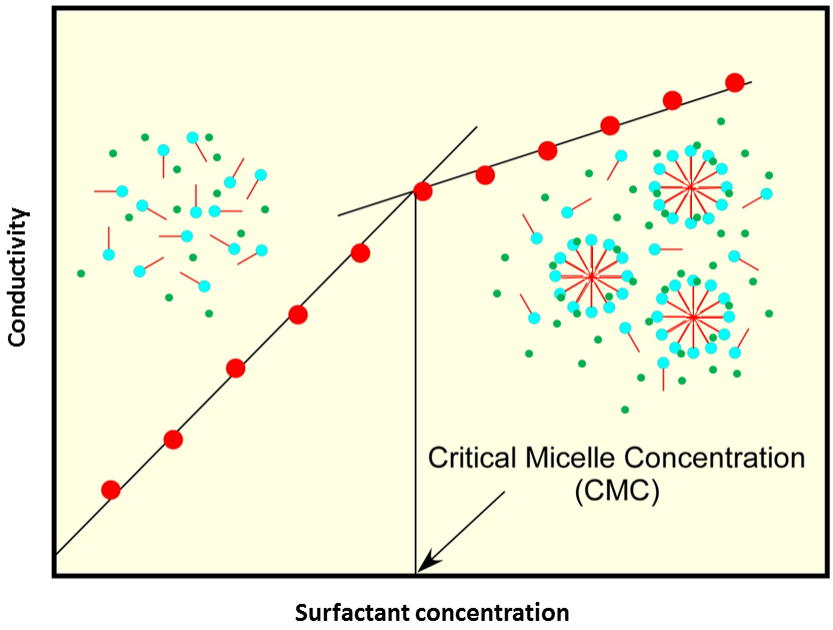

Figure 1.5: Schematic illustration of the determination of cmc by conductivity method

Therefore, the viscoelastic worm-like micelles have been extensively used in oilfield and in personal care products.[21]

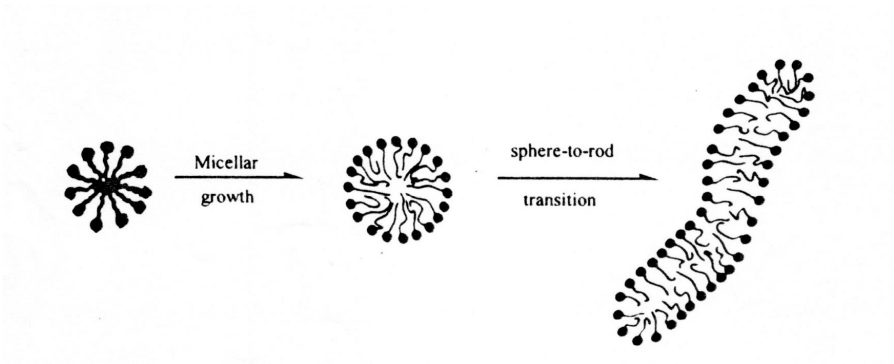

Figure 1.6: Micellar growth and sphere-to-rod transition

Vesicles, Figure 1.3, are spherical or ellipsoidal single- or multi-compartment closed bi-layer structures.[29] Surfactants arrange themselves such that the hydrophilic headgroups are in contact with the inner and outer aqueous regions, the hydrophobic tails associate

to form the interior in the bilayer for unilamellar vesicles (ULV) or layers for multilamellar vesicles (MLV). Specifically, vesicles composed of phospholipids commonly formed in biological membranes, such as 1-palmitoyl-2-oleoyl-sn-glycero-3-phosphocholine (POPC), are frequently called liposomes.[30] Vesicles are a class of interesting aggregates that have been used not only as model for cell membranes,[31, 32] but also microreactors and drug carriers.[33, 34, 35] Sonication, dialysis, extrusion of lamellar suspensions, and reverse-phase evaporation, are some common but energetically costly methods for vesicle preparation.[36] Thermodynamically stable spontaneous vesicles, however, can formed in some systems containing mixtures of two cationic surfactants[37], cationic and anionic surfactants (catanionic surfactants)[11], nonionic and ionic surfactants[38], or ionic surfactant and additives, i.e., alcohols and salts.[39, 40] For catanionic mixtures, surfactants pair with different chain lengths are preferred to avoid liquid crystalline lamellar phase and crystalline precipitates.[41, 42] The addition of salts into a micellar solution may induce a spontaneous micelle-to-vesicle transition, where critical salt concentration (CSC) can be defined as above which micelles grows into vesicles. Evidence of vesicle formations is demonstrated by a variety of techniques, such as, cryogenic transmission electron microscopy (cryo-TEM), dynamic light-scattering (DLS), small-angle neutro scattering (SANS), and video-enhanced microscopy.

1.1.3 Gemini surfactants

Gemini surfactants are made up of two conventional surfactants connected by a spacer group.[43] The two surfactants are identical or different. The spacer can be polar (polyether) or nonpolar (aliphatic); flexible (methylene) or rigid (stilbene); and short or long.[44] Although the structures of the spacer group varies a lot, the spacer groups have to connect the two moeities' headgroups, instead of the tails. Otherwise, the surfactant is simply called bolaform surfactant. Figure 1.7 gives schematic representations of both gemini and bolaform surfactants.

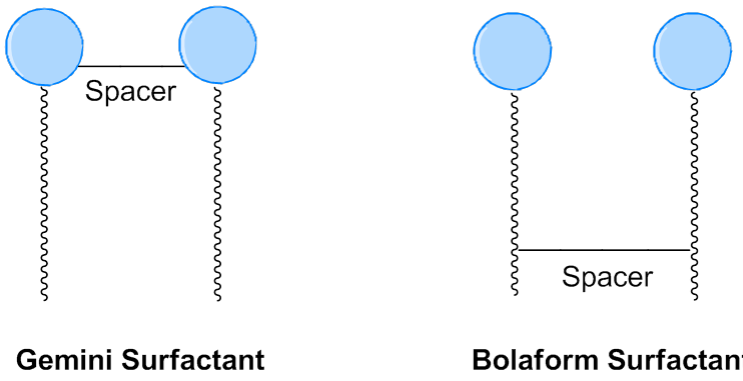

Figure 1.7: Schematic representations of gemini and bolaform surfactant

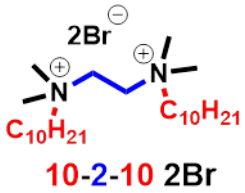

Figure 1.8: Chemical structure of gemini surfactant 10-2-10 2Br

The most studied gemini surfactants are bis(quaternary ammonium bromide) surfactants, $C_nH_{2n} - \alpha,\omega - (Me_2N^+C_mH_{2m}Br^-)_2$, known as m-n-m 2Br, where m is the carbon chain length and n is the methylene spacer length. For example, the structure of gemini surfactant 10-2-10 2Br is shown in Figure 1.8.

Table 1.2: List of cmc values of representative gemini surfactant and their correponding single-chain surfactants

Surfactant	cmc (mM)	Ref
$C_{12}H_{25}N^+(CH_3)_3Br^-$	16	[45]
$C_{16}H_{33}N^+(CH_3)_3Br^-$	1	[46]
$C_{12}H_{25}OSO_3^-Na^+$	8	[45]
$C_{12}H_{25}N^+(CH_3)_2 - (CH_2)_n - N^+(CH_3)_2C_{12}H_{25}2Br^-$ [a]	1	[47]
$C_{16}H_{33}N^+(CH_3)_2 - (CH_2)_2 - N^+(CH_3)_2C_{16}H_{33}2Br^-$	0.003	[48]
$C_{10}H_{21}O - CH_2 - CH(OSO_3^-) - CH_2 - O - (CH_2)_2 - O - CH_2 - CH(OSO_3^-) - CH_2 - OC_{10}H_{21}2Na^+$	0.01	[49]

[a] $n = 3 - 8$

Table 1.3: Comparison of the C_{20} values of representative gemini surfactant and conventional surfactants

Surfactant	C_{20} (mM)	Ref
$C_{12}H_{25}N^+(CH_3)_3Br^-$	8	[50]
$C_{12}H_{25}OSO_3^-Na^+$	3	[49]
$C_{12}H_{25}N^+(CH_3)_2-(CH_2)_2-O-(CH_2)_2-N^+(CH_3)_2C_{12}H_{25}2Br^-$	0.25	[51]
$C_{10}H_{21}O-CH_2-CH(OSO_3^-)-CH_2-O-(CH_2)_2-O-$ $CH_2-CH(OSO_3^-)-CH_2-OC_{10}H_{21}2Na^+$	0.001	[49]

Gemini surfactants have attracted significant attention because of their interesting physicochemical properties. First, The cmc's of gemini surfactants are one to two orders of magnitude lower than the corresponding conventional single-chain surfactants, Table 1.2. Second, gemini surfactants are usually orders of magnitude more surface-active then their single chain analogs.[52, 44] In other words, gemini surfactants are more efficient in adsorbing at the air/water interface and decreasing the surface tension of water. The value C_{20}, defined as the surfactant concentration required for lowering the surface tension of water by 0.02 N/m, is usually used to characterize this efficiency, Table 1.3. Third, micellar solutions of some gemini surfactants with short spacers undergo sphere-to-rod transitions at relatively low concentrations. Therefore, the aqueous solutions of such gemini surfactants can have very high viscosities at a low surfactant concentration.

1.2 Ion Specific Effects

1.2.1 Hofmeister series

The striking effects of a variety of salts on the solubility of proteins was first discovered by Franz Hofmeister in 1888.[53] These specific ion effects exhibit a recurring order that is now called Hofmeister series. Typical ordering of anions and cations in Hofmeister series is summarized in Figure 1.9.[54] It's the strongly hydrated hard cations of high charge density that tend to increase the solubility of proteins. However, this trend reverses for anions. In that case, weakly hydrated soft anions of low charge density tend to increase the solubility of proteins. This difference is actually related to the fact that the negative

charges on proteins, carboxylates, are strongly hydrated, whereas the positive charges on proteins, derivatives of ammonium, are weakly hydrated, and can be explained later by Collins' concept of matching water affinities (detailes in 1.2.2).

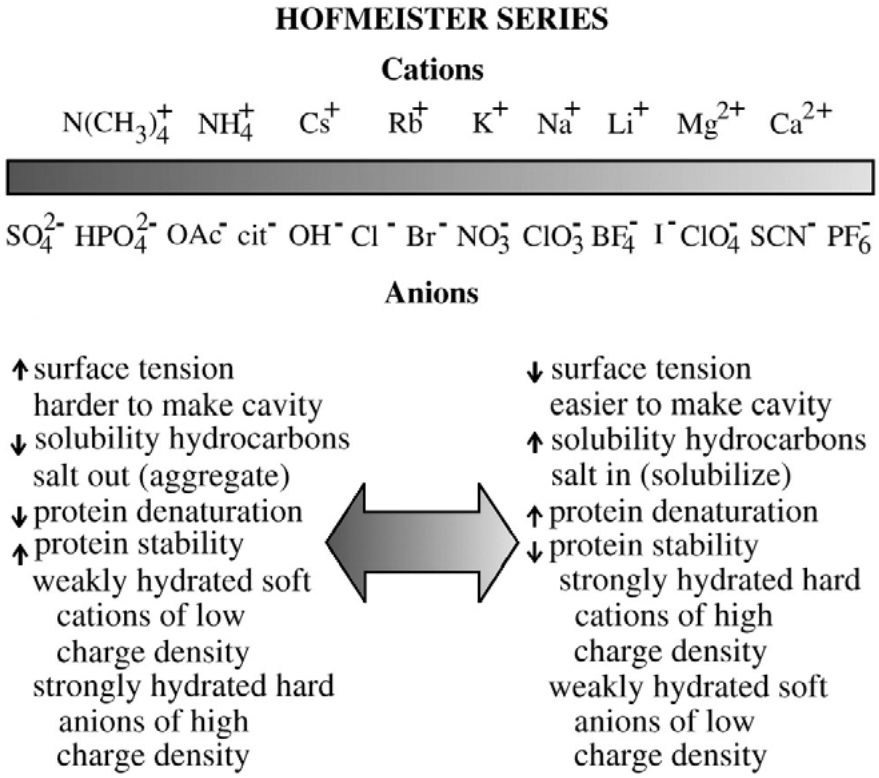

Figure 1.9: Typical ordering of anions and cations in Hofmeister series [54]

There have been numerous attempts trying to explain ion specific effects over the last century. For example, the specific interaction between ions and water was studied by measuring viscosities of salt solutions.[55, 56, 57] By measuring the time required for a salt solution to flow through a small hole at the bottom of a tube, the viscosity of the solution can be determined. For salt solutions whose concentrations below 0.1 M, the viscosity results can be fitted into equation 1.1:

$$\eta/\eta_0 = 1 + Ac^{1/2} + Bc \tag{1.1}$$

where η and η_0 are the viscosities of a salt solution and pure water, respectively; A is a electrostatic term which is close to 1; and B, known as Jones-Dole viscosity B coefficient, is

a direct measure of the strength of ion-water interactions. Ions with positive B coefficients are defined as strongly hydrated ions, while ions with negative B coefficients are called weakly hydrated ions.

Table 1.4: Jones-Dole viscosity B coefficients[58]

Cations	B	Anions	B
Mg^{2+}	0.385	PO_4^{3-}	0.590
Ca^{2+}	0.285	$CH_3CO_2^-$	0.250
Ba^{2+}	0.22	SO_4^{2-}	0.208
Li^+	0.150	F^-	0.10
Na^+	0.086	HCO_2^-	0.052
K^+	-0.007	Cl^-	-0.007
NH_4^+	-0.007	Br^-	-0.032
Rb^+	-0.030	NO_3^-	-0.046
Cs^+	-0.045	ClO_4^-	-0.061
		I^-	-0.068
		SCN^-	-0.103

The Jones-Dole viscosity B coefficient changes sign between Na^+ and K^+, indicating the strong hydration for Na^+ and weaker hydration for K^+. This result is also confirmed by solution neutron and X-ray diffraction techniques, Figure 1.10.[59, 60] The smallest distance between Li^+ and nearest water oxygen indicate the strongest hydration of Li^+. The Na^+ to oxygen distance is smaller than the oxygen-oxygen distance in liquid water, showing the hydration of Na^+ is strong; while the K^+ to oxygen distance is larger than the oxygen-oxygen distance in liquid water, confirming that K^+ is weakly hydrated.

Hydration of an ion is not the only important interaction which is used to describe specific ion effects. Over the last decades, molecular dynamic (MD) simulations have been widely employed to simulate the interactions between ions and macromolecules or molecular assembly systems. The features or parameters for properly describing specific ion effects are[54]: (1) The charge density of ions. One of the most important parameters and the choice is not trivial because choosing the proper radius, Pauling's radius or radius including the first hydration sphere, remain an unsolved question. (2) The structuring of water at interfaces. For example, non-hydrogen-bonded water molecules are detected at hydrophobic

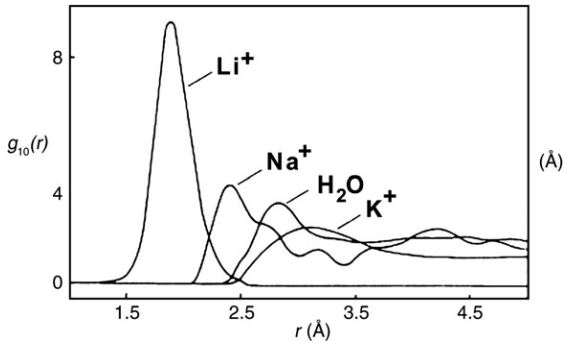

Figure 1.10: The radial distribution functions for Li^+, Na^+, water, and K^+ in liquid water. These curves measure the distance from the cations to the nearest water oxygen. The curve labeled "H_2O" measures the oxygen-oxygen distance in liquid water. Both neutron and X-ray diffractions were used to generate the data. [59, 60]

molecule-water interfaces by Raman Spectroscopy System.[61] Another example is that hydronium ions are energetically slightly more favorable in the air-water interface than in the bulk. [62] (3) Ion properties depend strongly on the environment, especially, neighboring headgroups and counterions. There is no single group of well-defined parameters for a particular ion. This also explains why the reversals of the Hofmeister Series are observed.[63] (4) To study the specific interaction between ions and macromolecules, the structure and chemical composition of the macromolecules must be known. The model cannot be simplified by using "protein surface". (5) Ion specific effects dependent on salt concentration. Ion specific effects are usually measured from intermediate to high salt concentrations, whereas electrostatic forces dominate at low salt concentation (<0.1 M). (6) Ion polarizability is also believed to be important[64, 65], however, it is extremely difficult to estimate ion polarizabilities in solutions. Recent MD simulations studied ion specificity by using nonpolarizable force fields.[66, 67, 68]

1.2.2 Collins' concept of matching water affinities

Collins developed us a relative simple idea called the "concept of matching water affinities" to explain ion specific effects.[58, 59] Cations and anions are first classified into two groups based on the strengths of their interactions with water, indicated by Figure 1.11. Strongly

hydrated ions (ions with positive B coefficient) are called kosmotropes (water-structure makers), while weakly hydrated ions (ions with negative B coefficients) are named chaotropes (water-structure breakers). However, recent research shows that for monovalent ions, the only influence is the first hydration shell [69], in other words, there is actually no significant long-range structuring of water due to ions. Therefore, the terms "kosmotropes" and "chaotropes" are only used for historical reasons here. For example, Figure 1.12 shows the division of the IA cations and VII halides into kosmotropes and chaotropes.[58]

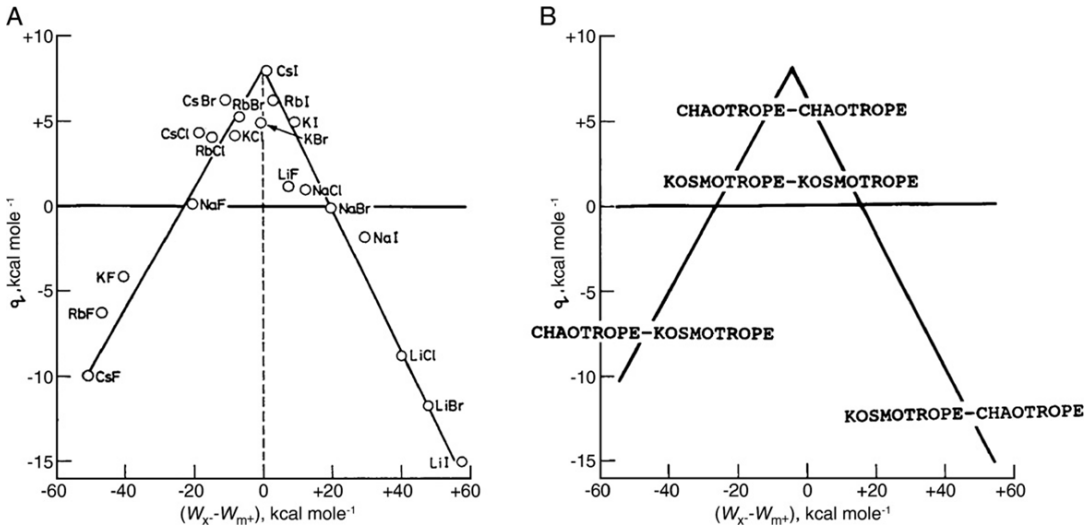

Figure 1.11: (A)Relationship between the standard heat of solution of a crystalline alkali halide (at infinite dilution) in kcal/mol and the difference between the absolute heats of hydration of the corresponding gaseous anion and cation, also in kcal/mol. (B) Identification of ions as chaotropes (weakly hydrated) or kosmotropes (strongly hydrated). The enthalpy of solution of chaotrope-chaotrope and kosmotrope-kosmotrope salts tends to be positive (takes up heat), whereas for the enthalpy of solution to be negative (gives off heat), the salt must have a kosmotropic and a chaotropic ion.[59]

The specific effect of ions can then be explained by "oppositely charged ions with equal water affinity tend to come together in solution to form contact ion pairs whereas oppositely charged ions with differing water affinities tend to stay apart". In short, chaotropes pair with chaotropes and kosmotropes pair with kosmotropes. The formation of ion pair requires a partial dehydration of both cation and anion, therefore, ion pairing forms readily when they have similar water affinity. For chaotropes and chaoptropes ions, the cost for dehydration is minimized; while for kosmotropes and kosmotropes ions, the formation of ion pairs release

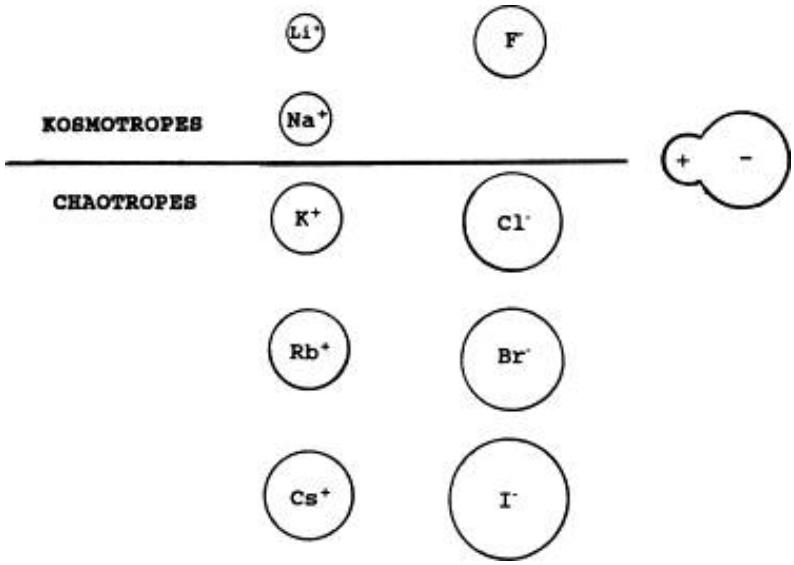

Figure 1.12: Division of the IA cations and VII halides into kosmotropes and chaotropes.[58]

more energy although the cost for dehydration of both ions is relatively high. Otherwise, if one ion is much more strongly hydrated than its partner, dehydrating the strongly hydrated ion costs more in energy than is gained by forming an ion pair.

1.2.3 Interfacial ion pairing and hydration in ionic surfactant aggregates

Ion specific effects also affect many micellar properties such as the cmc, Krafft temperature, aggregation number, ionization degree, and sphere-to-rod transition concentratons.[70] Table 1.5 lists the sensitivity of the sphere-to-rod transitions to the substitution of Br^- for a Cl^- for surfactants with the same headgroup and chain length.

Table 1.5: Effect of counterion type on the cmc and sphere-to-rod transition concentrations of some cationic surfactants

Surfactant[a]	No. of carbons on tail	headgroup,X	cmc (mM)	sphere-to-rod (M)	Ref
CTABr	16	$-N(Me)_3^+Br^-$	0.9	~ 0.1	[64]
CTACl	16	$-N(Me)_3^+Cl^-$	1	~ 1.0	[71]
DTABr	12	$-N(Me)_3^+Br^-$	14.6	~ 1.8	[72]
DTACl	12	$-N(Me)_3^+Cl^-$	19.4	none	[73]

[a] CTABr and CTACl cetyltrimethylammonium bromide and chloride; DTABr and DTACl, dodecyltrimethylammonium bromide and chloride.

There are two important equilibria controlling micelle formation, Figure 1.13. The

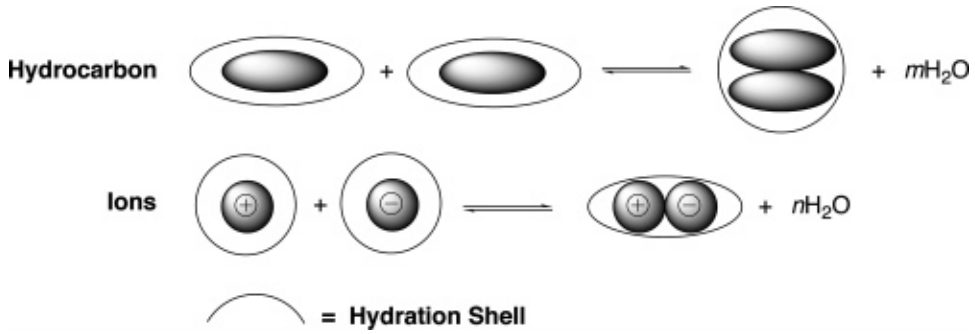

Figure 1.13: Schematic representations of the hydrophobic effect (top) and the ion-pair/hydration model (bottom).[58]

top equilibrium shows the hydrophobic effect, the minimization of contact between the hydrocarbon tails of surfactants with water, which is the driving force of surfactant aggregation. The increase in entropy from release of water in the hydrocarbon hydration shell to the surrounding bulk water is believed to be a major contributor to the self-assembly of surfactants.[74, 75] The bottom equilibrium is an ion-pair equilibrium in the interfacial region of ionic micelles and other surfactant aggregates. The cation (or anion) works as a simple representation of the headgroup for a cationic (or anionic) surfactant whereas its partner represents the counterion. Similar to the first equilibrium, the formation of ion-pairs also corresponds to partial dehydration of both headgroups and counterions and the release of interfacial water into the surrounding bulk water. The size and morphology of micelle is determined by the balance-of-forces controlled by these two equilibria.

The ion specific effects in ionic surfactant aggregates can be explained by the shift of interfacial ion-pair/hydration equilibrium. The ion-pair equilibrium depends on headgroups structures, counterion types, added salts, and interfacial hydration. According to Collins' concept of matching water affinity, headgroup and counterion with similar water affinities tend to form ion pairs in the interfacial region. For example, a weakly hydrated soft headgroup, e.g., -$N(Me)_3^+$, tends to form more ion-pairs with weakly hydrated counterions, e.g., Br^-, than more strongly hydrated counterions, e.g., Cl^-. Therefore, replacing Cl^- with Br^- shifts the ion-pair equilibrium to the right side, more interfacial water is released into the

surrounding bulk water, making micellar growth occur at a lower surfactant concentration.

To support our hypothesis, interfacial water and counterion concentrations estimated by chemical trapping method are provided as evidence in the current thesis. Specific anions effects on cationic gemini surfactants, 10-2-10 2X, aggregates in the absence (Chapter 2) and present (Chapter 3) of salt, and specific salt effects on anionic surfactants, AOT, aggregates (Chapter 4) are reported.

1.3 Chemical Trapping Method

1.3.1 Reactivity of arenediazonium ions

Arenediazonium ions have a rich and extensively explored chemistry. The four main reaction types for aromatic as opposed to aliphatic diazonium ions are shown in Figure 1.14: replacement of nitrogen by a nucleophile, reaction of a nucleophile at the terminal nitrogen, nucleophilic aromatic displacements activated by the diazonium group, and free radical reactions. Only the first two types of reactions are discussed here.

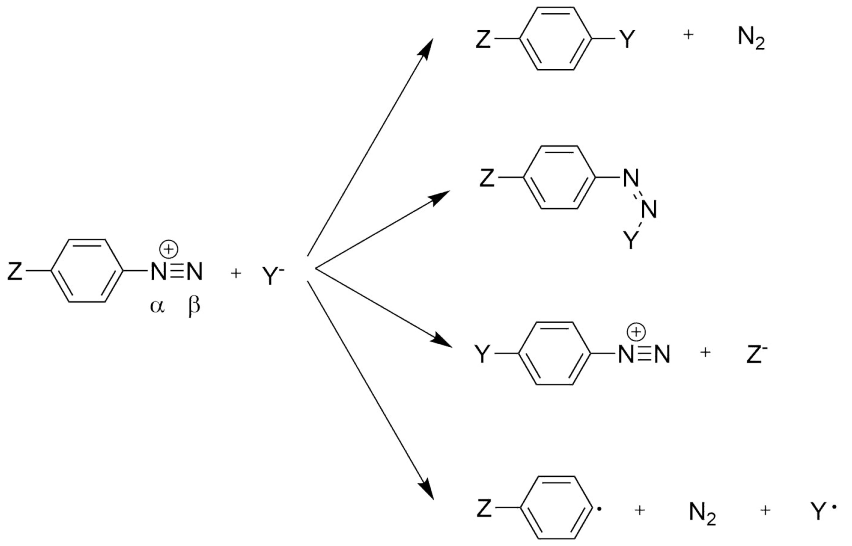

Figure 1.14: Main reaction types shown for arenediazonium ions[76]

1.Dediazoniation

The word dediazoniation was introduced by Bunnett as early as 1954. It refers to all the

reactions of diazonium compounds where an N_2 molecule is one of the products.[77] In the absence of UV light, strong nucleophiles, reducing and electron transfer agents, and in acidic to neutral solutions, arenediazonium ions generally undergo spontaneous dediazoniation, which is also the foundation of chemical trapping method. Figure 1.15 summarizes three ionic pathways for dediazoniation reactions.

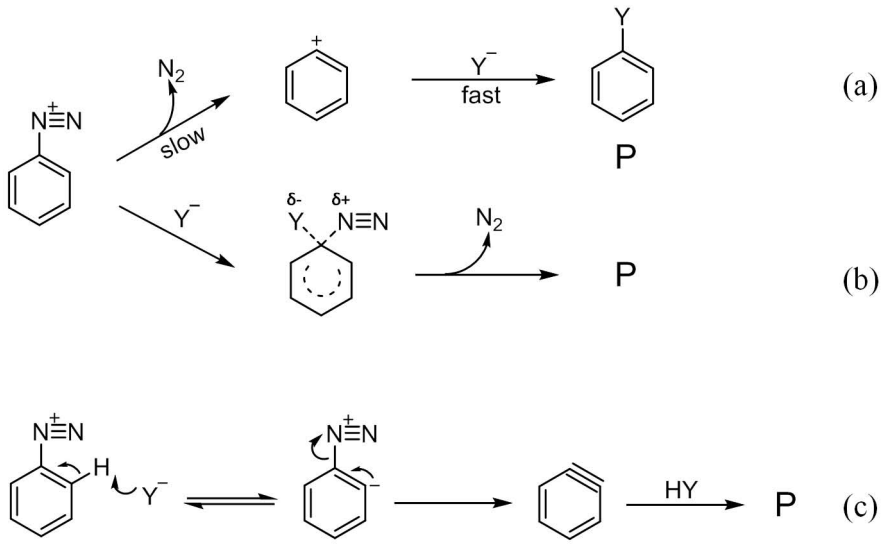

Figure 1.15: Three ionic pathways for dediazoniation reaction[76]

Pathway (a), i.e., phenyl cation pathway, is analogous to the S_N1 mechanism. The lifetime of the phenyl cation intermediate is estimated to be in the picosecond time scale, and has never been directly observed in solution.[78, 79, 80] However, this pathway is supported by evidence from kinetic experiments. The first-order rate constants for dediazoniation of benzenediazonium tetrafluoroborate is extraordinary insensitive to solvent polarity, Table 1.6.[81] The rate constants for the dediazoniation vary only 9-fold in nonpolar CH_2Cl_2 and dioxane, in dipolar, aprotic DMSO, in dipolar, protic alcohols, and in dilute and concentrated, aqueous H_2SO_4 solutions. In other words, solvents of various polarity affect the ground and transition state to similar extents suggesting the phenyl cation pathway. Mechanisms involving the build-up of appreciable charge on water oxygen in the transition state are ruled out by the absence of a solventisotope effect.[82] There is also evidence supporting the reversible, rate-determining, heterolytic C-N bond cleavage, exchange between ^{15}N in

the beta-nitrogen and $^{14}N_2$ in trifluoroethanol under 300 atm nitrogen;[83] and the dediazoniation reaction is inhibited by high concentrations of dissolved N_2.[84]

Table 1.6: First-order rate constants for dediazoniation of benzenediazonium tetrafluoroborate in various solvents at 25 °C

Solvent	$10^5 k_{obs}$ (s^{-1})	Dielectric constant	Ref
Dioxane	1.15	2.21	[85]
0.1% (0.01 M) H_2SO_4	4.55	80.1	[85]
105% (21 M) H_2SO_4	2.15	110.0	[85]
100% CH_3COOH	2.26	6.2	[85]
100% CH_3COOH + 1.0 M LiCl	4.51		[85]
CH_2Cl_2	2.20	8.9	[86]
CH_3CN	3.3	37.5	[86]
DMSO	4.16	48.9	[86]

Pathway (b) represent a bimolecular nucleophilic aromatic substitution with a simultaneously loss of N_2 and attacking by Y^-. There are also evidence to support this pathway. The rate of dediazoniation reaction increases linearly with increasing Br^- and SCN^- was observed.[87, 88] However, the rate increase is fairly small and may depend on a correction for the effect of added sodium ion on the activity of water.

Pathway (c) is an elimination-addition pathway involving the formation of an aryne followed by the addition of HY. However, this pathway is not important for normal arenediazonium ions in aqueous solution in the absence of very strong bases, which is demonstrated by the absence of products from rearrangement.[85]

These three pathways represent mechanistic extremes and, therefore, it's not uncommon for some reactions to have the characteristics of two pathways, especially, pathways (a) and (b) in aqueous solutions.

2. Reaction of nucleophiles at the terminal nitrogen

Arenediazonium ions are Lewis acids in which the beta-nitrogen may react with strong nucleophiles.[89] Based on the atom of the nucleophile that provides the electron long pair, O-, S-, N-, P-, or C-coupling may occur. As shown in Figure 1.16, a strong nucleophile with charge n, Nu^n, is covalently bonded to the terminal nitrogen. Usually, the primary

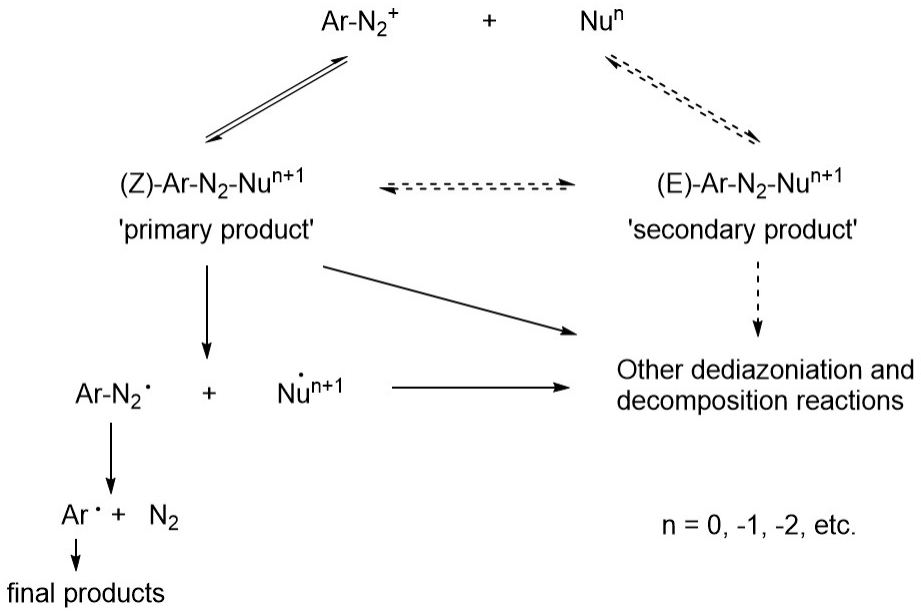

Figure 1.16: Schematic illustration of the addition of nucleophiles with charge n to arenediazonium ions.[89]

product is in the (Z)-configuration. The stability of the primary adduct depends on the leaving group abilitu of Nu^n and the stability of the radical $Nu\cdot^{n+1}$. The primary adduct may also be stabilized by conversion to the conjugate base or its (E)-configuration. For example, the attack of hydroxide ion on the terminal nitrogen gives diazohydroxides that further ionize to diazotates, Ar-N=N-O^-, which are stable in basic solution. Another important O-coupling reaction is the formation of diazo ethers with the attack of alkoxide and phenoxide. With N- and C-coupling, a group of important compounds can be formed, namely azo dyes. Arenediazonium ions also undergoes intramolecular coupling including the formation of indazoles under alkaline conditions, Figure 1.17.

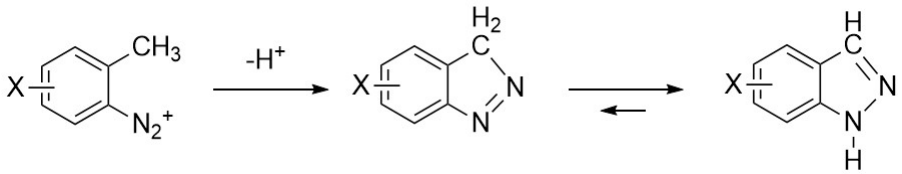

Figure 1.17: Schematic illustration of the formation of indazoles[89]

1.3.2 Logic of chemical trapping method

The chemical trapping method, which is a probe method, was developed by our group to estimate the molarities of weakly basic nucleophiles within association colloid interfaces. The method is based on the reaction between the two specifically designed probes 4-alkyl-2,6-dimethylarenediazonium ion, z − ArN_2BF_4 (z=16, hexadecyl, z=1, methyl), and weakly basic nucleophiles, such as water, halides, and alcohols at the interface of micelles and other association colloid. Figure 1.18 summarized the known reactions of the probe with many different reactants.

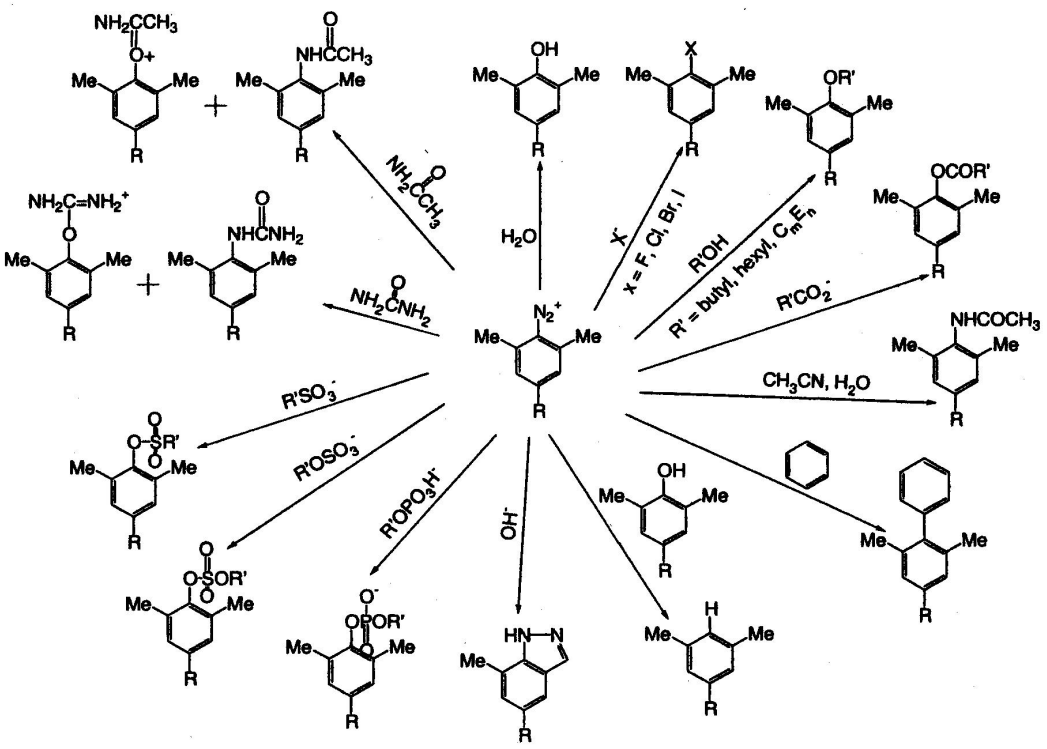

Figure 1.18: Reactions of the chemical trapping probe with different reactants.[90]

The long-chain probe 4-hexadecyl-2,6-dimethylbenzenediazonium ions, 16-ArN_2^+, is used to probe the interfacial regions of association colloids and emulsions, whereas its short-chain analog, 2,4,6-trimethylbenzenediazonium ion, 1-ArN_2^+, is used to determine the selectivity of the probe towards different weakly nucleophiles in reference salt solutions containing

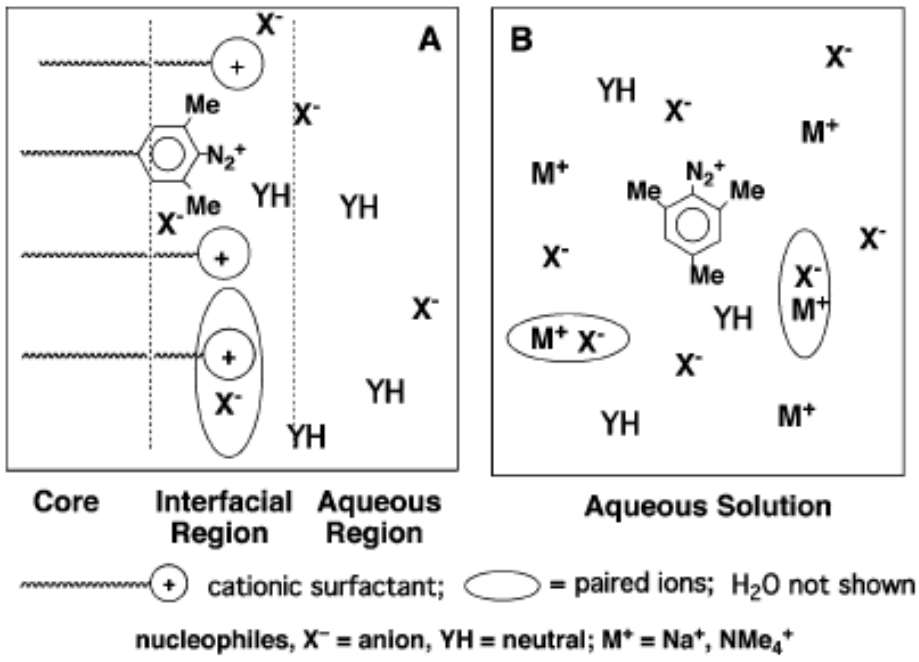

Figure 1.19: Box A illustrates a small section of an aqueous solution of cationic micelles where 16-ArN_2^+ is trapped by water (not shown), anionic, X^-, and neutral, YH, nucleophiles in the interfacial region. Box B shows an aqueous reference solution in which the stoichiometric component concentrations are fixed during solution preparation.[91]

surfactants' headgroup model, Figure 1.19. The probe undergoes dediazoniation reaction in aqueous solution of either an association colloid or salts in the absence of light at pH $<$ 7, and the concentration of 16-ArN_2^+ is kept equal to or less than 10^{-4} M. Weakly basic nucleophiles react competitively with probe to generate products that can be analyzed by HPLC equipped with UV detector, Figure 1.20. The product yields are proportional to the concentrations of reactive z-$ArN_2^+ \cdot H_2O$ and z-$ArN_2^+ \cdot X^-$ pairs.

The fundamental assumption of chemical trapping method is that the selectivity of the dediazoniation reaction in the interfacial region of association colloids and in reference solution is the same when the yields are the same. The selectivity of the dediazoniation reaction towards X^- compared to water in the interfacial region is defined in Equation 1.2:

$$S_w^X = \frac{H_2O_m(\%16 - ArX)}{X_m(\%16 - ArOH)} \tag{1.2}$$

where the subscript m indicates the interfacial molarity in moles per liter of interfacial

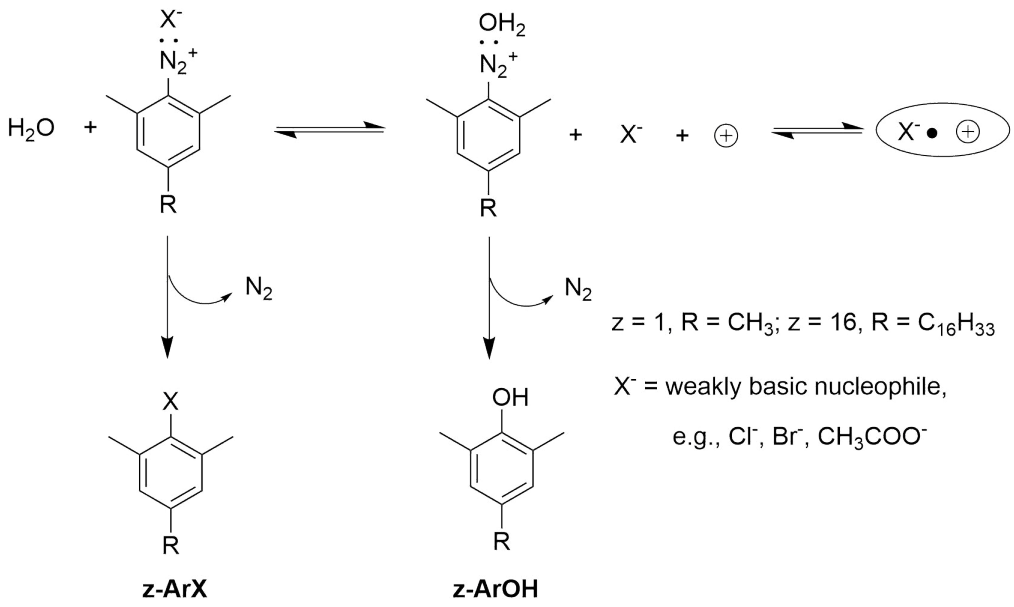

Figure 1.20: The probe, z-ArN_2^+ , and weakly nucleophiles are assumed to be in dynamic equilibrium in association colloids and bulk solution. There is a competition between the water and anions, X^-, to generate dediazoniation products, z-ArOH, and z-ArX, respectively. X^- may also form neutral ion-pairs which are assumed not to react with the probe.

volume; % represents percent yield of a product; 16-ArX and 16-ArOH are products from the dediazoniation reaction between 16-ArN_2^+ and X^- or water, respectively. This selectivity value in the reference solution is defined in Equation 1.3:

$$S_w^X = \frac{[H_2O](\%1 - ArX)}{[X](\%1 - ArOH)} \tag{1.3}$$

where square bracket indicates the stoichiometric concentration in moles per liter of total solution volume; 1-ArX and 1-ArOH are products from the dediazoniation reaction between 1-ArN_2^+ and X^- and water, respectively. Therefore, the above assumption can be mathematically represent in Equation 1.4:

$$S_w^X = \frac{[H_2O](\%1 - ArX)}{[X](\%1 - ArOH)} = \frac{H_2O_m(\%16 - ArX)}{X_m(\%16 - ArOH)} \tag{1.4}$$

The second assumption is a corollary of Equation 1.4: when the percent yield of long-chain product 16-ArX {and 16-ArOH} in the interfacial region equals to the percent yield

of short-chain product 1-ArX {and 1-ArOH} in the reference solution, the interfacial concentration of X^- {and water}, X_m {and H_2O_m}, equals to the stoichiometric concentration of X^- {and water}, $[X^-]$ {and $[H_2O]$}, in the reference solution. In short, when the yields are the same, the concentrations are the same.

1.3.3 Estimating interfacial molarities

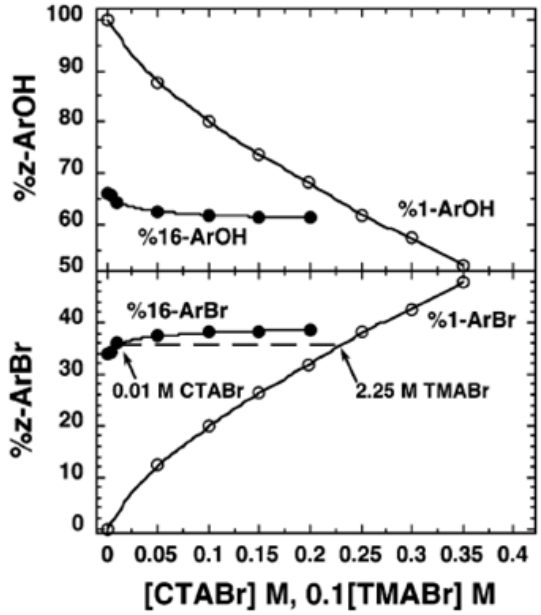

Figure 1.21: Chemical trapping product yields from reaction with H_2O (top) and Br^- (bottom) at 40 ^oC from reaction of 16-ArN_2^+ in CTABr micelles (•) and 1-ArN_2^+ in TMABr solutions (○). To put the CTABr and TMABr data on the same scale, each stoichiometric TMABr concentration is multiplied by 0.1.[91]

The estimates of interfacial Br^- concentration, Br_m, in CTABr micellar solutions is used as an example.[81] First, the composition of reference solutions is selected to mimic the CTABr micellar interface. Aqueous tetramethylammonium bromide, TMABr, was used to mimic the headgroup region of CTABr. Second, the product yields from chemical trapping reactions with 1-ArN_2^+ in aqueous reference solutions are obtained over a wide range of salt concentrations. For TMABr, the chemical trapping reaction with 1-ArN_2^+ was carried out in 0-3.5 M TMABr aqueous solutions, and a standard curve showing the relationship between %1-ArBr versus the stoichiometric Br^- concentration, [TMABr], was obtained.

Third, the product yields from chemical trapping reactions with 16-ArN_2^+ in the interfacial region of association colloid are obtained. The chemical trapping reaction with 16-ArN_2^+ was carried out in CTABr micellar solutions, to obtain the product yields of both 16-ArBr and 16-ArOH. Finally, interfacial molarities were estimatedby assuming that when the yields are the same, the concentrations are the same. The dashed line in Fiugre 1.21 indicates that the interfacial Br^- molarity in 0.01 M CTABr micellar solution is assumed equal to the stoichiometric Br^- concentration in the corresponding reference TMABr solution, 2.25 M, because %16-ArBr = %1-ArBr = 36%. The corresponding interfacial water molarity, H_2O_m, is estimated from Equation 1.4 using the known or measured values of molarities, product yields and the selectivity at the %1-ArX yield that give [X].

Chapter 2

Determination of Interfacial Molarities in 10-2-10 2X (X=AcO, MsO, Cl, Br, I) Micellar Solutions

2.1 Introduction

The elucidation of specific ion effects on the spontaneous self-assembly, structures and stabilities of association colloids of ionic amphiphiles remains a major unsolved problem in colloid and interface science, see Chapter 1. Here, the ion specific effects of acetate (AcO^-), mesylate (MsO^-), chloride (Cl^-), bromide (Br^-), and iodide (I^-) on micelles composed of the twin tail gemini surfactants 1,2-ethanebis(dimethyldecylammonium) (10-2-10 2X) are investigated by chemical trapping method, Figure 2.1. The interfacial counterion, X_m, and water, H_2O_m, molarities are estimated by chemical trapping method. The interfacial counterion molarities follow the order: $I_m > Br_m > Cl_m > MsO_m > AcO_m$. The interfacial water molarities follow the order: $AcO^- > Cl^- > MsO^- > Br^- > I^-$. The result of AcO_m, Cl_m, and Br_m are further confirmed by molecular dynamic (MD) simulations. For 10-2-10 2Br micelles, the fraction of Br^- ion-pairs in the interfacial region calculated by CT and MD method is around 0.5.

The specifically designed aggregate-bound probe, 4-hexadecyl-2,6-dimethylarenediazonium ion, 16-ArN_2^+,[81] reacts with weakly basic nucleophiles, e.g., halide ions and water in the interfacial regions of 10-2-10 2X micelles and the product yields measured by HPLC are used to estimate their interfacial molarities. The dediazoniation reactions were carried out above the measured cmc of those gemini surfactants to ensure micelles were present. To

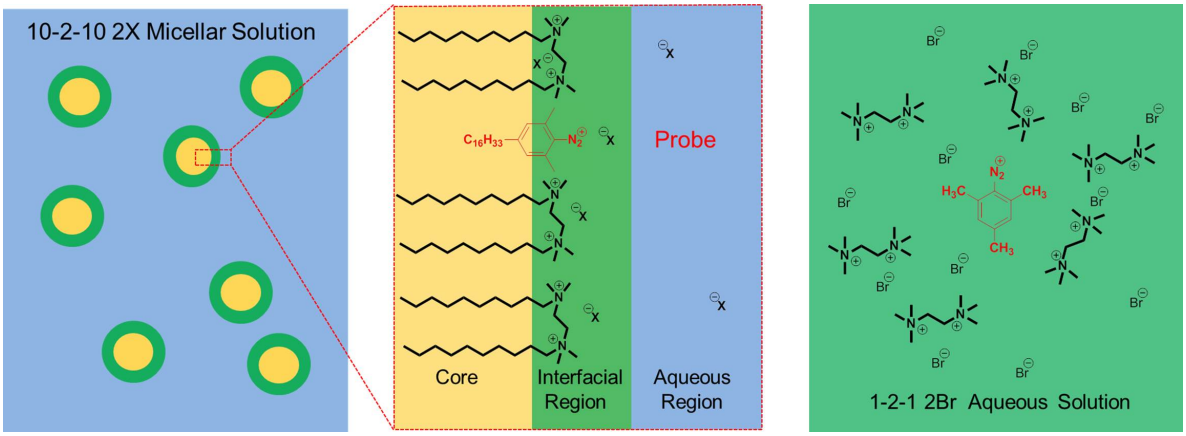

Figure 2.1: Chemical trapping in 10-2-0 2X micellar solutions and 1-2-1 2X reference solutions

estimate the interfacial molarities of the counterions, X_m, and water, H_2O_m, product yields, 1-ArX and 1-ArOH, from reactions of the short-chain probe, 1-ArN_2^+, and 0.5 to 4 M aqueous solutions of 1-2-1 2X solutions in the absence of micelles were also obtained. We assume that the selectivity of the reaction at the micellar interface and the aqueous solution is the same as in the interfacial regions of 10-2-10 2X micelles such that when the produce yields in the aqueous solutions are the same as those in the micelles, the molarities of the reference solution and the interfacial region are the same.

Molecular dynamics (MD) simulations were also used to characterize the interfacial regions of cationic 10-2-10 2X and their counterions (X = AcO, Cl, Br) gemini micelles. The distributions and concentrations of the counterions and water at the interfacial regions of the micelles are investigated by our collaborator, Massimiliano Porrini. A manuscript is in preparation on their work.

What's interesting about this chapter is that the estimates of interfacial molarities by chemical trapping and MD can be directly compared. We find that the estimated interfacial molarities of the three counterions, acetate (AcO^-), chloride (Cl^-), and bromide (Br^-) are in good agreement. The micelles with bromide ions show the highest interfacial counterion concentration and lowest hydration, followed by those with chloride ions, then acetate ions. The chemical trapping and MD simulation also provide independent estimates of the fraction

of gemini headgroup-Br^- ion-pairs and both methods show that almost half of the micellized gemini headgroups form ion-pairs in the interfacial region of the 10-2-10 2Br micelles.

2.2 Results and Discussion

2.2.1 Chemical trapping in aqueous 1-2-1 2X (X=AcO, MsO, Cl, Br, I) reference solutions

Tables 2.1-2.6 list HPLC peak areas, observed and normalized product yields and values for total X^-, H_2O concentration, selectivities, S_w^X and H_2O/X molar ratios for dediazoniation of 1-ArN_2^+ in aqueous 1-2-1 2X with 1 mM HX (X = MsO, Cl, Br, I), 1-2-1 2AcO at pH 6 with variable amounts of acetic acid at 25 ^{o}C (except for 1-2-1 2I, for which the dediazoniation reactions were carried out at 50 ^{o}C because of the high Krafft temperature of 10-2-10 2I). The molarities of X, [X_t], which are approximately two times of the molarities of 1-2-1 2X, [1-2-1 2X], vary from 0 to 4.5 M. The water molarities were obtained by weight (See Experimental). The observed yields of 1-ArOH and 1-ArX (X=AcO, MsO, Cl, Br, I) were calculated from HPLC peak areas measured in triplicate and their calibration curves respectively. The total yields combing the observed yields of 1-ArOH and 1-ArX were well above the lowest average yields of 86%. For the sake of comparison, all of the percent yields were converted to normalized yields, see notes below Table 2.1-2.6. The results for Br^- were run in duplicate with $\lambda = 220$ nm, and $\lambda = 230$ nm. The results are in good agreement and demonstrate the general reproducibility of the chemical trapping method.

Table 2.1: HPLC peak areas, observed and normalized (subscript N) product yields for dediazoniation of 1-ArN_2^+ in aqueous 1-2-1 2AcO solutions at 25 ^{o}C and pH 6, and values for salts, acetic acid, water concentration, selectivities, S_w^{AcO} and H_2O/AcO molar ratios.[a]

$[AcO_t]$[b] (M)	[1-2-1 2AcO] (M)	[AcOH][c] (M)	pH	$[H_2O]$ (M)	Peak Area[d] (10^6 μv•s)		Observed Yields (%)			Normalized Yields[e] (%)		S_w^{AcOf}	$[H_2O]/[AcO_t]$
					1-ArOH	1-ArOAc	1-ArOH	1-ArOAc	Total	1-$ArOH_N$	1-$ArOAc_N$		
0.520	0.250	0.020	6.0	52.3	12.659	0.045	97.4	1.14	98.5	98.8	1.16	1.18	100
1.057	0.500	0.057	6.0	49.0	11.344	0.088	97.0	2.47	99.4	97.5	2.48	1.18	46.4
2.249	1.000	0.249	5.9	42.2	10.809	0.201	92.4	5.62	98.0	94.3	5.74	1.14	18.7
4.266	1.500	1.266	5.9	32.7	9.919	0.517	79.8	13.6	93.4	85.4	14.6	1.31	7.65

a. Reaction time ca. 24 hours. The concentrations of 1-ArN_2^+ were around 4 x 10^{-3} M but vary in each experiment. 100 μL of cyclohexane was layered on top of 1-2-1 2AcO solutions in 2 mL volumetric flasks to prevent the evaporation of 1-ArOAc. Prior to HPLC analysis, the product mixture was diluted 5 fold with methanol to dissolve both the cyclohexane and the aqueous salt solution.
b. $[AcO_t]$ represents the total acetate (CH_3COOH and CH_3COO^-) concentration in solution. ($[AcO_t] = 2$[1-2-1 2AcO] + $[CH_3COOH]$)
c. Glacier acetic acid was added to control the pH. $[CH_3COOH]$ is not the actual finally concentration in the solution, but the amount of CH_3COOH which was added to the 1-2-1 2AcO solution.
d. 50 μL sample injections. Peak areas are average of triplicate injections. Eluting solvents: 80%MeOH/20%H2O; Flow rate: 0.6 mL/min; Detector wavelength: 230 nm.
e. % 1-$ArOAc_N$ = 100 (%1-ArOAc)/(%1-ArOH + %1-ArOAc); % 1-$ArOH_N$ = 100 (%1-ArOH)/(%1-ArOH + %1-ArOAc).
f. $S_w^{AcO} = [H_2O](\%1\text{-ArOAc})/[AcO_t](\%1\text{-ArOH})$.

Table 2.2: HPLC peak areas, observed and normalized (subscript N) product yields for dediazoniation of 1-ArN_2^+ in aqueous 1-2-1 2MsO solutions at 25 ^{o}C and 1 mM $MeSO_3H$, and values for total MsO^-, water concentration, selectivities, S_w^{MsO} and H_2O/MsO molar ratios.[a]

$[MsO_t]$[b] (M)	$[H_2O]$ (M)	Peak Area[c] (10^6 μv•s)		Observed Yields (%)			Normalized Yields[d] (%)		S_w^{MsOe}	$[H_2O]/[MsO_t]$
		1-ArOH	1-ArOMs	1-ArOH	1-ArOMs	Total	1-ArOH_N	1-ArOMs_N		
0.049	55.2	15.06	0.0477	94.6	0.8	95.4	99.1	0.9	10.1	1126
0.098	54.9	14.91	0.0917	93.6	1.6	95.2	98.3	1.7	9.71	560
0.147	54.5	14.69	0.122	92.2	2.2	94.4	97.7	2.3	8.71	371
0.196	54.2	14.96	0.159	93.9	2.8	96.8	97.1	2.9	8.30	276
0.245	53.8	14.04	0.184	88.2	3.3	91.4	96.4	3.6	8.10	220
0.49	52.1	14.38	0.322	90.3	5.7	96.0	94.1	5.9	6.72	106
0.98	48.6	13.69	0.549	85.9	9.7	95.7	89.8	10.2	5.61	49.6
1.47	45.1	13.15	0.767	82.6	13.6	96.2	85.9	14.1	5.05	30.7
1.96	41.7	11.87	0.960	74.5	17.0	91.5	81.4	18.6	4.85	21.2
2.45	38.2	12.38	1.29	77.4	22.8	100	77.2	22.8	4.59	15.6
2.94	34.7	11.66	1.56	72.9	27.6	100	72.6	27.4	4.47	11.8
3.43	31.2	10.61	1.96	66.3	34.6	101	65.7	34.3	4.75	9.11
3.92	27.8	9.810	2.23	61.3	39.3	100	61.0	39.0	4.53	7.08
4.41	24.3	8.847	2.85	55.3	50.1	105	52.4	47.6	4.99	5.51

a. Reaction time ca. 48 hours. The concentrations of 1-ArN_2^+ were around 4 x 10^{-3} M but vary in each experiment. 50 μL of cyclohexane was layered on top of 1-2-1 2MsO solutions in 1 mL volumetric flasks to prevent the evaporation of 1-ArOMs. Prior to HPLC analysis, the product mixture was diluted 5 fold with methanol to dissolve both the cyclohexane and the aqueous salt solution.
b. $[MsO_t] = 2$[1-2-1 2MsO]
c. 50 μL sample injections. Peak areas are average of triplicate injections. Eluting solvents: 80%MeOH/20%H2O; Flow rate: 0.6 mL/min; Detector wavelength: 230 nm.
d. % 1-ArOMs_N = 100 (%1-ArOMs)/(%1-ArOH + %1-ArOMs); % 1-ArOH_N = 100 (%1-ArOH)/(%1-ArOH + %1-ArOMs).
e. $S_w^{MsO} = [H_2O](\%1\text{-ArOMs})/[MsO_t](\%1\text{-ArOH})$.

Table 2.3: HPLC peak areas, observed and normalized (subscript N) product yields for dediazoniation of 1-ArN_2^+ in aqueous 1-2-1 2Cl solutions at 25 ^{o}C and 1 mM HCl, and values for total Cl^-, water concentration, selectivities, S_w^{Cl} and H_2O/Cl molar ratios.[a]

$[Cl_t]$[b] (M)	$[H_2O]$ (M)	Peak Area[c] (10^6 μv•s)		Observed Yields (%)			Normalized Yields[d] (%)		S_w^{Cl}[e]	$[H_2O]/[Cl_t]$
		1-ArOH	1-ArCl	1-ArOH	1-ArCl	Total	1-$ArOH_N$	1-$ArCl_N$		
0.02	55.4	9.183	0.065	88.4	0.7	89.1	99.2	0.8	21.5	2772
0.04	55.3	9.028	0.107	85.3	1.1	86.4	98.7	1.3	18.1	1383
0.06	55.2	8.875	0.146	85.4	1.6	87.0	98.2	1.8	16.7	920
0.08	55.1	9.091	0.190	85.9	2.0	87.9	97.7	2.3	15.9	689
0.10	55.0	9.218	0.229	87.1	2.4	89.5	97.3	2.7	15.1	550
0.20	54.5	9.186	0.379	86.8	4.0	90.7	95.6	4.4	12.4	272
0.30	53.9	8.781	0.492	84.5	5.2	89.8	94.2	5.8	11.1	180
0.50	52.8	9.125	0.712	80.3	6.9	87.2	92.1	7.9	9.11	106
1.00	50.1	8.401	1.067	82.0	11.5	93.5	87.7	12.3	7.03	50.1
1.50	47.3	8.548	1.563	75.2	15.2	90.4	83.2	16.8	6.37	31.5
2.00	44.6	7.739	1.781	75.5	19.2	94.7	79.7	20.3	5.67	22.3
2.50	41.8	8.080	2.375	71.1	23.1	94.2	75.5	24.5	5.43	16.7
3.00	39.1	7.119	2.325	69.5	25.1	94.6	73.5	26.5	4.70	13.0
3.50	36.3	7.230	3.055	63.6	29.9	93.5	68.0	32.0	4.88	10.4
4.50	30.9	5.983	3.532	58.4	37.7	96.1	60.8	39.2	4.42	6.86

a. Reaction time ca. 48 hours. The concentrations of 1-ArN_2^+ were around 4 x 10^{-3} M but vary in each experiment. 50 μL of cyclohexane was layered on top of 1-2-1 2Cl solutions in 1 mL volumetric flasks to prevent the evaporation of 1-ArCl. Prior to HPLC analysis, the product mixture was diluted 5 fold with methanol to dissolve both the cyclohexane and the aqueous salt solution.
b. $[Cl_t]$ = 2[1-2-1 2Cl]
c. 50 μL sample injections. Peak areas are average of triplicate injections. Eluting solvents: 80%MeOH/20%H2O; Flow rate: 0.6 mL/min; Detector wavelength: 230 nm.
d. % 1-$ArCl_N$ = 100 (%1-ArCl)/(%1-ArOH + %1-ArCl); % 1-$ArOH_N$ = 100 (%1-ArOH)/(%1-ArOH + %1-ArCl).
e. $S_w^{Cl} = [H_2O](\%1\text{-ArCl})/[Cl_t](\%1\text{-ArOH})$.

Table 2.4: HPLC peak areas (230 nm), observed and normalized (subscript N) product yields for dediazoniation of 1-ArN_2^+ in aqueous 1-2-1 2Br solutions at 25 ^{o}C and 1 mM HBr, and values for total Br^-, water concentration, selectivities, S_w^{Br} and H_2O/Br molar ratios.[a]

$[Br_t]$[b] (M)	$[H_2O]$ (M)	Peak Area[c] (10^6 μv•s)		Observed Yields (%)			Normalized Yields[d] (%)		S_w^{Bre}	$[H_2O]/[Br_t]$
		1-ArOH	1-ArBr	1-ArOH	1-ArBr	Total	1-ArOH_N	1-ArBr_N		
0.00	55.5	12.146	-	94.2	0	94.2	100	0	-	-
0.04	55.3	12.890	0.447	99.9	1.94	102	98.1	1.91	18.9	1349
0.08	55.1	12.690	0.716	97.9	3.09	101	96.9	3.06	19.0	680
0.10	55.0	12.714	0.845	98.1	3.65	102	96.4	3.59	18.3	544
0.50	52.6	11.225	2.709	86.9	11.8	98.7	88.1	11.9	12.7	105
1.00	49.6	10.889	4.028	84.2	17.4	102	82.8	17.2	9.18	49.6
1.50	46.7	10.042	5.222	77.6	22.6	100	77.4	22.6	8.18	31.1
2.00	43.7	9.556	6.161	73.9	26.7	101	73.5	26.5	7.24	21.8
2.50	40.7	8.383	6.880	68.9	30.1	99.0	69.6	30.4	6.84	16.3
3.00	37.8	7.802	7.790	60.4	33.8	94.2	64.1	35.9	6.61	12.6
3.50	34.8	7.631	9.100	59.1	39.5	98.6	59.9	40.1	6.48	9.95
4.00	31.9	6.733	9.712	52.2	42.1	94.3	55.3	44.7	6.24	7.96
4.50	28.9	6.010	10.954	46.5	47.5	94.1	49.5	50.5	6.04	6.42

a. Reaction time ca. 48 hours. The concentrations of 1-ArN_2^+ were around 4 x 10^{-3} M but vary in each experiment. 100 μL of cyclohexane was layered on top of 1-2-1 2Cl solutions in 2 mL volumetric flasks to prevent the evaporation of 1-ArBr. Prior to HPLC analysis, the product mixture was diluted 5 fold with methanol to dissolve both the cyclohexane and the aqueous salt solution.
b. $[Br_t] = 2$[1-2-1 2Br]
c. 50 μL sample injections. Peak areas are average of triplicate injections. Eluting solvents: 80%MeOH/20%H2O; Flow rate: 0.6 mL/min; Detector wavelength: 230 nm.
d. % 1-ArBr_N = 100 (%1-ArBr)/(%1-ArOH + %1-ArBr); % 1-ArOH_N = 100 (%1-ArOH)/(%1-ArOH + %1-ArBr).
e. $S_w^{Br} = [H_2O](\%1\text{-ArBr})/[Br_t](\%1\text{-ArOH})$.

Table 2.5: HPLC peak areas (220 nm), observed and normalized (subscript N) product yields for dediazoniation of 1-ArN_2^+ in aqueous 1-2-1 2Br solutions at 25 ^{o}C and 1 mM HBr, and values for total Br^-, water concentration, selectivities, S_w^{Br} and H_2O/Br molar ratios.[a]

$[Br_t]$[b] (M)	$[H_2O]$ (M)	Peak Area[c] (10^6 μv•s)		Observed Yields (%)			Normalized Yields[d] (%)		S_w^{Bre}	$[H_2O]/[Br_t]$
		1-ArOH	1-ArBr	1-ArOH	1-ArBr	Total	1-ArOH_N	1-ArBr_N		
0.00	55.5	11.148	-	93.2	0	93.2	100	0	-	-
0.04	55.3	11.838	0.239	99.0	1.39	100	98.6	1.38	26.2	1349
0.08	55.1	12.777	0.512	106	2.96	109	97.3	2.71	21.5	680
0.10	55.0	12.682	0.614	105	3.55	109	96.7	3.26	20.3	544
0.50	52.6	10.934	1.904	91.3	11.1	102	89.2	10.8	14.2	105
1.00	49.6	11.117	2.960	92.7	17.2	110	84.4	15.6	10.3	49.6
1.50	46.7	9.977	3.775	83.2	21.9	105	79.2	20.8	9.06	31.1
2.00	43.7	9.398	4.476	78.3	26.0	104	75.1	24.9	7.89	21.8
2.50	40.7	8.445	5.099	71.0	29.8	101	70.4	29.6	7.11	16.3
3.00	37.8	7.387	5.575	61.7	32.4	94.1	65.6	34.4	7.04	12.6
3.50	34.8	7.254	6.789	60.6	39.4	100	60.6	39.4	6.65	9.95
4.00	31.9	6.362	7.165	53.1	41.6	94.8	56.1	43.9	6.44	7.96
4.50	28.9	6.010	8.125	50.2	47.2	97.4	51.5	48.5	6.56	6.42

a. Reaction time ca. 48 hours. The concentrations of 1-ArN_2^+ were around 4 x 10^{-3} M but vary in each experiment. 100 μL of cyclohexane was layered on top of 1-2-1 2Cl solutions in 2 mL volumetric flasks to prevent the evaporation of 1-ArBr. Prior to HPLC analysis, the product mixture was diluted 5 fold with methanol to dissolve both the cyclohexane and the aqueous salt solution.
b. $[Br_t] = 2$[1-2-1 2Br]
c. 20 μL sample injections. Peak areas are average of triplicate injections. Eluting solvents: 80%MeOH/20%H2O; Flow rate: 0.6 mL/min; Detector wavelength: 220 nm.
d. % 1-ArBr_N = 100 (%1-ArBr)/(%1-ArOH + %1-ArBr); % 1-ArOH_N = 100 (%1-ArOH)/(%1-ArOH + %1-ArBr).
e. $S_w^{Br} = [H_2O](\%1\text{-ArBr})/[Br_t](\%1\text{-ArOH})$.

Table 2.6: HPLC peak areas, observed and normalized (subscript N) product yields for dediazoniation of 1-ArN_2^+ in aqueous 1-2-1 2I solutions at 50 ^{o}C and 1 mM HI, and values for total I^-, water concentration, selectivities, S_w^I and H_2O/I molar ratios.[a]

$[I_t]$[b] (M)	$[H_2O]$ (M)	Peak Area[c] (10^6 μv•s)		Observed Yields (%)			Normalized Yields[d] (%)		S_w^I[e]	$[H_2O]/[I_t]$
		1-ArOH	1-ArI	1-ArOH	1-ArI	Total	1-ArOH_N	1-ArI_N		
0.02	55.4	1.828	0.158	88.4	1.80	90.2	98.0	2.0	57.4	2772
0.04	55.3	1.993	0.291	88.6	3.10	91.7	96.6	3.4	48.2	1383
0.06	55.2	1.976	0.390	87.9	4.10	92.0	95.5	4.5	43.4	920
0.08	55.1	1.967	0.490	87.5	5.20	92.7	94.4	5.6	41.0	688
0.10	54.9	1.822	0.519	88.1	6.00	94.1	93.6	6.4	37.4	549
0.20	54.3	1.918	0.915	85.2	9.70	95.0	89.8	10.2	31.0	272
0.30	53.7	1.674	1.116	81.0	12.9	93.9	86.3	13.7	28.5	179
0.50	52.5	1.529	1.466	78.9	18.1	97.0	81.4	18.6	24.1	105
1.00	49.4	1.621	2.639	68.9	26.8	95.7	72.0	28.0	19.2	49.4
1.50	46.4	0.957	2.347	60.3	35.4	95.7	63.0	37.0	18.1	30.9
2.00	43.3	1.092	3.658	51.2	41.0	92.2	55.5	44.5	17.4	21.7
2.50	40.3	0.765	3.134	48.2	47.2	95.5	50.5	49.5	15.8	16.1
3.00	37.2	0.895	4.651	42.0	52.2	94.1	44.6	55.4	15.4	12.4
3.50	34.2	0.604	3.823	38.1	57.6	95.7	39.8	60.2	14.8	9.76
4.00	31.1	0.764	5.570	35.8	62.5	98.3	98.3	63.6	13.6	7.78

a. Reaction time ca. 7 hours. The concentrations of 1-ArN_2^+ were around 4 x 10^{-3} M but vary in each experiment. 100 μL of cyclohexane was layered on top of 1-2-1 2I solutions in 2 mL volumetric flasks to prevent the evaporation of 1-ArI. Prior to HPLC analysis, the product mixture was diluted 25 fold with methanol/H_2O to dissolve both the cyclohexane and the aqueous salt solution.
b. $[I_t] = 2[1\text{-}2\text{-}1\ 2I]$
c. 50 μL sample injections. Peak areas are average of triplicate injections. Eluting solvents: 80%MeOH/20%H2O; Flow rate: 0.6 mL/min; Detector wavelength: 230 nm.
d. % 1-ArI_N = 100 (%1-ArI)/(%1-ArOH + %1-ArI); % 1-ArOH_N = 100 (%1-ArOH)/(%1-ArOH + %1-ArI).
e. $S_w^I = [H_2O](\%1\text{-ArI})/[I_t](\%1\text{-ArOH})$.

Figure 2.2 shows the plots of the normalized product yields (%1-ArX) from the dediazoniation reactions in 1-2-1 2X reference solutions as a function of the countererion concentrations ($[X_t]$=2[1-2-1 2X]), also known as standard curves. The selectivities of dediazoniation reactions toward X^- and H_2O, S_w^x, in aqueous 1-2-1 2X solutions were estimated and plotted versus counterion concentrations $[X_t]$, Figure 2.3. The selectivities are the highest for the most hydrophobic counterion I^-, and lowest for the most hydrophilic counterion AcO^-. Similar trend are also observed in standard curves. Interestingly, the selectivity values for MsO^-, Cl^-, Br^-, and I^- decrease gradually with increasing counterion concentrations $[X_t]$. Counterions probably form ion-pairs at relatively high concentrations and not react with the probe.

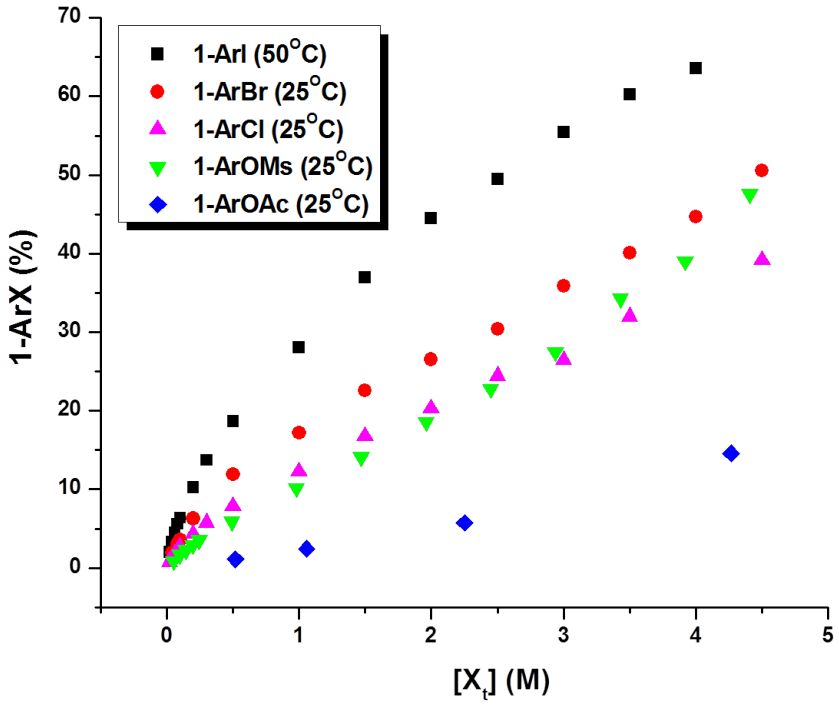

Figure 2.2: Normalized product yields %1-ArX (X=AcO, MsO, Cl, Br, I) as a function of counterion concentrations $[X_t]$=2[1-2-1 2X].

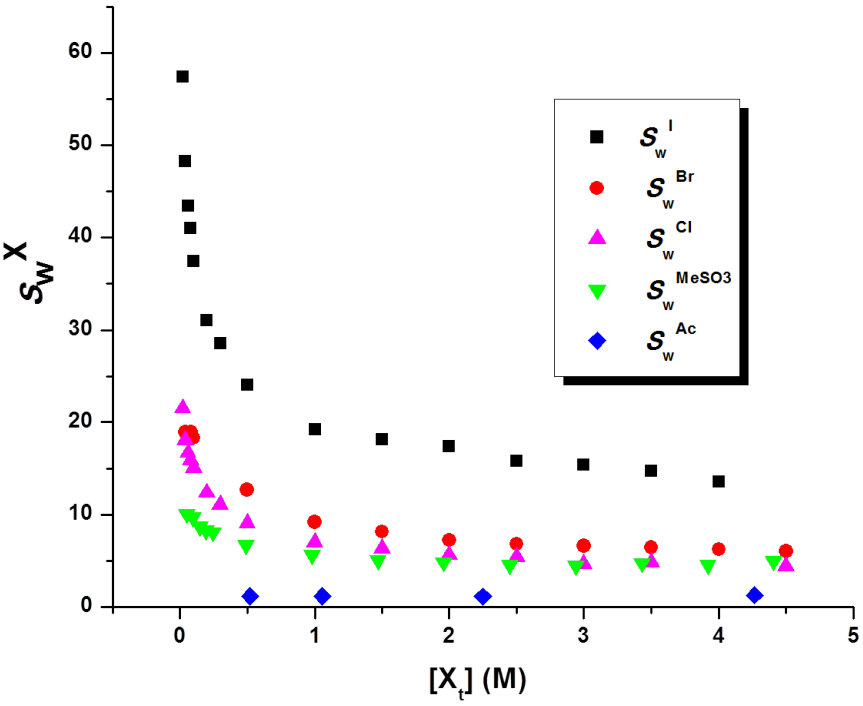

Figure 2.3: The selectivities of dediazoniation reactions toward X^- and H_2O, S_w^x, in aqueous 1-2-1 2X solutions (X=AcO, MsO, Cl, Br, I) as a function of counterion concentrations $[X_t]$=2[1-2-1 2X].

2.2.2 Interfacial molarities estimated by chemical trapping in aqueous 10-2-10 2X (X=AcO, MsO, Cl, Br, I) gemini micellar solutions

To estimate interfacial molarities in 10-2-10 2X (X=AcO, MsO, Cl, Br, I) micelles, chemical trapping experiments were carried out in a series 10-2-10 2X micellar solutions whose concentrations above at least twice their cmc values to ensure the existence of micelles in these solutions. The cmc values of 10-2-10 2X gemini surfactants were determined by conductivity measurements described in Chapter 1, and carried out by our collaborator, Alla Malinenko, Table 2.7.[92]

Table 2.7: List of cmc values of 10-2-10 2X gemini[92]

Surfactant	cmc (mM)	Temperature ^{o}C
10-2-10 2AcO	23.3	30
10-2-10 2MsO	15.3	30
10-2-10 2Cl	12.8	30
10-2-10 2Br	6.5	30
10-2-10 2I	3.0	50

Tables 2.8-2.12 list chemical trapping results including average peak areas, observed prodcut yields, and normalized yields in aqueous 10-2-10 2X (X=AcO, MsO, Cl, Br, I) gemini micellar solutions. The footnotes give the reaction conditions, the HPLC conditions, and equations used to calculate total yields, and normalized yields of 16-ArX (X=AcO, MsO, Cl, Br, I) and 16-ArOH products using calibration curves (See Appendix). Note that 1 mM of HX (X=MsO, Cl, Br, I) was added to control the acidity of the corresponding 10-2-10 2X gemini solutions. Because AcO^- is a weak acid, experiments with AcO^- as the counterion are run under different experimental condition (See Experimental) and additional products are observed. The results with AcO^- as the counterion and the mystery peak are discussed separately below.

Table 2.8: HPLC Average peak areas, observed yields and normalized yields (subscript N) for reaction of 16-ArN_2^+ in 10-2-10 2AcO micelles from 50 mM to 250 mM at 25 ^oC.[a]

[10-2-10 2AcO] (mM)	[AcOH][b] (mM)	pH	Average Peak Areas[c] (10^6 $\mu v \bullet s$)					Observed Yields (%)						Normalized Yields[e] (%)	
			16-ArOH	16-ArH	16-ArOAc	16-ArInd	Azoether	16-ArOH	16-ArH	16-ArOAc	16-ArInd	Azoether	Total[d]	16-$ArOH_N$	16-$ArOAc_N$
50	52	5.0	4.550	0.322	0.123	3.557	1.882	40.9	2.8	1.2	21.0	16.8	85.5	97.8	2.2
100	157	5.0	3.344	0.430	0.119	5.381	2.223	27.4	3.4	1.0	29.7	18.1	83.1	97.5	2.5
150	218	5.0	3.853	0.341	0.152	6.354	2.557	31.6	2.7	1.3	35.4	20.8	94.4	97.1	2.9
200	262	5.0	3.612	0.274	0.156	6.855	2.246	29.6	2.1	1.4	38.3	18.3	91.7	96.8	3.2
250	314	5.0	3.517	0.331	0.204	6.791	1.871	29.6	2.7	1.8	38.8	15.6	91.1	95.7	4.3
50	558	4.0	2.834	0.691	0.176	3.520	8.975	25.3	6.1	1.7	20.6	7.9	63.7	95.7	4.5

a. Reaction time ca. 24 hours to ensure the complete dediazoniation reaction. Measured yields are based on the weighed amount of 16-ArN_2^+ which is ca. 10^{-4} M.

b. Glacial acetic acid was added to control the pH. [AcOH] is not the actual final concentration in the solution, but the amount of CH_3COOH that was added to the 1-2-1 2AcO solution.

c. 100 μL sample injections. Peak areas are average of triplicate injections. Eluting solvents: 65%MeOH/35%H_2O; Flow rate: 0.4 mL/min; Detector wavelength: 220 nm.

d. %Total = %16-ArOH + %16-ArOAc + 2(%16-ArH) + %16-ArInd + 2(%azoether) (Assuming the extinction coefficient of azoether equal approximately twice of that of 16-ArOH)

e. % 16-$ArOAc_N$ = 100 (%16-ArOAc)/(%16-ArOH + %16-ArH + %16-ArOAc + %azoether); % 16-$ArOH_N$ = 100 (%16-ArOH + %16-ArH + %azoether)/(%16-ArOH + %16-ArH + %16-ArOAc + %azoether).

Table 2.9: HPLC Average peak areas, observed yields and normalized yields (subscript N) for reaction of 16-ArN_2^+ in 10-2-10 2MsO micelles from 25 mM to 250 mM at 25 ^{o}C.[$MeSO_3H$]=1 mM.[a]

[10-2-10 2MsO] (mM)	Average Peak Areas[b] (10^6 μv•s)			Observed Yields (%)				Normalized Yields[d] (%)	
	16-ArOH	16-ArH	16-ArOMs	16-ArOH	16-ArH	16-ArOMs	Total[c]	16-ArOH_N	16-ArOMs_N
25	11.24	0.06	1.02	85.4	0.3	11.5	97.6	88.1	11.9
50	11.32	0.06	1.10	86.0	0.3	12.4	99.1	87.4	12.6
75	11.29	0.03	1.16	85.7	0.1	13.1	99.1	86.7	13.3
100	11.27	0.03	1.22	85.6	0.1	13.8	99.6	86.1	13.9
125	11.46	0.02	1.31	87.0	0.0	14.8	101	85.5	14.5
150	11.47	0.04	1.36	87.1	0.2	15.4	102	85.0	15.0
175	11.42	0.05	1.40	86.7	0.3	15.8	103	84.6	15.4
200	11.39	0.04	1.45	86.5	0.2	16.4	103	84.1	15.9
225	11.36	0.03	1.47	86.3	0.1	16.6	103	83.9	16.1
250	11.00	0.03	1.45	83.6	0.1	16.4	100	83.7	16.3

a. Reaction time ca. 48 hours to ensure the complete dediazoniation reaction. Measured yields are based on the weighed amount of 16-ArN_2^+ which is ca. 10^{-4} M.
b. 100 μL sample injections. Peak areas are average of triplicate injections. Eluting solvents: 80%MeOH/20%H_2O; Flow rate: 0.4 mL/min; Detector wavelength: 220 nm.
c. %Total = %16-ArOH + %16-ArOMs + 2(%16-ArH)
d. % 16-ArOMs_N = 100 (%16-ArOMs)/(%16-ArOH + %16-ArH + %16-ArOMs); % 16-ArOH_N = 100 (%16-ArOH + %16-ArH)/(%16-ArOH + %16-ArH + %16-ArOMs).

Table 2.10: HPLC Average peak areas, observed yields and normalized yields (subscript N) for reaction of 16-ArN_2^+ in 10-2-10 2Cl micelles from 25 mM to 250 mM at 25 ^{o}C.[HCl]=1 mM.[a]

[10-2-10 2Cl] (mM)	Average Peak Areas[b] (10^6 μv•s)			Observed Yields (%)				Normalized Yields[d] (%)	
	16-ArOH	16-ArH	16-ArCl	16-ArOH	16-ArH	16-ArCl	Total[c]	16-ArOH_N	16-ArCl_N
25	9.086	0.046	1.898	77.2	0.3	14.8	92.6	84.0	16.0
50	9.549	0.029	2.080	83.3	0.1	16.6	100.2	83.4	16.6
75	9.485	0.021	2.158	82.7	0.1	17.3	100.1	82.7	17.3
100	9.544	0.031	2.277	83.2	0.1	18.2	101.7	82.1	17.9
125	9.668	0.027	2.379	84.3	0.1	19.0	103.6	81.6	18.4
150	9.709	0.046	2.549	76.7	0.2	18.5	95.6	80.6	19.4
200	9.675	0.041	2.616	76.4	0.2	19.0	95.8	80.2	19.8
250	9.528	0.048	2.692	75.2	0.3	19.5	95.3	79.5	20.5

a. Reaction time ca. 48 hours to ensure the complete dediazoniation reaction. Measured yields are based on the weighed amount of 16-ArN_2^+ which is ca. 10^{-4} M.
b. 100 μL sample injections. Peak areas are average of triplicate injections. Eluting solvents: 65%MeOH/35%H_2O; Flow rate: 0.4 mL/min; Detector wavelength: 220 nm.
c. %Total = %16-ArOH + %16-ArCl + 2(%16-ArH)
d. % 16-ArCl_N = 100 (%16-ArCl)/(%16-ArOH + %16-ArH + %16-ArCl); % 16-ArOH_N = 100 (%16-ArOH + %16-ArH)/(%16-ArOH + %16-ArH + %16-ArCl).

Table 2.11: HPLC Average peak areas, observed yields and normalized yields (subscript N) for reaction of 16-ArN_2^+ in 10-2-10 2Br micelles from 25 mM to 250 mM at 25 ^{o}C.[HCl]=1 mM.[a]

[10-2-10 2Br] (mM)	Average Peak Areas[b] (10^6 μv•s)			Observed Yields (%)				Normalized Yields[d] (%)	
	16-ArOH	16-ArH	16-ArBr	16-ArOH	16-ArH	16-ArBr	Total[c]	16-ArOH_N	16-ArBr_N
10	7.832	0.148	4.269	69.1	1.2	26.8	98.3	72.4	27.6
20	8.143	0.108	4.553	71.8	0.8	28.6	102	71.7	28.3
30	7.807	0.104	4.549	68.9	0.8	28.6	99.0	70.9	29.1
50	8.484	0.113	5.230	74.8	0.9	32.9	109	69.7	30.3
100	6.936	0.462	4.674	56.7	3.7	27.2	91.3	68.9	31.1
150	3.224	0.300	2.228	53.0	4.7	25.9	88.3	69.0	31.0
250	3.137	0.458	2.348	51.6	7.3	27.3	93.5	68.3	31.7

a. Reaction time ca. 48 hours to ensure the complete dediazoniation reaction. Measured yields are based on the weighed amount of 16-ArN_2^+ which is ca. 10^{-4} M.
b. 100 μL sample injections. Peak areas are average of triplicate injections. Eluting solvents: 65%MeOH/35%H_2O; Flow rate: 0.4 mL/min; Detector wavelength: 220 nm.
c. %Total = %16-ArOH + %16-ArBr + 2(%16-ArH)
d. % 16-ArBr_N = 100 (%16-ArBr)/(%16-ArOH + %16-ArH + %16-ArBr); % 16-ArOH_N = 100 (%16-ArOH + %16-ArH)/(%16-ArOH + %16-ArH + %16-ArBr).

Table 2.12: HPLC Average peak areas, observed yields and normalized yields (subscript N) for reaction of 16-ArN_2^+ in 10-2-10 2I micelles from 6 mM to 25 mM at 50 ^{o}C.[HI]=1 mM.[a]

[10-2-10 2I] (mM)	Average Peak Areas[b] (10^5 μv•s)			Observed Yields (%)				Normalized Yields[d] (%)	
	16-ArOH	16-ArH	16-ArI	16-ArOH	16-ArH	16-ArI	Total[c]	16-ArOH_N	16-ArI_N
6	6.460	1.876	21.648	28.3	7.4	59.0	102	37.7	62.3
10	6.860	2.880	22.611	27.1	20.5	55.5	103	40.3	59.7
15	6.570	2.500	20.458	29.5	10.3	57.2	107	41.1	58.9
20	7.021	2.350	19.127	30.7	9.4	52.1	102	43.5	56.5
25	6.737	2.614	19.457	30.3	10.8	54.4	106	43.0	57.0

a. Reaction time ca. 20 hours to ensure the complete dediazoniation reaction. The concentration of 16-ArN_2^+ were around 10^{-4} M but vary in each experiments. The solution was diluted by 5 times with methanol before HPLC analysis.
b. 100 μL sample injections. Peak areas are average of triplicate injections. Eluting solvents: 65%MeOH/35%H_2O; Flow rate: 0.4 mL/min; Detector wavelength: 220 nm.
c. %Total = %16-ArOH + %16-ArI + 2(%16-ArH)
d. % 16-ArI_N = 100 (%16-ArI)/(%16-ArOH + %16-ArH + %16-ArI); % 16-ArOH_N = 100 (%16-ArOH + %16-ArH)/(%16-ArOH + %16-ArH + %16-ArI).

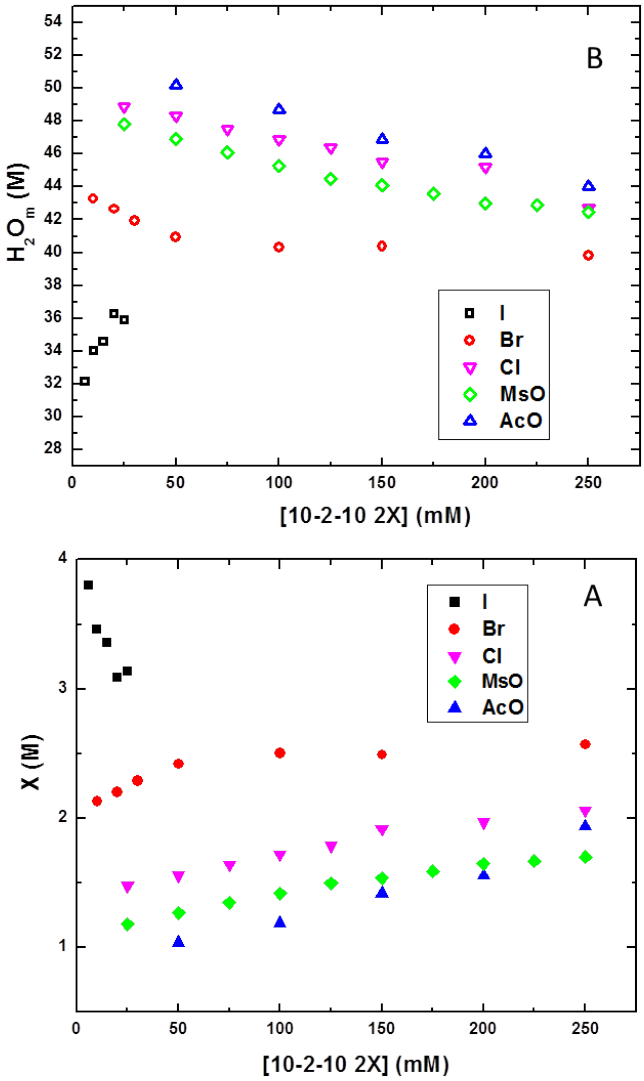

Figure 2.4: Interfacial molarity of counterions, X_m (A), and water, H_2O_m (B), in 10-2-10 2X micelles versus the stoichiometric concentraiton.

The interfacial molarities of counterion and water in 10-2-10 2X micelar solutions, denoted as X_m and H_2O_m respectively, estimated by chemical trapping are shown in Figure 2.4 and Tables 2.13-2.17. The estimated interfacial molarities of counterions are in the range of 1-4 M, except that the stoichiometric surfactant concentrations are only on the order of mM. These molarities depend strongly on conterion type. The interfacial counterion molarities are higher for hydrophobic counterions, I^- and Br^-, and lowest for hydrophilic

Table 2.13: Estimated values of AcO_m, H_2O_m, S_w^{AcO} in 10-2-10 2AcO micellar solutions from 50 mM to 250 mM, at 25 ^oC at pH 5.

[10-2-10 2AcO] (mM)	AcO_m (CH_3COOH_m + $CH_3COO^-_m$) (M)	S_w^{AcO}	H_2O_m (M)	H_2O_m/AcO_m
50	0.93	1.24	50.7	54.7
100	1.04	1.23	49.1	47.2
150	1.19	1.22	48.9	41.1
200	1.30	1.21	47.3	36.3
250	1.72	1.18	44.5	26.0

Table 2.14: Estimated values of MsO_m, H_2O_m, S_w^{MsO} in 10-2-10 2MsO micellar solutions from 25 mM to 250 mM, at 25 ^oC with 1 mM $MeSO_3H$.

[10-2-10 2MsO] (mM)	MsO_m (M)	S_w^{MsO}	H_2O_m (M)	H_2O_m/MsO_m
25	1.18	5.44	47.8	40.6
50	1.27	5.33	46.9	37.0
75	1.35	5.24	46.1	34.2
100	1.42	5.16	45.3	32.0
125	1.50	5.08	44.5	29.7
150	1.54	5.04	44.1	28.6
175	1.59	5.00	43.6	27.5
200	1.65	4.94	43.0	26.1
225	1.67	4.93	42.9	25.7
250	1.70	4.90	42.5	25.0

AcO^-. The interfacial counterion molarities generally increase with increasing surfactant concentration, although there is a decline for I_m as the surfactant concentration increase. The corresponding H_2O_m in those micellar solutions follow the opposite order. Specifically, the estimated X_m at twice cmc of 10-2-10 2X (X= I, Br, Cl, MsO, AcO) are 3.8 M, 2.1 M, 1.5 M, 1.2 M and 0.9 M respectively, while the corresponding H_2O_m are 32 M, 43 M, 49 M, 48 M, 51 M respectively. These trends correlate very well with the cmc values of 10-2-10 2X surfactants: AcO > MsO > Cl > Br > I. The correlation between the interfacial property and the physical property can be conceptually explained by a ion-pairing hydration model.

$$\triangle G_{mic} = RT[ln(cmc)] \tag{2.1}$$

$$\triangle G_{mic} = \triangle H_{mic} - T \triangle S_{mic} \tag{2.2}$$

Equation 2.1 shows the linear relationship between the change of free energy of micellization

Table 2.15: Estimated values of Cl_m, H_2O_m, S_w^{Cl} in 10-2-10 2Cl micellar solutions from 25 mM to 250 mM, at 25 ^{o}C with 1 mM HCl.

[10-2-10 2Cl] (mM)	Cl_m (M)	S_w^{Cl}	H_2O_m (M)	H_2O_m/Cl_m
25	1.48	6.31	48.90	33.1
50	1.56	6.18	48.27	31.0
75	1.65	6.04	47.55	28.9
100	1.72	5.94	46.94	27.2
125	1.79	5.86	46.46	26.0
150	1.92	5.71	45.53	23.7
200	1.97	5.66	45.18	22.9
250	2.06	5.34	42.68	20.7

Table 2.16: Estimated values of Br_m, H_2O_m, S_w^{Br} in 10-2-10 2Br micellar solutions from 10 mM to 250 mM, at 25 ^{o}C with 1 mM HBr.

[10-2-10 2Br] (mM)	Br_m (M)	S_w^{Br}	H_2O_m (M)	H_2O_m/Br_m
10	2.13	7.75	43.27	20.3
20	2.20	7.64	42.66	19.4
30	2.29	7.52	41.96	18.3
50	2.42	7.37	40.96	16.9
100	2.50	7.27	40.31	16.1
150	2.49	7.28	40.39	16.2
250	2.57	7.20	39.84	15.5

per surfactant, $\triangle G_{mic}$, and $ln(cmc)$.[93] The more negative of $\triangle G_{mic}$, the smaller of cmc value. Also, measured changes of enthalpy, $\triangle H_{mic}$, are small compared to the dominant entropic term ($-T \triangle S_{mic}$) in Gibbs Equation 2.2.[94] The water molecules in the immediate vicinity of surfactant monomeric form are postulated to be more ordered than water molecules in bulk water.[95, 96] Thus, transfer of an surfactant tail from bulk water to a micellar core releases that water into bulk solution, resulting in net increase in $\triangle S_{mic}$ for the whole solution. Similarly, in the interfacial region, the headgroup and counterions may associate reversibly to form ion pairs that are less hydrated than free ions, resulting the release of more water into the bulk solution with a net increase in $\triangle S_{mic}$, Figure 2.5. Therefore, the high interfacial counterion concentrations and low interfacial water concentrations of the 10-2-10 2I and 10-2-10 2Br, indicating more ion-pairing in the interfacial region, are consistent with their relative low cmc values.

Table 2.17: Estimated values of I_m, H_2O_m, S_w^I in 10-2-10 2I micellar solutions from 6 mM to 25 mM, at 50 ^{o}C with 1 mM HI.

[10-2-10 2I] (mM)	I_m (M)	S_w^I	H_2O_m (M)	H_2O_m/I_m
6	3.80	13.9	32.2	8.47
10	3.46	14.6	34.0	9.83
15	3.36	14.7	34.6	10.3
20	3.09	15.2	36.3	11.7
25	3.14	15.2	35.9	11.4

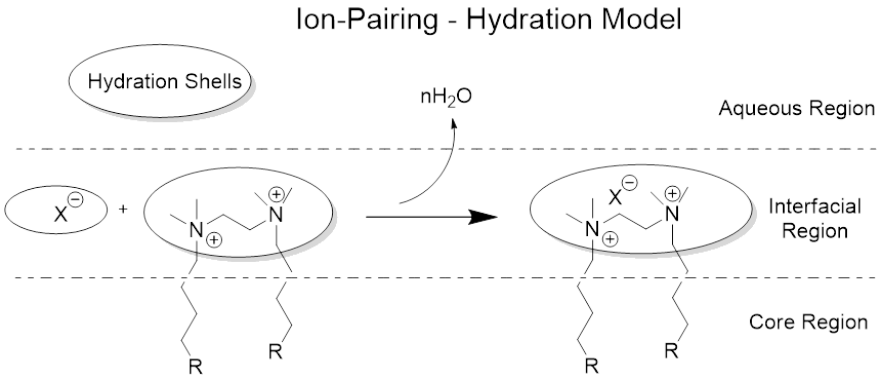

Figure 2.5: Schematic illustration of the ion-pairing hydration model in gemini micelles.

2.2.3 The agreement between chemical trapping and MD Simulations on the interfacial molarities of 10-2-10 2X (X = AcO, Cl, Br)

Molecular dynamics (MD) simulation was used to characterize the interfacial region of three 10-2-10 2X (X =AcO, Cl, Br) gemini micelles by our collaborator, Massimiliano Porrini. The results are summarized here to confirm that the interfacial molarities estimated by chemical trapping is reasonable. Structural parameters such as radius of gyration (R_g) and solvent accessible surface area (SASA) of the surfactant aliphatic tails were calculated[97, 98] to estimate the compactness and roughness of the gemini micelles, respectively. The radius of gyration, a mass weighted scalar length of each atom from the center-of-mass (COM), can be calculated by equation 2.3:

$$R_g = \sqrt{\frac{\sum(r^2 m)}{\sum(m)}} \tag{2.3}$$

where r is radius and m is mass of each atom. Solvent accessible surface area is the surface area of a macromolecule that is accessible to a solvent. Both the mean value of R_g and SASA

are the highest for Br^-, defining the most compact and least rough micelle, whereas the reverse is true for AcO^-. In other words, stronger interactions between Br^- and the headgroup of the micelle (ion pairing) create tighter packing of the whole micelle, subsequently lowering the mean value of R_g and SASA of the hydrophobic tails. The snapshots from MD simulations for 10-2-10 2X, in Figure 2.6, despite the modest differences in structural properties between three micelles.

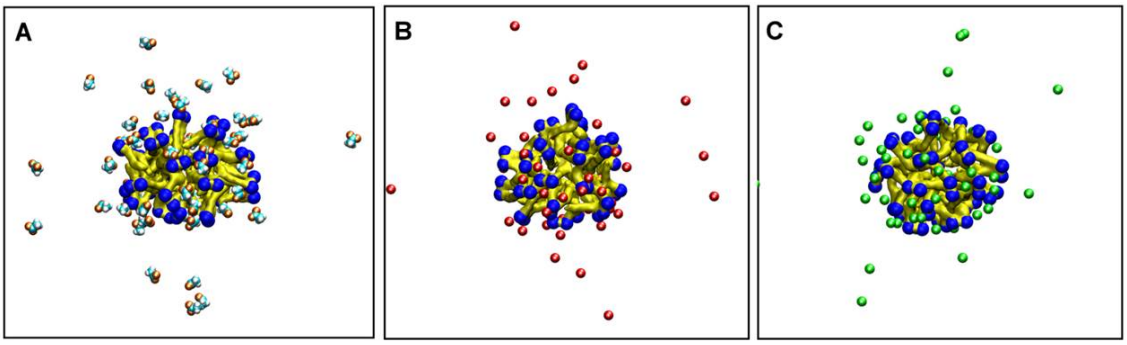

Figure 2.6: Snapshots from MD simulations of 10-2-10 2X micelle with AcO (A), Cl (B) and Br (C). Yellow and white surfaces for aliphatic tails of 10-2-10 2X, and blue beads for the tetramethylammonium polar heads. The counterions are depicted with VDW representation: orange, cyan, white, red and green balls for oxygen, carbon, hydrogen, chlorine and bromine atoms, respectively. Water molecules are omitted for clarity.

Figure 2.7 shows the RDFs calculated from the nitrogen atoms of surfactant head groups and counterions, respectively. The maxima of the counterion distributions are close to that of the headgroup nitrogens, but the distributions are broader and extends out into the aqueous region.

Compared to Cl^- and Br^-, AcO^- has a broader distribution. Its distribution extends both further into the hydrophobic core of the micelle and into bulk solution, and has the lowest concentration at its maximum. First, the results are consistent with the hydrophilic nature of its carboxylate group, showing further distribution in the bulk solution. Second, the RDF of AcO^- is higher at a shorter distance also indicate that the slightly hydrophobic character of AcO^- methyl group plays a role in its slight distribution into the hydrophobic core. A RDF of the methyl hydrogen of acetate anion (not shown) actually shows that the

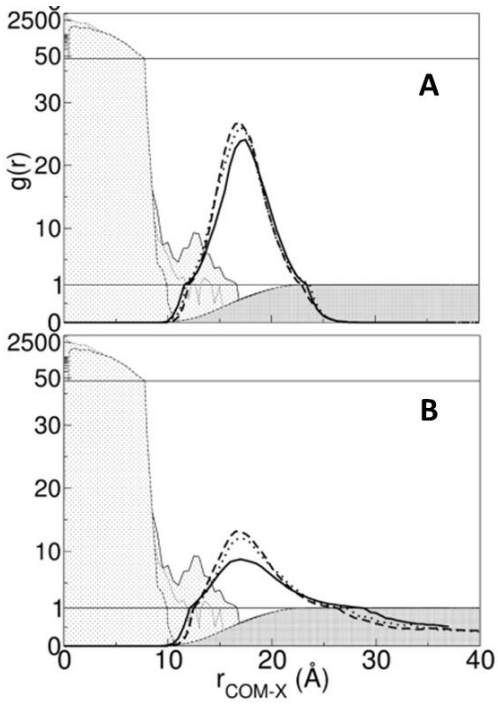

Figure 2.7: RDFs (g(r)) derived from the micelle COM. Solid, dotted and dashed lines refer to the system in presence of AcO^-, Cl^-, and Br^-, respectively. (A)the nitrogen atoms of the gemini headgroups and (B)the counterions.

-CH_3 group is partially buried in the micelle, whereas the carboxylate moiety faces towards the polar headgroups.

The concentration distributions of counterions and water along the RDF from the micelle COM were estimated by summing the number of Br^- and Cl^- in each 1.0 $\AA$ thick concentric spherical layer centered at the micelle COM, Figure 2.8. For AcO^-, the average location of the two nucleophilic oxygens was chosen as the most comparable population to the single Br^- and Cl^- atoms. The thick vertical dash-dot lines correspond to the maximum interfacial concentrations of each counterion, are used to compare with the interfacial concentrations estimated by chemical trapping method.

The simulated and measured interfacial molarities for anions and water are summarized in Table 2.18. Overall, the agreement between the two independent methods is striking, but not perfect. Although the calculated values of interfacial water concentrations are somewhat lower than the experimental values, the basic agreement for both the interfacial

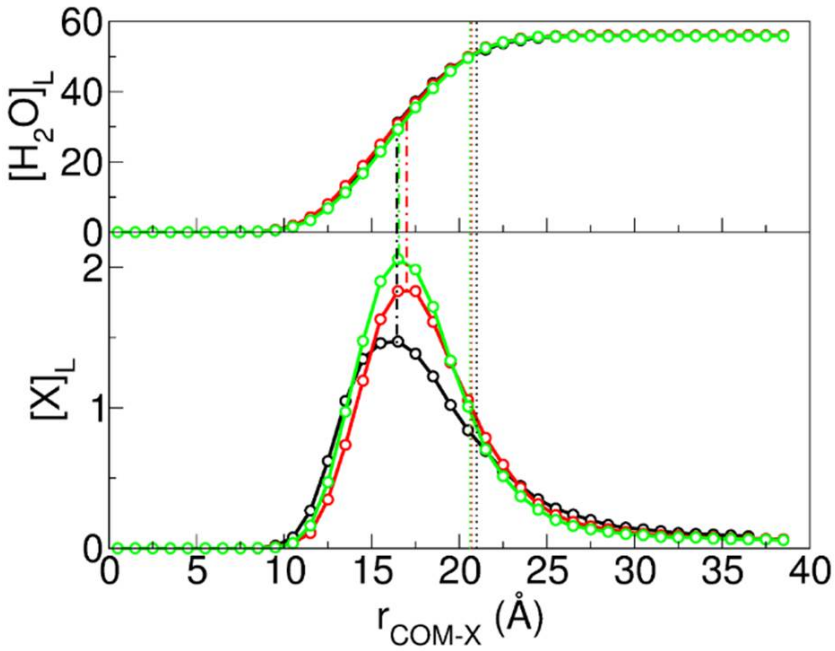

Figure 2.8: The concentration distribution of counterions in 10-2-10 2X gemini micelles. The x-axis defines the radial distance of the spherical layers from the micelle COM. The y-axis of the top and bottom graphs defines the local (within each 1.0 $\AA$ thick layer) molarity of water and counterions (X), respectively. Black, red and green lines refer to solution with AcO^-, Cl^- and Br^-, respectively.

Table 2.18: Experimental and calculated interfacial molarities for ions and water in 10-2-10 2X (X = AcO, Cl, Br) micelles. The calculated ion interfacial concentrations refer to the peaks of their distributions, whereas the calculated water concentrations are from the projection of the location of these peaks onto the respective water concentration gradients Figure 2.8. The experimental values are those at the stoichiometric concentrations of 2 x cmc.

Interfacial molarities	Counterions		
	AcO^-	Cl^-	Br^-
X_m (exp.)	0.9	1.5	2.1
X_m (calc.)	1.5	1.8	2.1
H_2O_m (exp.)	51	49	43
H_2O_m (calc.)	31	34	29

counter anions and water validates the MD simulation approach (the choice of the force field, i.e. the use of the set of mixed parameters within CHARMM force field) and the chemical trapping method used to obtain quantitative estimates of the interfacial counterion molarities at the interfacial volume of cationic association colloids.

2.2.4 The Location of the Chemical Trapping Probe in Gemini Micelles

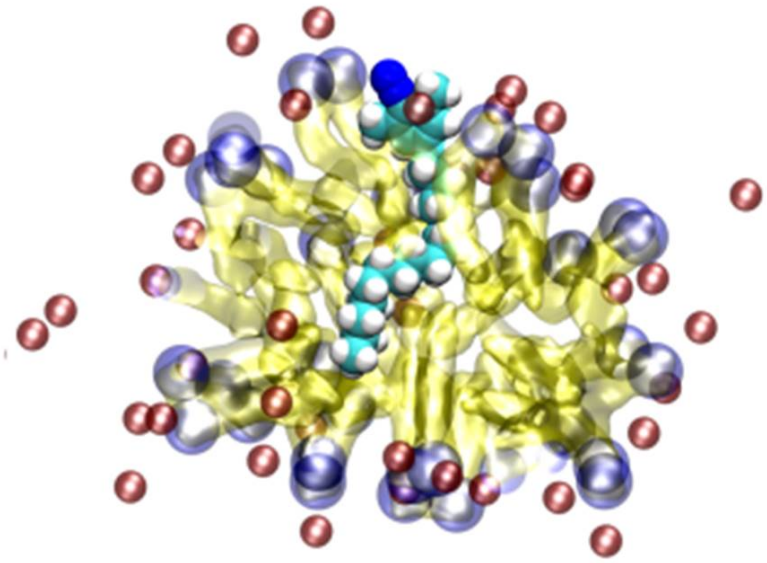

Figure 2.9: A MD simulation of the chemical trapping probe, 16-ArN_2^+ , nested in a 10-2-10 2Cl micelle. Depicted are chloride ions (red), a spaghetti-like core of decyl tails (golden yellow), gemini nitrogens (steel blue), and the chemical probe with carbons (cyan), hydrogens (white), and diazonio group (dark blue). For esthetic purposes, various groups in the gemini micelle cross section are not quite to scale.

The radial distribution of the chemical trapping probe, 16-ArN_2^+ , nested in a 10-2-10 2X micelle containing 27 gemini surfactant molecules was also investigated by MD simulation. Figure 2.9 shows that although the aliphatic 16-carbon tail of the probe is longer than the 10-carbon tail of the 10-2-10 2X surfactants, it snuggles easily within the micellar core, consistent with its fluid properties. Also, Figure 2.10 shows the cationic arenediazonium group has the same basic RDF as the cations on the gemini headgroups and indicates that the reactive group samples the same interfacial volume as the gemini headgroups, confirming

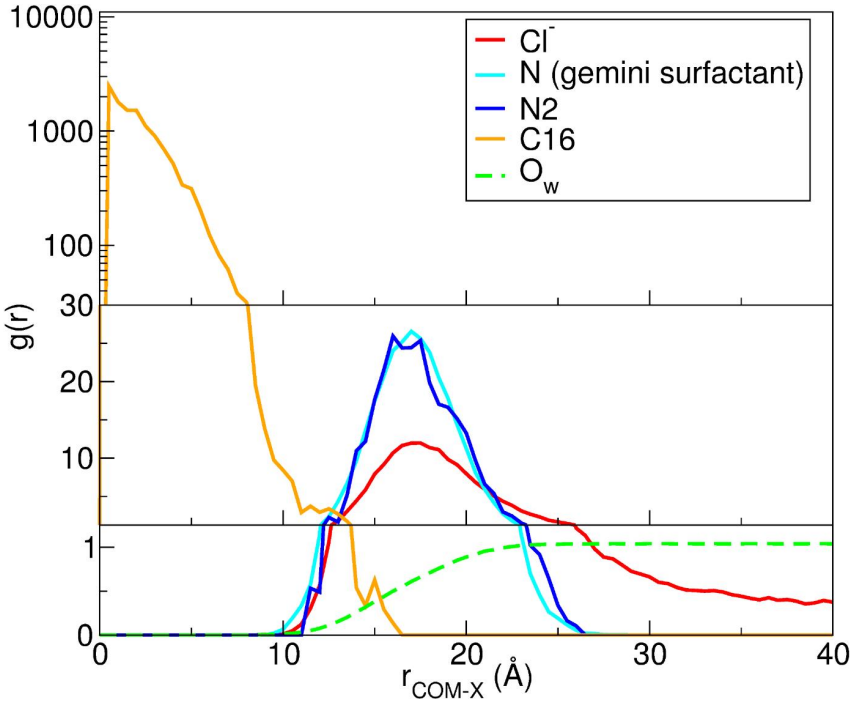

Figure 2.10: RDFs of selected probe and surfactant atoms with respect to the 10-2-10 2Cl micelle COM. The atoms are: the terminal carbon atom C16 of the 16-ArN_2^+ hydrophobic tail (gold line), the nitrogen atom N_2 bound to benzene moiety of 16-ArN_2^+ (blue line), the nitrogen atom N of the 10-2-10 2Cl gemini surfactant (cyan line), the counterion Cl^- (red line) and the oxygen atom of water molecules (dashed green line)

one of the assumptions of the chemical trapping method.[99]

2.2.5 Estimates of the fractions of Br^- ion-pairs in the interfacial regions

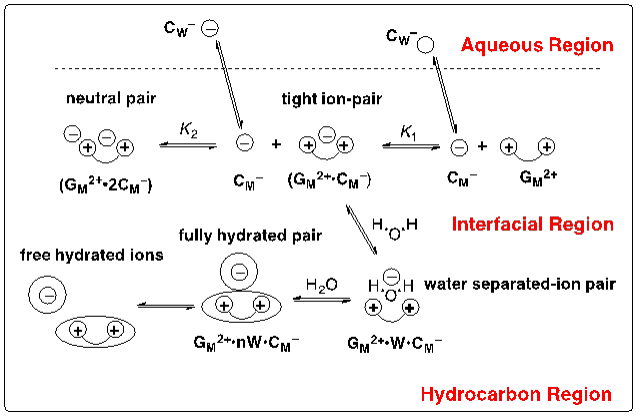

Figure 2.11: Illustration of the equilibria that contribute to ion-pairing within the interfacial region of 10-2-10 2X micelles as defined in the MD RDF and CT methods. To minimize clutter, the surfactant tails and most water of the water molecules are not shown. The three regions demarked by lines do not represent their relative volumes and the physical locations of anions relative to cations in the interfacial region are for representation purposes only.

Figure 2.11 shows the equilibria that govern the formation of different types of ion-pairs: tight water-separatedand fully-hydrated counterion gemini headgroups ion-pairs at the interface. K_1 is the ion pairing constant of the tight ion-paired gemini, K_2 is the ion pairing constant of the second more loosely held counterion leading to neutral gemini. The transition between the tight pair and water separated ion-pair can be described by the addition of H_2O.

The fraction of ion-pairs in the interfacial region cannot be obtained directly from our chemical trapping experiments because the molarities of the free and paired counterions in the interfacial region are not directly measured by the probe. Our approach as developed previously,[100, 101] is to determine the ion-pairing constant, K_1, in bulk 1-2-1 2Br aqueous solution from plots of normalized yields, %1-ArBr, versus stoichiometric counterion concentration, [Br_t], (Figure 2.2) and assume that the value of K_1 in the micelles is the same as in the aqueous reference solution. The method is based on our assumption that the probe only

react with free Br^- in solution but not paired Br^- (tight and water separated), which is consistant with our measured selectivity curve, Figure 2.3. Therefore, the fraction of tight and water separated ion-paired Br^- cannot be estimated separately.

$$G^{2+} + C^- \rightleftharpoons G^{2+} \cdot C^- \qquad K_1 = \frac{[G^{2+} \cdot C^-]}{[G^{2+}][C^-]} \tag{2.4}$$

$$G^{2+} \cdot C^- + C^- \rightleftharpoons G^{2+} \cdot 2C^- \qquad K_2 = \frac{[G^{2+} \cdot 2C^-]}{[G^{2+} \cdot C^-][C^-]} \tag{2.5}$$

Two ion pairing constant K_1 and K_2 for 1-2-1 2Br can be defined in aqueous solution of 1-2-1 2Br by equations 2.4 and 2.5, where G^{2+} is the free dication, C^- is the free counterion, and $G^{2+} \cdot C^-$ is the tight or hydrated mono-ion pair, and $G^{2+} \cdot 2C^-$ is the neutral ion pair. However, we set $K_2 = 0$ for 1-2-1 2Br because initial estimates of K_2 by our curve fitting method gave values that were extremely small, ca. 0.0013 and therefore unreliable, probably because the normalized yield, 1-ArBr, within experimental error, is a linear function of the stoichiometric bromide concentrations, $[Br_t]$, above 0.5 M $[Br_t]$ (Figure 2.2).

$$[C_T] = [C^-] + [G^{2+} \cdot C^-] \tag{2.6}$$

$$[G_T] = [G^{2+}] + [G^{2+} \cdot C^-] \tag{2.7}$$

$$[C_T] = 2[G_T] + 0.001M \tag{2.8}$$

$$K_1[C^-]^2 + (1 - 0.5K_1(C_T + 0.001))[C^-] - [C_T] = 0 \tag{2.9}$$

$$\%1 - ArX = A[C^-] \tag{2.10}$$

$$\frac{K_1}{A}(\%1 - ArX)^2 + \frac{(1 - 0.5K_1(C_T + 0.001))}{A}(\%1 - ArX) - [C_T] = 0 \tag{2.11}$$

Equations 2.6-2.8 are mass balance equations defining the total concentration of C_T and G_T. The value 0.001 M is the concentration of added HBr to control solution acidity. Combining Equations 2.4 and 2.6-2.8 gives a quadratic equation for free counterion concentration, $[C^-]$, in 1-2-1 2Br aqueous solutions, Equation 2.9. Linear equation 2.10, in which

A is an empirical constant, is based on the assumption that the product yield %1-ArBr depends only on the concentration of free and not paired counterions. Equation 2.11, derived by combining Equation 2.9 and 2.10, and was used to fit the chemical trapping normalized product yields, %1-ArBr, as a function of stoichiometric bromide concentration, [Br_t], in 1-2-1 2Br up to 0.5 M.

Values for the ion pairing constants K_1 and the empirical constant A were obtained by fitting the quadratic equation by using a program written in "R" by the R Project for Statistical Computing (See Appendix).[102] The inputs were the total bromide concentration, [Br_t] ([Br_t] ≤ 0.5), and the corresponding normalized bromo-product yield, %1-ArBr_N from combined data sets at λ = 220 and 230 nm. The values of K_1 and A were selected by a grid search for the optimal values. For each pair (K_1,A), a series of $(\%1\text{-ArBr})_{cal}$ values were calculated corresponding to all [Br_t] values. The best pair of K_1 and A was selected by minimizing F in Equation 2.12:

$$F = \frac{\sum[\%1 - ArBr_N - (\%1 - ArBr)_{cal}]^2}{(\%1 - ArBr)_{cal}} \tag{2.12}$$

The estimated ion pairing constant for 1-2-1 2Br is $K_1 = 10.9$, and when A = 43. Marcus concluded that measured ion pairing constants ≥ 10 provide meaningful evidence for ion pairing.[103]

The optimized values K_1 were used to estimate the interfacial concentration of free counterions, $\{C_M^-\}$, free headgroup, $\{G_M^{2+}\}$, counterion headgroup ion pairs, $\{G_M^{2+} \bullet C_M^-\}$, in the interfacial regions of 10-2-10 2Br micellar solutions, where {} indicates interfacial molarity in units of moles per liter of interfacial volume.

$$K_1 = \frac{\{G_M^{2+} \bullet C_M^-\}}{\{G_M^{2+}\}\{C_M^-\}} \tag{2.13}$$

$$\{C_M\} = \{C_M^-\} + \{G_M^{2+} \bullet C_M^-\} \tag{2.14}$$

$$\{G_M\} = \{G_M^{2+}\} + \{G_M^{2+} \bullet C_M^-\} \tag{2.15}$$

$$\{C_M\} = 2(1 - \alpha)\{G_M\} \tag{2.16}$$

$$K_1\{C_M^-\}^2 + (1 + \frac{\alpha - 0.5}{1-\alpha} K_1\{C_M\})\{C_M^-\} - \{C_M\} = 0 \tag{2.17}$$

$$\{G_M^{2+} \bullet C_M^-\} = \{C_M\} - \{C_M^-\} \tag{2.18}$$

$$\{G_m^{2+}\} = \frac{\{C_M\}}{2(1-\alpha)} - \{G_M^{2+} \bullet C_M^-\} \tag{2.19}$$

Equations 2.13-2.16 are analogous to Equations 2.4 and 2.6-2.8, but the symbols represent components for the interfacial region of 10-2-10 2Br micellar solutions. $\{C_M\}$ is the total interfacial molarity of counterions obtained from the chemical trapping results (Table 2.16), and $\{G_M\}$ is the total interfacial headgroup molarity and $2\{G_M\}$ is the interfacial molarity of cationic charges that are calculated from $\{C_M\}$ and α by using Equation 2.16. The factor 2 indicates that each gemini headgroup is dicationic and $(1-\alpha)$ is the fraction of counterions within the interfacial region. Equation 2.16 shows that the relationship between interfacial counterion and headgroup molarities depend on α. Equation 2.17 is obtained by combining Equations 2.13-2.16 and is used to calculate the molarity of unpaired counterions in the interfacial region, $\{C_M^-\}$, from K_1 and α. Equations 2.18 and 2.19 are used to estimate the ion pair and free headgroup molarities, respectively.

Table 2.19: Calculated ion pairing fraction in the interfacial regions of 10-2-10 2Br micelles ($\alpha = 0.37$).

[10-2-10 2Br] (mM)	$\{C_M\}$ (M)	$\{C_M^-\}$ (M)	$\{G_M^{2+}\}$ (M)	$\{G_M^{2+} \bullet C_M^-\}$ (M)	$2\{G_M\}$ (M)	$\frac{\{C_M^-\}}{\{C_M\}}$	$\frac{\{G_M^{2+} \bullet C_M^-\}}{\{C_M\}}$	$\frac{\{G_M^{2+} \bullet C_M^-\}}{2\{G_M\}}$
10	2.13	0.65	0.21	1.48	3.38	0.30	0.70	0.44
20	2.20	0.67	0.21	1.53	3.49	0.30	0.70	0.44
30	2.29	0.69	0.21	1.60	3.63	0.30	0.70	0.44
50	2.42	0.72	0.22	1.70	3.84	0.29	0.70	0.44
100	2.50	0.74	0.22	1.76	3.97	0.29	0.71	0.44
150	2.49	0.73	0.22	1.76	3.95	0.29	0.71	0.44
250	2.57	0.75	0.22	1.82	4.08	0.29	0.71	0.44

The columns in Tables 2.19-2.22 list various interfacial molarities and fractions of counterions at 4 different α values for 10-2-10 2Br estimated either by conductivity[104] (Table 2.22) or MD simulations of r_{N-X} (Tables 2.20-2.22). Each table shows: the stoichiometric molarity of 10-2-10 2Br (Column 1, denoted as C1); the total interfacial counterion molarity measured by chemical trapping ($\{C_M\}$,C2); the interfacial molarity of free counterion

Table 2.20: Calculated ion pairing fraction in the interfacial regions of 10-2-10 2Br micelles ($\alpha = 0.31$).

[10-2-10 2Br] (mM)	$\{C_M\}$ (M)	$\{C_M^-\}$ (M)	$\{G_M^{2+}\}$ (M)	$\{G_M^{2+} \bullet C_M^-\}$ (M)	$2\{G_M\}$ (M)	$\frac{\{C_M^-\}}{\{C_M\}}$	$\frac{\{G_M^{2+} \bullet C_M^-\}}{\{C_M\}}$	$\frac{\{G_M^{2+} \bullet C_M^-\}}{2\{G_M\}}$
10	2.13	0.75	0.17	1.38	3.09	0.35	0.64	0.44
20	2.20	0.78	0.17	1.42	3.19	0.35	0.65	0.45
30	2.29	0.80	0.17	1.49	3.32	0.35	0.65	0.45
50	2.42	0.84	0.17	1.58	3.51	0.35	0.65	0.45
100	2.50	0.86	0.17	1.64	3.62	0.34	0.65	0.45
150	2.49	0.86	0.17	1.63	3.61	0.34	0.65	0.45
250	2.57	0.88	0.18	1.69	3.72	0.34	0.65	0.45

Table 2.21: Calculated ion pairing fraction in the interfacial regions of 10-2-10 2Br micelles ($\alpha = 0.23$).

[10-2-10 2Br] (mM)	$\{C_M\}$ (M)	$\{C_M^-\}$ (M)	$\{G_M^{2+}\}$ (M)	$\{G_M^{2+} \bullet C_M^-\}$ (M)	$2\{G_M\}$ (M)	$\frac{\{C_M^-\}}{\{C_M\}}$	$\frac{\{G_M^{2+} \bullet C_M^-\}}{\{C_M\}}$	$\frac{\{G_M^{2+} \bullet C_M^-\}}{2\{G_M\}}$
10	2.13	0.88	0.13	1.25	2.77	0.41	0.59	0.45
20	2.20	0.90	0.13	1.30	2.86	0.41	0.59	0.45
30	2.29	0.93	0.13	1.35	2.97	0.41	0.59	0.46
50	2.42	0.98	0.13	1.44	3.14	0.41	0.59	0.46
100	2.50	1.01	0.13	1.49	3.25	0.40	0.60	0.46
150	2.49	1.00	0.13	1.48	3.23	0.40	0.60	0.46
250	2.57	1.04	0.14	1.53	3.34	0.40	0.60	0.46

Table 2.22: Calculated ion pairing fraction in the interfacial regions of 10-2-10 2Br micelles ($\alpha = 0.16$).

[10-2-10 2Br] (mM)	$\{C_M\}$ (M)	$\{C_M^-\}$ (M)	$\{G_M^{2+}\}$ (M)	$\{G_M^{2+} \bullet C_M^-\}$ (M)	$2\{G_M\}$ (M)	$\frac{\{C_M^-\}}{\{C_M\}}$	$\frac{\{G_M^{2+} \bullet C_M^-\}}{\{C_M\}}$	$\frac{\{G_M^{2+} \bullet C_M^-\}}{2\{G_M\}}$
10	2.13	0.97	0.11	1.16	2.53	0.46	0.54	0.46
20	2.20	1.00	0.11	1.20	2.62	0.45	0.54	0.46
30	2.29	1.04	0.11	1.25	2.73	0.45	0.55	0.46
50	2.42	1.09	0.11	1.32	2.88	0.45	0.55	0.46
100	2.50	1.12	0.11	1.38	2.98	0.45	0.55	0.46
150	2.49	1.12	0.11	1.37	2.96	0.45	0.55	0.46
250	2.57	1.15	0.11	1.42	3.06	0.45	0.55	0.46

($\{C_M^-\}$,C3, Equation 2.17); free headgroup molarity ($\{G_M^{2+}\}$,C4, Equation 2.19); and interfacial molarity of counterion headgroup ion-pairs, ($\{G_M^{2+} \bullet C_M^-\}$,C5, Equation 2.18); and interfacial total head group charge molarity ($2\{G_M\}$,C6, Equation 2.15. Tables also list: (a) the fraction of free counterions ($\frac{\{C_M^-\}}{\{C_M\}}$,C7, (C3/C2)); (b) the fraction of ion-pairs in terms of interfacial counterion molarity ($\frac{\{G_M^{2+} \bullet C_M^-\}}{\{C_M\}}$,C8, (C5/C2)); and (c) the fraction of ion-pairs in terms of interfacial headgroup molarities ($\frac{\{G_M^{2+} \bullet C_M^-\}}{2\{G_M\}}$,C9, (C5/C6)).

The values in C9 showing the ratio of the sum of the interfacial molarities of tight and water separated ion-paired headgroups divided by total interfacial cation molarity, can also be defined as the fraction of gemini headgroups paired with one counterion, f_{Br}. Interestingly, a 25 fold increase in stoichiometric surfactant concentration (from 10 mM to 250 mM 10-2-10 2Br) results in significant decreases in H_2O_m (44 M to 39 M) and increases in Br_m at micellar interface (Figure 2.4), but these changes have almost no effect on f_{Br}, suggesting that f_{Br} is buffered by ion-pairing equilibrium. Also, regardless of the ionization degrees, computed α_{MD}^n or measured, α_E, used to derive the f_{Br}, its average value remains the same, 0.45 $\pm$ 0.1, as in Tables 2.19-2.22, i.e. 45% of the headgroups are ion-paired.

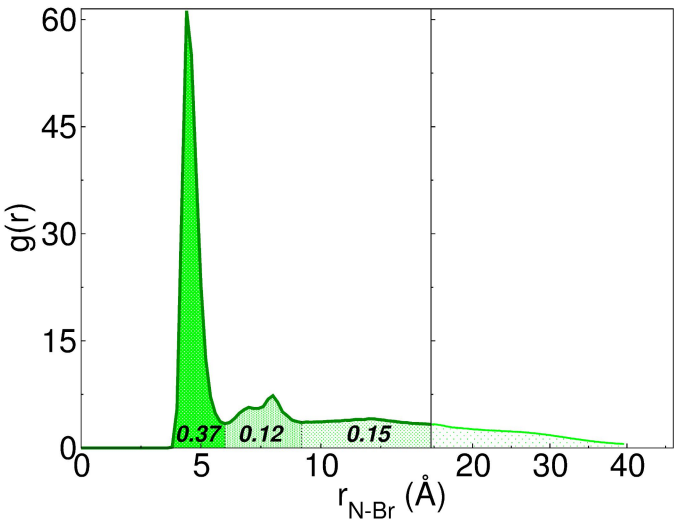

Figure 2.12: Fraction areas of the RDFs of the counterions with respect to nitrogen atoms of the micelle. The first, second, and third peaks correspond to the tight, water-shared and fully-hydrated ion pairs, respectively.

The RDF profiles from MD simulations were also employed to calculate the fraction

of ion-pairs in 10-2-10 2Br micelles, and similar results were obtained, Figure 2.12. The first peak in the RDF is at ca. 4.5 $\AA$, and is consistent with the cation-anion distance of contact or tight ion-pair.[105] The second peak is at ca. 7.5 $\AA$, and is consistent with the distance of water-shared or water-separated ion-pairs. The third peak at ca. 12 $\AA$ is probably represents fully-hydrated ion-pairs or condensed counterions[106, 107] that are associated within the interfacial region, but not paired with specific dicationic headgroups. The fractional area of the first and second peaks is 0.37 and 0.12 respectively, for a total of 0.49 of the Br^- ions are ion-paired. This value is in good agreement with that from the chemical trapping result of 45%.

To our knowledge, this is the first time that the distributions and molarities of counterions, water and headgroups and the fraction of paired counterions in the interfacial regions of micelles have been coherently elucidated by two totally different methods. Both MD and CT methods show that almost 50% of the dicationic headgroups are paired with one Br^-. Together these results provide solid evidence of ion-pairing in the interfacial regions of gemini micelles.

2.2.6 Chemistry in 10-2-10 2AcO micelles

Table 2.8 lists several products formed from reaction with acetate that are not found or are uncommon with other counterions MsO^-, Cl^-, Br^-, and I^-. 16-ArInd, 16-ArH, 16-ArOAc, and a mystery peak are found in significant yields. The "mystery peak" forms at pH 5 in 10-2-10 2AcO micelles, shown in Figure 2.13 (middle), and listed in Table 2.8, is assumed to be a diazoether, Figure 2.14, which is formed by deprotonation of 16-ArOH by AcO^- acting as a general base that deprotonats an α-methyl and speeds reaction with 16-ArN_2^+. The 16-ArH product is also formed by reaction of 16-ArOH with unreacted 16-ArN_2^+. It is commonly observed in small yields in a variety of different micelles,[90, 91] but becomes the dominant reduction product in the presence of added antioxidants such as ascorbic acid, α-tocopherol, and t-butylhydroquinone with 16-ArN_2^+ in emulsions.[108] The

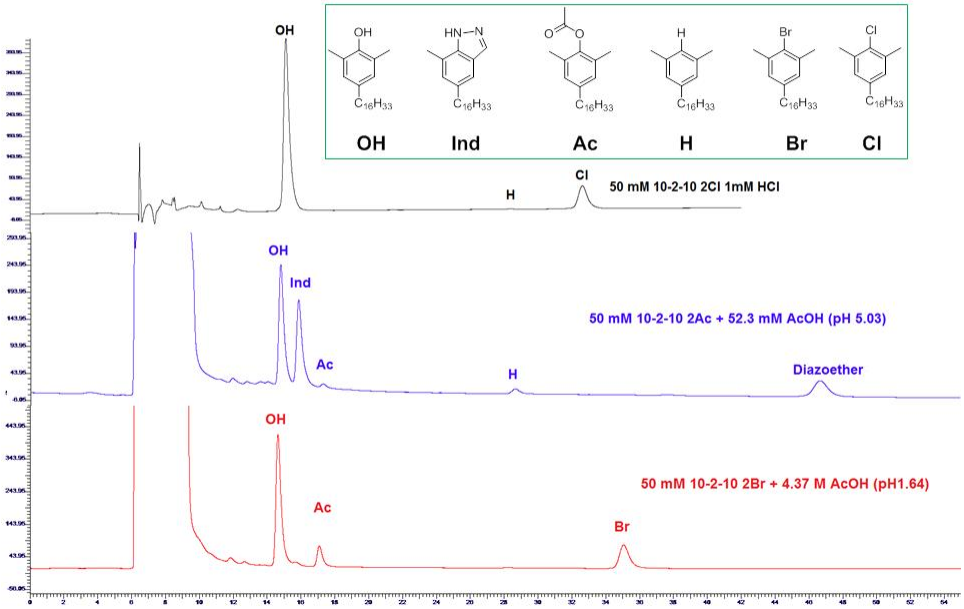

Figure 2.13: Sample HPLC chromatograms for reaction of 16-ArN_2^+ in micelles of 10-2-10 2Cl (top), 10-2-10 2AcO (middle) or 10-2-10 2Br with added acetic acid (bottom) at 25^{o}C.

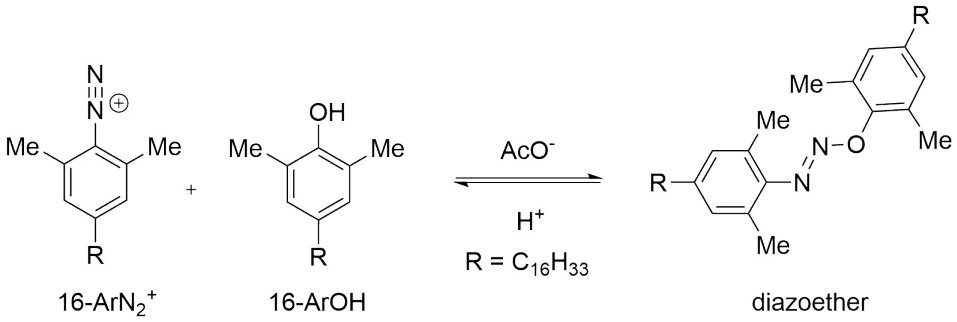

Figure 2.14: Diazoether formation. Proposed general base catalyzed reaction between unreacted 16-ArN_2^+ and the reaction product, 16-ArOH in gemini micelles of 10-2-10 2AcO at pH 5.

16-ArInd product is formed by general base induced deprotonation of a methyl side chain to give a carbanion that reacts with the arenediazonium headgroup and then rearranges.[90] This peak is observed whenever carboxylate groups are present in high concentration in the micellar interface, such as in micelles of dodecanoylglycine and dodecanoylsarcosine.[109] However, at high acidity such as in the addition of 4 M HOAc to 10-2-10 2Br (or add concentrated HBr to 10-2-10 2AcO, same result), only acetate ester is formed by trapping of 16-ArN_2^+ by acetic acid, Figure 2.13. Neither 16-ArInd nor the mystery peak is formed because the carboxylate groups are protonated and the concentration of the remaining carboxylate groups in the micellar interface are too low. Finally, 1-ArH, 1-ArInd, and the mystery peak do not appear in reactions of 1-ArN_2^+ in aqueous solutions in the absence of micelles because unlike the micellar solutions in which both 16-ArN_2^+ and 16-ArOH are concentrated within the micellar interface, there is no concentration effect in the aqueous salt solutions containing 1-ArN_2^+ and 1-ArOH. Consequently, the general base catalyzed reactions do not compete with spontaneous dediazoniation in the absence of micelles.

Several lines of evidence point to the diazoether as the mystery peak. Deprotonation of the phenolic product by interfacial carboxylate groups facilitate its attack on 16-ArN_2^+ at the micellar interface, is a reasonable mechanism. This product is also observed in micellar solutions of surfactants that have carboxylate headgroups, in which the carboxylate concentration is 1 M because the carboxylate group is part of the surfactant, i.e., >1 M.[109] Its retention time is long, ca. 43 min, consistent with a hydrophobic molecule on a reversed phase column, Figure 2.13. The compound is stable in micellar solutions at pH 5 for at least 1.5 years. However, all attempts at isolating this product from HPLC separations gave multiple products. Addition of concentrated HCl to the dediazonation product mixture (final pH ca. 0.77) reduces the size of the mystery peak to about 4% of its original size in ca. 40 hours, consistent with acid catalyzed hydrolysis of a diazoether.[108]

2.3 Conclusions

Chemical trapping method was used to characterize the interfacial region of 10-2-10 2X (X = AcO, MsO, Cl, Br, and I) cationic gemini micelles. The interfacial counterions and water molarities follow the Hofmeister series: the interfacial counterion molarities follow the order: I > Br > Cl > MsO > AcO; while the interfacial water molarities follow the order: AcO > Cl > MsO > Br > I. MD simulations were also applied to 10-2-10 2X (X = AcO, Cl, and Br) micelles. The interfacial molarities obtained by CT and MD are remarkable similar to each other.

Together these results provide a more detailed representation of the micellar interface that belies the traditional cartoon representation of micelles with arbitrary and often sharp boundaries between the core, interfacial, and aqueous volumes.[110] The interfacial region, as seen by MD simulation, containing the headgroups, counterions and interfacial water is thicker than the micellar core by about 25 $\mathring{A}$ thick in these gemini micelles. Indeed, the distribution of H_2O molecules begins at about 10 $\mathring{A}$ and then increases steadily to a plateau as the interfacial polarity changes from that of nearly pure hydrocarbon to that of water across the headgroup region from about 10-25 $\mathring{A}$. The counterions distribution shows a maximum at ca. 18 $\mathring{A}$, and decreases gradually out into the aqueous region. Strikingly, the RDF for the N_2 nitrogen on the 16-ArN_2^+ probe covers the same region as the gemini headgroup nitrogens, both with a maximum at around 18 $\mathring{A}$, providing powerful evidence that the reactive headgroup of the probe 16-ArN_2^+ , reacts in same cross section as the headgroups despite the fact that the length of its tail is significantly longer than the 10-2-10 surfactant. Thus both probe and surfactant tails are in a fluid hydrocarbon-like region while the probes are capable of sampling the interfacial volume with its reactive head.

The tight and water-separated pairs are located within the headgroup region and, therefore the micellar interfacial region is not smooth with all the headgroups on a spherical surface around the core, but rough with more ion-pairs near the core and more hydrated

and unpaired headgroup and counterions further away.

Both chemical trapping and MD simulations support the interpretation of high (1-4 M) local ion concentrations that are 1-2 orders of magnitude higher than the stoichiometric concentrations, and a competition between water and ions in the interfacial region. Formation of 50% headgroup ion-pairs in the headgroup region of 10-2-10 Br micelles suggests a new explanation for the often surprisingly low cmc values of gemini surfactants.[43] That ion-pair formation significantly reduces the net surface charge and makes the gemini micelles more hydrophobic than expected. Our approach lays the foundations to employ the combination of MD and chemical trapping methods to investigate other surfactants interacting with other counterions. The results could produce new insight into the delicate balance-of-forces controlling micelle formation and growth.

2.4 Experimental

2.4.1 General method

HPLC measurements were performed on a Perkin-Elmer Series 200 equipped with a UV/Vis detector, a Varian Microsorb MV C18 column (length, 25 cm; particle size, 5 μm) or a Agilent ZORBAX Eclipse XDB-C18 column (4.6x150 mm, 3.5 μm)(for X=I), and a computer-controlled Perkin-Elmer 600 Series Interface. Kinetic measurements were carried out on a Perkin-Elmer Lambda 45 UV/Vis spectrophotometer equipped with a Peltier Temperature Programmer 6 operated with UV WinLab 6.0.3 software. All pH values were obtained by a Fisher AR50 dual channel pH/Ion/Conductivity Meter. ^{1}H NMR spectra were recorded on Varian VNMRS 300, 400 and 500 MHz spectrometers.

2.4.2 Materials

All aqueous solutions were prepared from water that was distilled, passed over activated carbon, an ion exchange resin and then redistilled. All solvents, MeCN, *i*-PrOH, MeOH,

and cyclohexane were of the highest commercially available reagent grade. 10-2-10 2X (X=AcO, MsO, Cl, Br, I) were synthesized by our collaborator, Alla Malinenko, based on the procedure developed by Manet et al for the syntheses of 14-2-14 2X.[70, 92] 1-2-1 2X (X = AcO, MsO, Cl, Br, I) were prepared by the same procedure as for 10-2-10 2X. The chemical trapping probe salts 1-ArN_2BF_4 and 16-ArN_2BF_4 were prepared as needed by a previously developed synthetic procedure.[81] Reaction products 1-ArX, 16-ArX, (X = Cl, Br), 1-ArI, 1-ArOH, 16-ArOH, 16-ArInd and 16-ArH, which were used to create needed calibration curves, were either commercially available or prepared by established procedures.[81, 90] The products, 1-ArOAc, 1-ArOMs, 16-ArOAc, and 16-ArOMs were synthesized for these experiments (see below).

Figure 2.15 shows the basic synthesis conditions used to prepare the short tail ester, mesityl acetate, 1-ArOAc, and long tail, 4-hexadecyl-2,6-dimethylphenyl acetate, 16-ArOAc, esters.

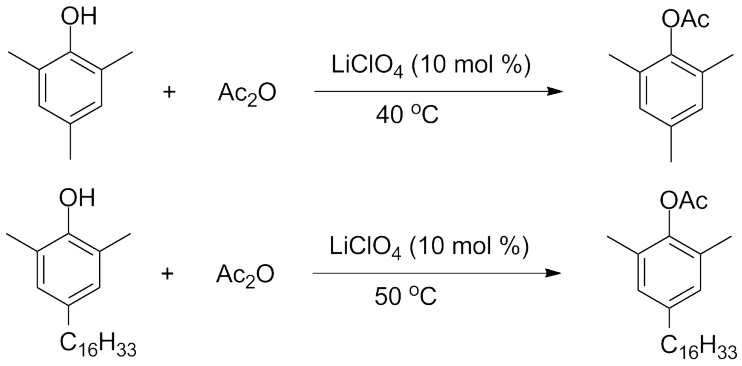

Figure 2.15: Syntheses of acetate esters

Mesityl acetate, 1-ArOAc. The short tail acetate ester was prepared by acetylation of mesityl alcohol,1-ArOH, using acetic anhydride in the presence of $LiClO_4$ under solvent free conditions, Nakae et al.[111] A mixture of 1-ArOH (3.40 g, 25 mM; Aldrich, 97%), acetic anhydride (5.10g, 50 mM; J.T.Baker, 99.2%), and $LiClO_4$ (0.266 g, 2.5 mM; Aldrich, dry, 99.99%) was placed in a 50 mL, three-neck, round-bottom, flask fitted with a heating mantle, stirrer, condenser, and thermometer and heated under dry N_2 at 40 ^{o}C for 18 hours. The

reaction was quenched with 80 mL H_2O. The crude product was extracted with ethyl acetate (2 x 80 mL). The organic layer was washed first with saturated $NaHCO_3$ solution (2 x 80 mL), then saturated NaCl solution (80 mL), and dried with Na_2SO_4. Further purification was conducted on silica gel column (5% EtOAc/hexane) giving a colorless liquid. ^{1}H NMR ($CDCl_3$) δ (PPM): 6.86 (2H, s), 2.32 (3H, s), 2.25 (3H, s), 2.11 (6H, s), Figure 2.16.

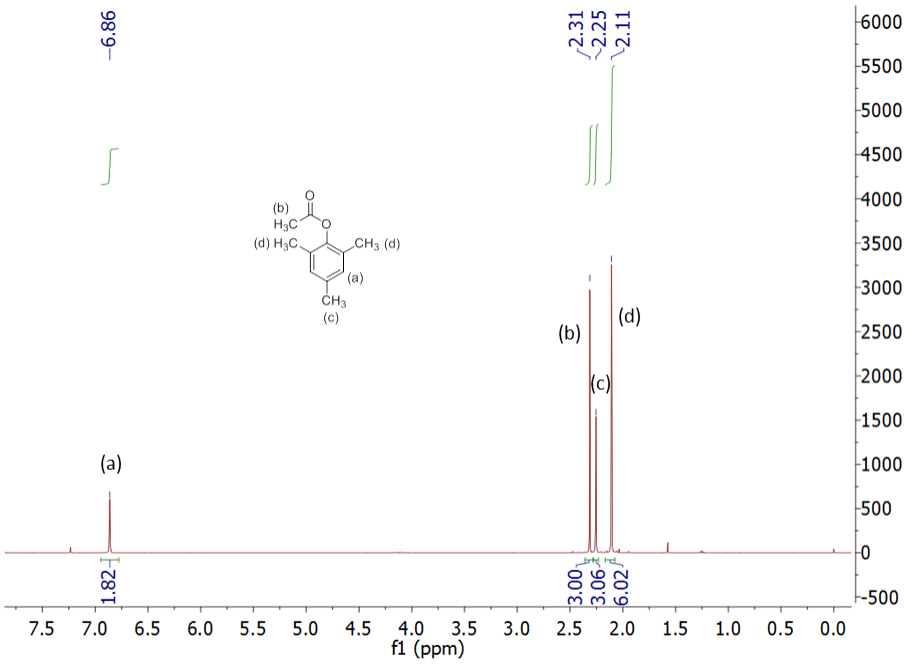

Figure 2.16: ^{1}H NMR spectrum of mesityl acetate at 400 MHz in $CDCl_3$

4-Hexadecyl-2,6-dimethylphenyl acetate, 16-ArOAc. The long tail 16-ArOAc was synthesized using a same procedure as for 1-ArOAc with minor modifications. 16-ArOH was used instead of 1-ArOH, 60 fold excess acetic anhydride was added instead of 2 fold, and the reaction mixture was heated to 50 ^{o}C instead of 40 ^{o}C to ensure complete dissolution of the reactants and products. The crude product was purified by elution with 1% EtOAc/hexane over a silica gel column, giving a white solid. ^{1}H NMR ($CDCl_3$) δ (PPM): 6.86 (2H, s), 2.50 (2H, t), 2.32 (3H, s), 2.12 (6H, s), 1.56 (2H, br), 1.26 (26H, br), 0.87 (3H, t), Figure 2.17.

2,4,6-trimethylphenyl methanesulfonate, 1-ArOMs. Figure 2.18 shows the basic synthesis scheme used to prepare 1-ArOMs. The short tail mesylate ester was prepared by carrying

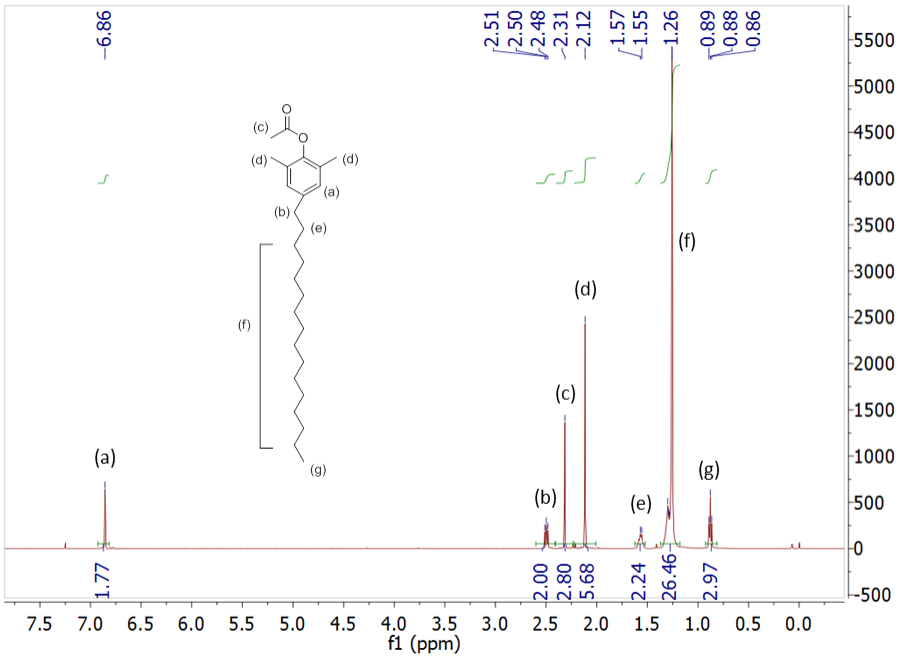

Figure 2.17: ^{1}H NMR spectrum of 4-hexadecyl-2,6-dimethylphenyl acetate at 500 MHz in $CDCl_3$

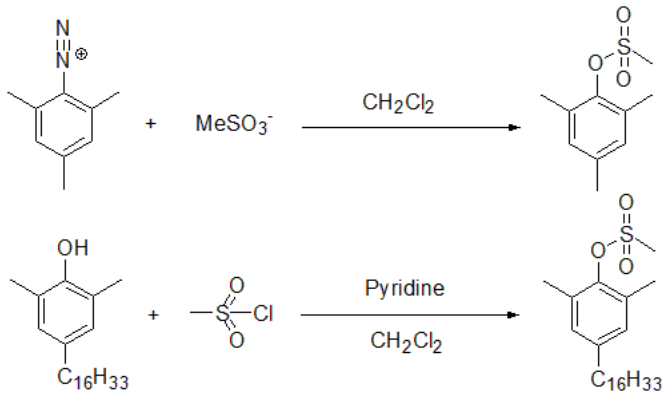

Figure 2.18: Syntheses of mesylate esters

out the dediazoniation reaction between short-chain probe, 1-ArN_2^+, and methanesulfonate, MsO^-.[78] 1-ArN_2BF_4 (0.102 g, 0.44 mmol) was added to a mixture of 10-2-10 2MsO (0.335 g, 0.57 mmol)and CH_2Cl_2 (5 ml). The reaction mixture was stirred under room temperature for 24 h. The color of the reaction mixture turned from red, then orange, to yellow. The crude product was purified by elution with 20% EtOAc/hexane over a silica gel column, giving a final yield of 30%. ^{1}H NMR ($CDCl_3$) δ (PPM): 6.88 (2H, s), 3.26 (3H, s), 2.34 (6H, s), 2.26 (3H, s), Figure 2.19.

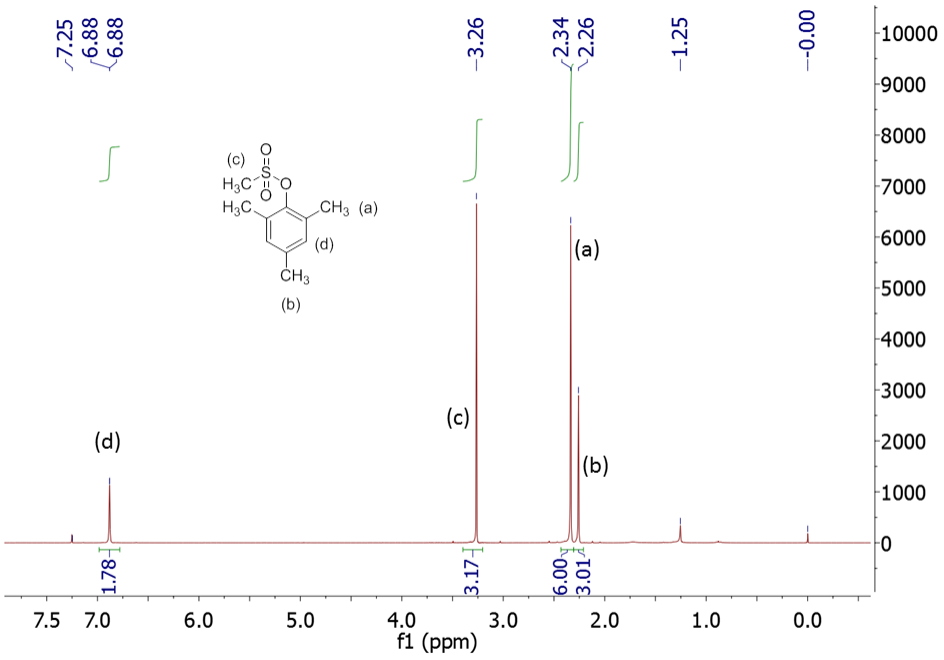

Figure 2.19: ^{1}H NMR spectrum of 2,4,6-trimethylphenyl methanesulfonate at 300 MHz in $CDCl_3$

4-Hexadecyl-2,6-dimethylphenyl methanesulfonate, 16-ArOMs. The long tail mesylate ester was prepared by the reaction of mesyl chloride with the 16-ArOH in dichloromethane and pyridine, Figure 2.18.[112] 16-ArOH (5 mg, 0.014 mmol), anhyrous dichloromethane (500 μL), and anhydrous pyridine (60 μL)were mixed in an oven dried round bottom flask and give a clear solution. The reaction mixture was not cooled in an ice bath because of the small-scale. Mesyl chloride (20 μL, 0.26 mmol)was added dropwise into the mixture. The

reaction was allowed to stirred overnight at room temperature. The complete consumption of the starting material was observed by HPLC. The reaction was quenched by addition of water (1 mL) and the organic phase was separated. The aqueous phase was further extracted with dichloromethane (3 x 0.5 mL) and all the organic layers were combined and washed with 15% HCl (2 x 0.5 mL) and saturated NaCl solution (3 x 0.5 mL), and dried with $MgSO_4$. The solvent was evaporated after filtration. The crude product was purified by HPLC with a 65% MeOH/35% *i*-PrOH (v/v) mobile phase. ^{1}H NMR ($CDCl_3$) δ (PPM): 6.88 (2H, s), 3.28 (2H, s) 2.50 (2H, t), 2.35 (6H, s), 1.54 ($\beta - CH_2-$ and residual water, br), 1.26 (26H, br), 0.88 (3H, t), Figure 2.20.

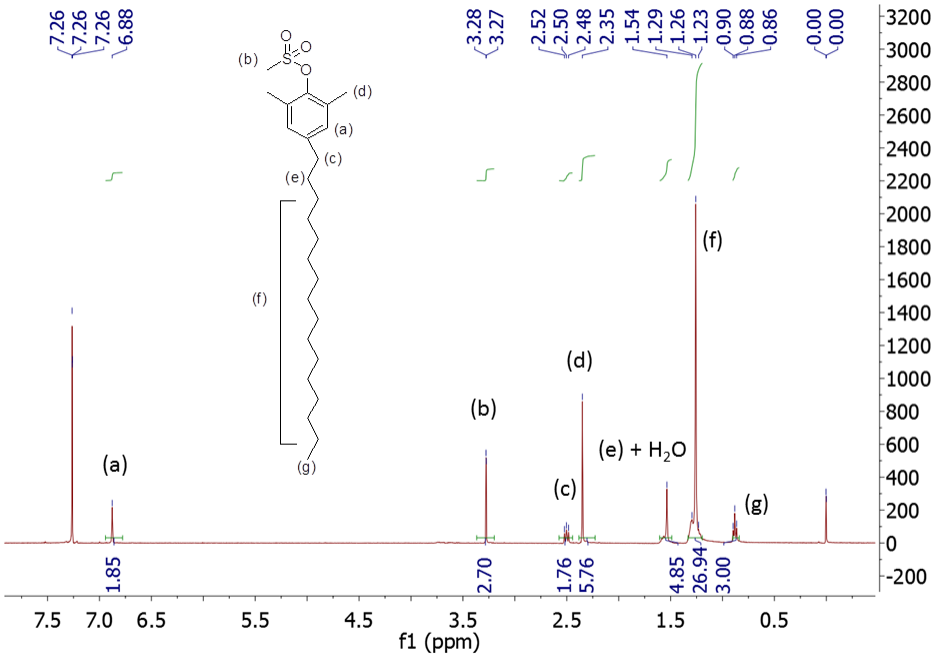

Figure 2.20: ^{1}H NMR spectrum of 4-Hexadecyl-2,6-dimethylphenyl methanesulfonate at 400 MHz in $CDCl_3$

2.4.3 Chemical trapping with 1-ArN_2^+ in aqueous 1-2-1 2X (X = MsO, Cl, Br) reference solutions

Aqueous 1-2-1 2X (X = MsO, Cl, Br) stock solutions were prepared via a routine procedure in which the weights of both the salt and the water were obtained by measuring them in weighed 10 mL volumetric flasks. The salt was vacuum dried for several days until it reached constant weight. Each salt was weighed in a 10 mL flask and sufficient water was added to dissolve it and then the solution was diluted to the mark. The weight of water was determined by difference between the total weight minus the total weight of salt and the flask. The stock solutions were used to prepare sets of 1-2-1 2X (X = MsO, Cl, Br) solutions containing incremental amounts of the stock solutions in 1-2 mL volumetric flasks. The solution acidity was set by adding 10-20 μL of 0.1 M HX, to give a final HX concentration of 1 mM. The weight of water in each 1-2 mL flask was obtained from the calculated weight of water in the aliquot of the stock solution plus the weight of water added to fill the 1-2 mL flask to the mark. These weights were used to calculate the molarities of X^- and H_2O because the solutions were concentrated and salt occupies a significant fraction of the total solution volume. To initiate the dediazoniation reactions, 10-20 μL of freshly prepared stock solutions of 1-ArN_2BF_4 in ice-cold MeCN were added to give a final probe concentration of 4-4.5 x 10^{-3} M. 50-100 μL of cyclohexane were layered on top of the solutions to prevent the evaporation of volatile 1-ArX and 1-ArOH products (the long chain products, 16-ArX and 16-ArOH, are involatile). The volumetric flasks were sealed with Parafilm and equilibrated at 25 ^{o}C for 2 days. Prior to HPLC analysis, the product mixture was diluted 5-fold with MeOH or MeCN to dissolve both the cyclohexane and the aqueous salt solution. Conditions for product separation on the HPLC for 1-2-1 2X (X=Cl, Br) were the following: an 80% MeOH/20% H_2O (v/v) mobile phase; flow rate = 0.6 mL/min; detector wavelength = 230 nm; the injection volume was 50 μL. For 1-2-1 2MsO, the conditions for product separation were: an 55% MeOH/45% H_2O (v/v) mobile phase; flow rate = 0.4 mL/min; detector wavelength = 230 nm; the injection volume was 50 μL.

Percent yields were obtained from average values of peak areas from triplicate or duplicate injections with the calibration curves obtained for the particular product. Product yields are in the data tables in the Results section below.

2.4.4 Chemical trapping with 1-ArN$_2^+$ in aqueous 1-2-1 2AcO reference solutions

Prior to 1-ArN$_2$BF$_4$ addition, the initially basic solutions were titrated to about pH 6 by adding glacial acetic acid. The titration was monitored by using a pH meter. The reaction solutions were equilibrated at 25 ^{o}C for 24 hours. All the other procedures were the same as the chemical trapping in 1-2-1 2Br and 1-2-1 2Cl solutions.

2.4.5 Chemical trapping with 1-ArN$_2^+$ in aqueous 1-2-1 2I reference solutions

The reaction solutions were kept at 50 ^{o}C for 7 hours. The gemini 10-2-10 2I has a high Krafft temperature and not soluble at 25 ^{o}C, and the chemical trapping experiment in 10-2-10 2I micelles were carried out at 50 ^{o}C. Therefore the chemical trapping reaction with 1-ArN$_2^+$ in 1-2-1 2I reference solutions were also carried out at the same temperature for comparison. Prior to HPLC analysis, the product mixtures were diluted 25-fold with methanol and H_2O to keep both product and salt in the solutions at room temperature. However, the methods for sample preparation, HPLC analysis, and percent yields obtaining were the same as the chemical trapping in 1-2-1 2Br and 1-2-1 2Cl solutions.

2.4.6 Chemical trapping with 16-ArN$_2^+$ in aqueous 10-2-10 2X (X= MsO, Cl, Br) micellar solutions.

The reaction was initiated by adding 20 μL freshly prepared stock solutions of 16-ArN$_2$BF$_4$ dissolved in ice-cold MeCN to 2 mL of the aqueous micellar containing solution, the 10-2-10 2X (X = Br or Cl) of the needed concentration, 1 mM HX, and a final probe concentration

of 10^{-4} M. The volumetric flasks were sealed and thermostated at 25 ^{o}C for 2 days. Conditions for product separation on the HPLC for 10-2-10 2Br and 10-2-10 2Cl were: a 65% MeOH/35% i-PrOH (v/v) mobile phase; flow rate = 0.4 ml/min; detector = 220 nm; and the injection volume was 100 μL. For 10-2-10 2MsO, the conditions for product separation were: a 80% MeOH/20% *i*-PrOH (v/v) mobile phase; flow rate = 0.4 mL/min; detector = 220 nm; and the injection volume was 100 μL. Percent yields were obtained from average values of peak areas from triplicate or duplicate injections with the appropriate calibration curves.

2.4.7 Chemical trapping with 16-ArN_2^+ in aqueous 10-2-10 2AcO micellar solutions.

Prior to 16-ArN_2BF_4 addition, the solutions were titrated dropwise with glacial acetic acid to about pH 5. The reaction solutions were equilibrated at 25 ^{o}C for 24 hours. All the other procedures were the same as the chemical trapping in 10-2-10 2Br and 10-2-10 2Cl solutions.

2.4.8 Chemical trapping with 16-ArN_2^+ in aqueous 10-2-10 2I micellar solutions.

The reaction solutions were kept at 50 ^{o}C for 20 hours because of the high Krafft temperature of 10-2-10 2I. Prior to HPLC analysis, the product mixtures were diluted 5-fold with methanol to keep both product and surfactants in the solutions at room temperature. The methods for sample preparation, HPLC analysis, and percent yields obtaining were the same as the chemical trapping in 10-2-10 2Br and 10-2-10 2Cl solutions.

2.4.9 Molecular dynamics (MD) simulations for 10-2-10 2X (X=AcO, Cl, Br)

Molecular dynamics (MD) simulations were carried out by our collaborator, Massimiliano Porrini. The CHARMM36 [113] force field with its parametrization for the surfactant

molecules, and the OPLS parameters [114, 115, 116] for the three counterions were used to describe the interactions between surfactants, counterions and water.

Micelles composed of 27 10-2-10 surfactants were built using Packmol software.[117] The micelles were immersed in boxes with volumes of 83x80x82 $\AA^3$ and 17900 water molecules. The systems were neutralized with 54 counterions (AcO^-, Cl^-, and Br^-), randomly placed in the box. The resulting counterions concentrations were ca. 164 mM, corresponding to a gemini stoichiometric concentration of ca. 82 mM.

For the simulations in the presence of the arenediazonium probe, one molecule of 16-ArN_2^+ was inserted into the micelle and its +1 charge was neutralized by one more counterion. The protocol followed for minimization, equilibration and production run was the same for all the simulations. The CHARMM-compatible charges[118] of 16-ArN_2^+ were derived using the VMD[119] plugin force field ToolKit (ffTK),[120] aiming at reproducing the quantum mechanical interactions with TIP3P[121] water molecules.

2.5 Appendix

2.5.1 R programs

R is a language for statistical data manipulation and analysis. It's free and can be downloaded at http://cran.R-project.org. Please see the book *The Art of R Programming* by Norman Matloff for a basic introduction to R programing.

1. The following computer program in R was written to obtain the optimized value of ion pairing constant K for TMAX. Note everything on the line after a hashmark is a comment in R.

```
#Purpose: Association constant estimation (TMAX)   [HX]=1mM
rm(list=ls(all=TRUE))
#Input data set
data<-read.csv(file.choose())
```

```
#conc.t([TMAX]+[HX])     yield.e (experimental value of %1-ArX)
attach(data)
acid<-0.001                # 0.001M HX
plot(yield.e~conc.t,ylab="%1-ArX",xlab="[Xt]")

#define A, K, yield.c, error, error.sum
A<-seq(1,200,by=0.1)    #yield=A*[X-]
n<-length(A)
K<-seq(0.1,20,by=0.1)    #association constant of TMAX
m<-length(K)
p<-nrow(data)       #number of data points
yield.c<-c(NA,p)   #calculated value of %1-ArX
error<-c(NA,p) #(calculated yield - measured yield)^2/calculated yield
error.sum<-matrix(NA,n,m) #sum of errors chisq distribution

#search over the grid (A,K)
for (i in 1:n){
   for (j in 1:m) {
       for (k in 1:p) {
        yield.c[k]=((K[j]*acid-1)/A[i]+sqrt(((1-K[j]*acid)/A[i])^2+
        4*conc.t[k]*K[j]/A[i]^2))/(2*K[j]/A[i]^2)
        # root of (K/A^2)*x^2 +(1/A)*(1-K*acid)*x -[xt]=0
        error[k]<-(yield.c[k]-yield.e[k])^2/(yield.c[k])
                        }
     error.sum[i,j]<-sum(error)
                    }
}
```

```
apply(error.sum,2,min) #smallest error for each K value (changing A)
windows()
plot(K,apply(error.sum,2,min),xlab="Assciation Constant K",ylab="Error",
main="Best Association Constant K Selection")
windows()
plot(A,apply(error.sum,1,min),xlab="Fitting Parameter A",ylab="Error",
main="Best Fitting Parameter A Selection")
windows()
plot(A,apply(error.sum,1,min),xlim=c(50,200),ylim=c(0,7), xlab="Fitting
Parameter A",ylab="Error",main="Best Fitting Parameter A Selection")
Kmin_m<-which.min(apply(error.sum,2,min))
Kmin<-K[Kmin_m]
Kmin
Amin_n<-which.min(apply(error.sum,1,min))
Amin<-A[Amin_n]
Amin
error.sum[Amin_n,Kmin_m] #test statistic for selected fitting
1-pchisq(error.sum[Amin_n,Kmin_m],df=(p-2)) #p value of selected fitting
qchisq(0.95,df=(p-2))   # a=0.05 critical value for chisq dist
```

2. The following computer program in R was written to obtain the optimized value of ion pairing constants K_1 (assuming $K_2 = 0$) for 1-2-1 2X.

```
#Purpose: Association constant estimation (1-2-1 2Br) K2=0
#[HX]=1mM  chisq test    A=42.6
rm(list=ls(all=TRUE))


#Input data set
```

```
data<-read.csv(file.choose())
#conc.t(2*[1-2-1 2X]+[HX])     yield.e (experimental value of %1-ArX)
attach(data)
acid<-0.001                # 0.001M HX
plot(yield.e~conc.t,ylab="%1-ArX",xlab="[Xt]")

#define A, K, yield.c, error, error.sum
A<-42.6    #yield=A*[X-]
K<-seq(0.1,50,by=0.1)    #association constant of 1-2-1 2X
m<-length(K)
p<-nrow(data)     #number of data points
yield.c<-c(NA,p)  #calculated value of %1-ArX
error<-c(NA,p)    #(calculated yield - measured yield)^2/calculated yield
error.sum<-c(NA,m) #sum of errors chisq distribution

#search over the grid (A,K)
for (j in 1:m) {
       for (k in 1:p) {
        yield.c[k]=((0.5*K[j]*(conc.t[k]+acid)-1)/A+sqrt(((1-0.5*K[j]*acid-0.5
        *K[j]*conc.t[k])/A)^2+4*conc.t[k]*K[j]/A^2))/(2*K[j]/A^2)
        # root of (K/A^2)*x^2 +(1/A)*(1-0.5*K*([xt]+acid))*x -[xt]=0
        error[k]<-(yield.c[k]-yield.e[k])^2/(yield.c[k])
                        }
     error.sum[j]<-sum(error)
}

min(error.sum) #smallest error for each K value (changing A)
```

```
windows()
plot(K,error.sum,xlab="Assciation Constant K",ylab="Error",
main="Best Association Constant K Selection")
Kmin_m<-which.min(error.sum)
Kmin<-K[Kmin_m]
Kmin
error.sum[Kmin_m] #test statistic for selected fitting
1-pchisq(error.sum[Kmin_m],df=(p-1)) #p value of selected fitting
qchisq(0.95,df=(p-1))   # a=0.05 critical value for chisq dist
```

3. The following computer program in R was written to obtain the optimized value of ion pairing constants K_1 and K_2 at the same time for 1-2-1 2X, giving an estimation of $K_2 = 0.0013$.

```
#Purpose: Association constant K1 estimation (1-2-1 2Br)
#[HX]=1mM  A=42.6  tune both K1 and K2(0.0002~0.01)
rm(list=ls(all=TRUE))

#Input data set
data<-read.csv(file.choose())
#conc.t(2*[1-2-1 2X]+[HX])  yield.e (experimental value of %1-ArX)
attach(data)
plot(yield.e~conc.t,ylab="%1-ArX",xlab="[Xt]")

#Input variables
acid<-0.001               # 0.001M HX
A<-42.6                 # yield=A*[X-] calculated from TMAX data
```

```
K1<-seq(1.5,30,by=0.1)    #association constant K1
m<-length(K1)
K2<-seq(0.0002,0.01,by=0.0001 )
n<-length(K2)
p<-nrow(data)             #number of data points
yield.c<-array(NA,c(n,m,p))         #calculated value of %1-ArX
error<-c(NA,p) #(calculated yield-measured yield)^2/calculated yield
error.sum<-matrix(NA,n,m) #sum of errors, chisq dist

#Define Newton's Method (Give a real root of a polynomial function)
newton <- function(f, tol=1E-12,x0=1,N=20) {
        h <- 0.001
        i <- 1; x1 <- x0
        n <- numeric(N)
        while (i<=N) {
                df.dx <- (f(x0+h)-f(x0))/h
                x1 <- (x0 - (f(x0)/df.dx))
                n[i] <- x1
                i <- i + 1
                if (abs(x1-x0) < tol) break
                x0 <- x1
        }
        return(n[i-1])
}

#search over K1 K2
for (i in 1:n){
```

```
 for (j in 1:m) {
  for (k in 1:p) {
   f <- function(x) { K1[j]*K2[i]*(1/A)*x^3 + (K1[j]-K1[j]*K2[i]*acid)*
   (1/A^2)*x^2 + (1/A)*(1-0.5*K1[j]*(conc.t[k]+acid))*x - conc.t[k] }
   #cubic equation for yield.c
   yield.c[i,j,k]<- newton(f, x0=1, N=20)  #real root of the cubic equation
                  }
                 }
}
for (i in 1:n) {
    for(j in 1:m){
 if(all(yield.c[i,j,]>=0)) {
        error<-(yield.c[i,j,]-yield.e)^2/(yield.c[i,j,]) }
        error.sum[i,j]<-sum(error)
                 }
}
apply(error.sum,2,min) #smallest error for each K1 value (changing K2)
windows()
plot(K1,apply(error.sum,2,min),xlab="Assciation Constant K1",ylab="Error",
main="Best Association Constant K1 Selection")
windows()
plot(K2,apply(error.sum,1,min),xlab="Assciation Constant K2",ylab="Error",
main="Best Assciation Constant K2 Selection")
K1min_m<-which.min(apply(error.sum,2,min))
K1min<-K1[K1min_m]
K1min
K2min_n<-which.min(apply(error.sum,1,min))
```

```
K2min<-K2[K2min_n]
K2min
error.sum[K2min_n,K1min_m] #test statistic for selected fitting
1-pchisq(error.sum[K2min_n,K1min_m],df=(p-2)) #p value of selected fitting
qchisq(0.95,df=(p-2))   # a=0.05 critical value for chisq dist
```

4. The following computer program in R was written to obtain the ion pair concentrations in micellar interface of 10-2-10 2Br.

```
#Fractions of paired ions in the interfacial region of 10-2-10 2Br micelles

#Input data set
data<-read.csv(file.choose())  #conc Br.t
attach(data)
plot(Br.t~conc,ylab="Brm (M)",xlab="[10-2-10 2Br] (mM)")

p<-length(Br.t)
K1<- 10.9
K2<- 0
acid<- 0.001
beta<- 0.84
dicat.t<-c(NA,p)
Br.free<-c(NA,p)
dicat2<-c(NA,p)
dicatBr<-c(NA,p)
dicatBr2<-c(NA,p)
```

```
#Define Newton's Method (Give a real root of a polynomial function)
newton <- function(f, tol=1E-12,x0=1,N=20) {
        h <- 0.001
        i <- 1; x1 <- x0
        n <- numeric(N)
        while (i<=N) {
                df.dx <- (f(x0+h)-f(x0))/h
                x1 <- (x0 - (f(x0)/df.dx))
                n[i] <- x1
                i <- i + 1
                if (abs(x1-x0) < tol) break
                x0 <- x1
        }
        return(n[i-1])
}


for(k in 1:p)    {
dicat.t[k]<-(Br.t[k]-acid)/(2*beta)
f <- function(x) { K1*K2*x^3 + (K1+2*K1*K2*dicat.t[k]-K1*K2*Br.t[k])*x^2
                  + (1+K1*dicat.t[k]-K1*Br.t[k])*x - Br.t[k] }
Br.free[k]<- newton(f, x0=1, N=20)
dicat2[k]<-dicat.t[k]/(1+K1*Br.free[k]+K1*K2*Br.free[k]^2)
dicatBr[k]<-K1*Br.free[k]*dicat2[k]
dicatBr2[k]<-K2*Br.free[k]*dicatBr[k]
}
Br.free               #[Br-]
Br.free/Br.t          #fraction of free interfacial bromide ion
```

```
dicat2                #[dicat2+]

2*dicat2/Br.t         #fraction of free dication

dicatBr               #[(dicatBr)+]

dicatBr/Br.t          #fraction of monobromo dication pair

dicatBr2              #[dicatBr2]

2*dicatBr2/Br.t       #fraction of dibromo dication pair


dicatBr/(2*dicat.t)

#fraction of monobromo dication pair in the bulk solution (compare with MD )

2*dicatBr2/(2*dicat.t)

#fraction of dibromo dication pair in the bulk solution (compare with MD )
```

2.5.2 Tables

Table 2.23 lists observed rate constants, k_{obs}, half lives, $t_{1/2}$ values, and the squared correlation coefficients, R^2, for dediazonation reaction in 10-2-10 2X (X = Br, Cl, MsO, AcO, TFA) at 25.0 ^{o}C, with a separate run for CTAB run for comparison. The reactions were monitored for 4-5 $t_{1/2}$ at $\lambda = 284$ nm. The final 16-ArN_2^+ concentration were 1 x 10^{-4} M. The rate constant for AcO is almost four times faster than for the other reactions. This is probably caused by competing general base catalyzed bimolecular reactions.

Table 2.24 lists standard curves from reaction of 1-ArN_2^+ with X^- in 1-2-1 2X (X = I, Br, Cl, MsO, AcO) aqueous reference solutions.

Tables 2.25 and 2.26 list calibration curves for calcuation dediazoniation product yields.

Tables 2.27 and 2.28 list the chemical trapping results including HPLC peak areas, observed and normalized product yields and values for total X^-, H_2O concentration, selectivities, S_w^X and H_2O/X molar ratios in aqueous TMAI and TMABr solutions. The molarities of TMAI vary from 0 to 0.6 M, because higher concentrations phase separate at

50 ^{o}C.

Table 2.23: Dediazoniation rate constants, k_{obs}, half lives, $t_{1/2}$ values, and least squares fit, R^2, in various micellar solutions at 25.0 ^{o}C

Micellar Solutions	$10^5 k_{obs}$, s^{-1}	$t_{1/2}$, h	R^2
10 mM CTABr (1 mM HBr)	4.78	4.4	0.99995
10 mM 10-2-10 2Br (1 mM HBr)	3.91	4.9	0.99995
50 mM 10-2-10 2Cl (1 mM HCl)	3.97	4.9	0.99972
10 mM 10-2-10 2MsO (1 mM $MeSO_3H$)	3.17	6.0	0.99996
50 mM 10-2-10 2AcO (pH 5)	15.4	1.2	0.99447
10 mM 10-2-10 2TFA (1 mM CF_3COOH)	2.59	7.4	0.99998

Table 2.24: Standard curves from reaction of 1-ArN_2^+ with X^- in 1-2-1 2X (X = I, Br, Cl, MsO, AcO) aqueous reference solutions. (See Figure 2.2)

Micellar Solutions	Standard Curves[a]	R^2	Temp (^{O}C)
1-2-1 2I (1 mM HI)	Y = -1.986 X^2 + 21.691 X + 8.456	0.9990	50
1-2-1 2Br (1 mM HBr)	Y = 9.380 X + 7.6296	0.9980	25
1-2-1 2Cl (1 mM HCl)	Y = 7.708 X + 4.618	0.9955	25
1-2-1 2MsO (1 mM $MeSO_3H$)	Y = 8.735 X + 1.523	0.9993	25
1-2-1 2AcO (pH 6)	Y = 2.663 X - 0.270	0.9988	25

[a] Units: Y-normalized product yields, %1-ArX, (%); X-counterion concentration, [X^-], (M).

Table 2.25: Linear calibration equations for long-chain dediazoniation products.[a]

Reaction Products[a]	Calibration Equations[b]	R^2
16-ArI	Y = 1.542 x 10^{11}X	1.0000
16-ArCl	Y = 1.087 x 10^{11}X	1.0000
16-ArOMs	Y = 6.701 x 10^{10}X	0.9998
16-ArOAc	Y = 9.338 x 10^{10}X	1.0000
16-ArBr[c]	Y = 1.393 x 10^{11}X + 14530	1.0000
16-ArOH[c]	Y = 1.000 x 10^{11}X - 28660	0.9998
16-ArH[c]	Y = 9.883 x 10^{10}X + 14590	1.0000
16-ArInd[c]	Y = 1.404 x 10^{11}X + 249000	0.9980

[a] HPLC Eluting solvent: 35%/65% v/v, *i*-PrOH/MeOH (except 16-Ind: 40%/60%, v/v; 16-ArOMs: 20%/80%, v/v). Flow rate: 0.4 ml/min. Detector wavelength: 220 nm. Injection volume: 100 μL .

[b] Units: Y-peak area (in μv•s), X-concentration (in molarity), and R^2.

[c] Ref:[109]

Table 2.26: Linear calibration equations for short-chain dediazoniation products.

Reaction Products[a]	Calibration Equations[c]	R^2
1-ArI	Y = 5.436 x 10^{10}X	0.9998
1-ArCl	Y = 1.178 x 10^{10}X	0.9996
1-ArOMs[b]	Y = 6.459 x 10^{9}X	0.9999
1-ArOAc	Y = 3.965 x 10^{9}X	1.0000
1-ArOH	Y = 1.300 x 10^{10}X	0.9995
1-ArOH[b]	Y = 1.822 x 10^{10}X	1.0000
1-ArBr	Y = 2.321 x 10^{10}X + 14530	0.9998

[a] HPLC Eluting solvent: 80%/20% v/v, MeOH/H_2O. Flow rate: 0.6 ml/min. Detector wavelength: 230 nm. Injection volume: 50 μL .

[b] HPLC Eluting solvent: 55%/45% v/v, MeCN/H_2O. Flow rate: 0.4 ml/min. Detector wavelength: 230 nm. Injection volume: 50 μL .

[c] nits: Y-peak area (in μv•s), X -concentration (in molarity), and R^2.

Table 2.27: HPLC peak areas, observed and normalized (subscript N) product yields for dediazoniation of 1-ArN_2^+ in aqueous TMABr solutions at 25 ^{o}C and 1 mM HBr, and values for total Br^-, water concentration, selectivities, S_w^{Br} and H_2O/Br molar ratios.[a]

$[Br_t]$[b] (M)	$[H_2O]$ (M)	Peak Area[c] (10^6 μv•s)		Observed Yields (%)			Normalized Yields[d] (%)		S_w^{Bre}	$[H_2O]/[Br_t]$
		1-ArOH	1-ArBr	1-ArOH	1-ArBr	Total	1-ArOH_N	1-ArBr_N		
0.011	55.5	12.042	0.132	95.0	0.58	95.6	99.4	0.61	30.9	5044
0.021	55.4	11.708	0.228	92.4	1.01	93.4	98.9	1.08	28.8	2639
0.036	55.3	11.980	0.366	92.8	1.59	94.4	98.3	1.68	26.3	1536
0.054	55.2	11.803	0.514	91.4	2.23	93.7	97.6	2.38	25.0	1022
0.071	55.1	12.253	0.602	94.9	2.61	97.5	97.3	2.68	21.4	775
0.088	55.0	11.940	0.742	92.5	3.22	95.7	96.6	3.36	21.7	625
0.101	54.9	12.015	0.836	91.0	3.55	94.5	96.2	3.75	21.4	549
0.201	54.2	11.717	1.400	88.7	5.94	94.7	93.7	6.27	18.1	271
0.301	53.5	11.239	1.831	85.1	7.77	92.9	91.6	8.36	16.3	178
0.501	52.2	10.629	2.777	85.5	12.5	98.0	87.2	12.8	15.3	104
1.000	48.8	9.185	3.968	73.9	17.9	91.8	80.5	19.5	11.8	48.8
1.500	45.4	7.722	5.198	63.4	23.9	87.3	72.6	27.4	11.4	30.3
2.000	42.1	7.795	6.332	62.7	28.5	91.3	68.7	31.3	9.57	21.0
2.500	38.7	6.670	7.496	54.8	34.5	89.2	61.4	38.6	9.75	15.5
3.000	35.3	6.031	8.435	49.5	38.8	88.3	56.1	43.9	9.23	11.8
3.500	32.0	5.518	9.366	45.3	43.1	88.4	51.3	48.7	8.68	9.13

a. Reaction time ca. 48 hours. The concentrations of 1-ArN_2^+ were around 4 x 10^{-3} M but vary in each experiment. 100 μL of cyclohexane was layered on top of 1-2-1 2Cl solutions in 2 mL volumetric flasks to prevent the evaporation of 1-ArBr. Prior to HPLC analysis, the product mixture was diluted 5 fold with methanol to dissolve both the cyclohexane and the aqueous salt solution.
b. $[Br_t]$ = [TMABr]
c. 50 μL sample injections. Peak areas are average of triplicate injections. Eluting solvents: 80%MeOH/20%H_2O; Flow rate: 0.6 mL/min; Detector wavelength: 230 nm.
d. % 1-ArBr_N = 100 (%1-ArBr)/(%1-ArOH + %1-ArBr); % 1-ArOH_N = 100 (%1-ArOH)/(%1-ArOH + %1-ArBr).
e. $S_w^{Br} = [H_2O](\%1\text{-ArBr})/[Br_t](\%1\text{-ArOH})$.

Table 2.28: HPLC peak areas, observed and normalized (subscript N) product yields for dediazoniation of 1-ArN_2^+ in aqueous TMAI solutions at 50 ^{o}C and 1 mM HI, and values for total I^-, water concentration, selectivities, S_w^I and H_2O/I molar ratios.[a]

$[I_t]$[b] (M)	$[H_2O]$ (M)	Peak Area[c] (10^6 μv•s)		Observed Yields (%)			Normalized Yields[d] (%)		S_w^I[e]	$[H_2O]/[I_t]$
		1-ArOH	1-ArI	1-ArOH	1-ArI	Total	1-ArOH_N	1-ArI_N		
0.02	55.4	1.980	0.158	83.8	1.6	85.5	98.1	1.9	52.9	2772
0.04	55.2	2.004	0.308	84.9	3.1	88.0	96.5	3.5	50.8	1381
0.05	55.2	1.894	0.354	82.3	3.7	86.0	95.7	4.3	49.3	1103
0.06	55.1	2.069	0.431	87.6	4.4	92.0	95.3	4.7	45.8	918
0.08	54.9	1.993	0.536	84.4	5.4	89.8	94.0	6.0	44.2	687
0.09	54.9	1.974	0.584	85.8	6.1	91.8	93.4	6.6	43.1	610
0.10	54.8	1.887	0.622	79.9	6.3	86.2	92.7	7.3	43.2	548
0.15	54.4	2.066	0.913	86.4	9.1	95.5	90.4	9.6	38.4	363
0.20	54.0	1.944	1.065	82.3	10.8	93.1	88.4	11.6	35.4	270
0.30	53.3	1.658	1.308	75.9	14.3	90.2	84.1	15.9	33.5	178
0.40	52.5	1.621	1.530	74.2	16.7	91.0	81.6	18.4	29.6	131
0.50	51.7	1.532	1.750	70.1	19.2	89.3	78.5	21.5	28.3	103
0.60	51.0	1.584	2.098	72.5	23.0	95.5	75.9	24.1	26.9	85.0

a. Reaction time ca. 7 hours. The concentrations of 1-ArN_2^+ were around 4 x 10^{-3} M but vary in each experiment. 100 μL of cyclohexane was layered on top of 1-2-1 2I solutions in 2 mL volumetric flasks to prevent the evaporation of 1-ArI. Prior to HPLC analysis, the product mixture was diluted 25 fold with methanol/H_2O to dissolve both the cyclohexane and the aqueous salt solution.
b. $[I_t]$ = [TMAI]
c. 50 μL sample injections. Peak areas are average of triplicate injections. Eluting solvents: 80%MeOH/20%H_2O; Flow rate: 0.6 mL/min; Detector wavelength: 230 nm.
d. % 1-ArI_N = 100 (%1-ArI)/(%1-ArOH + %1-ArI); % 1-ArOH_N = 100 (%1-ArOH)/(%1-ArOH + %1-ArI).
e. $S_w^I = [H_2O](\%1\text{-ArI})/[I_t](\%1\text{-ArOH})$.

Chapter 3

Determination of Interfacial Molarities in 10-2-10 2X/NaX (X = MsO, Cl, Br) Solutions

3.1 Introduction

Many surfactant properties such as the cmc, sphere-to-rod transition, Krafft temperature, and degree of ionization depend not only on surfactant structure but also on surfactant counterion type. The ion specific effects on 10-2-10 2X gemini surfactant were investigated in Chapter 2, but the sphere-to-rod transition, usually induced by added salts, were not discussed. In this chapter, the ion specific effects are further elucidated by chemical trapping in 10-2-10 2X (X = MsO, Cl, Br) aqueous solutions in the present of added corresponding salts NaX (X = MsO, Cl, Br, respectively).

The chemical trapping experiments were applied to cetyltrialkylammonium bromide [(CTRA)X, R = Me, Et, n-Pr, and n-Bu] and cetyltrimethylammonium chloride (CTACl) in the present of added TMABr or TMACl, respectively.[99] The estimates of interfacial counterion molarities were successfully fitted in a two-site pseudophase ion exchange (PIE) model showing that, in a system of surfactant aggregates with added salts, the interfacial counterion concentration is the essentially sum of the aqueous counterion concentration and the concentration of counterions contributed by surfactant headgroups within the interfacial region. Also, the interfacial counterion molarities for CTMABr and CTACl increase significantly at their respective sphere-to-rod transitions ca. 0.1 M [Br_w] and ca. 1.2 M [Cl_w]. However, interfacial molarities in the present of added counterion salts have not been estimated for gemini surfactants nor more hydrophilic counterion as MsO^-. Here, the

interfacial counterion, X_m and water, H_2O_m, molarities are estimated by chemical trapping method in 10-2-10 2X/NaX (X = MsO, Cl, Br) solutions. The dependence of X_m and H_2O_m on the counterion concentration in the aqueous pseudophase, $[X_w]$ are investigated by using the two-site PIE model. The increase of interfacial counterion molarities with added counterion salt follow the order: $Br^- > Cl^- > MsO^-$. Moreover, the three counterions show complete different pattern in plots of interfacial counterion molarities, X_m, versus, counterion concentration in the aqueous pseudophase, $[X_w]$ estimated by assuming a value for alpha.

3.2 Results and Discussion

3.2.1 Interfacial molarities estimated by chemical trapping in 10-2-10 2X/NaX (X = MsO, Cl, Br) solutions

Tables 3.2-3.4 in the Appendix list chemical trapping results from the dediazoniation of 16-ArN_2^+ in aqueous 10-2-10 2X (X = MsO, Cl, Br) solutions containing variable amounts of NaX and 1 mM HX (X = MsO, Cl, Br) at 25 ^{o}C. Included in Tables 3.2-3.4 are the HPLC average peak areas, observed product yields, and normalized yields, and the estimated interfacial molarities of counterions and water, denoted as X_m and H_2O_m respectively. Note that 1 mM of HX (X = MsO, Cl, Br) was added to control the solution acidity. The observed yields of 16-ArOH and 16-ArX (X = MsO, Cl, Br) were calculated from HPLC peak areas and their calibration curves are listed in Table 2.25. The total yields combining the observed yields of 16-ArOH and 16-ArX were above 88%. All of the product yields were normalized to minimize experimental error. The footnotes give the reaction conditions and the HPLC conditions.

Figures 3.1-3.3 show the interfacial molarities of counterion, X_m, water, H_2O_m, and their ratio, H_2O_m/X_m, obtained from chemical trapping results in 10-2-10 2X gemini solutions in the presence and absence of the added corresponding salt NaX (X=MsO, Cl, Br). The

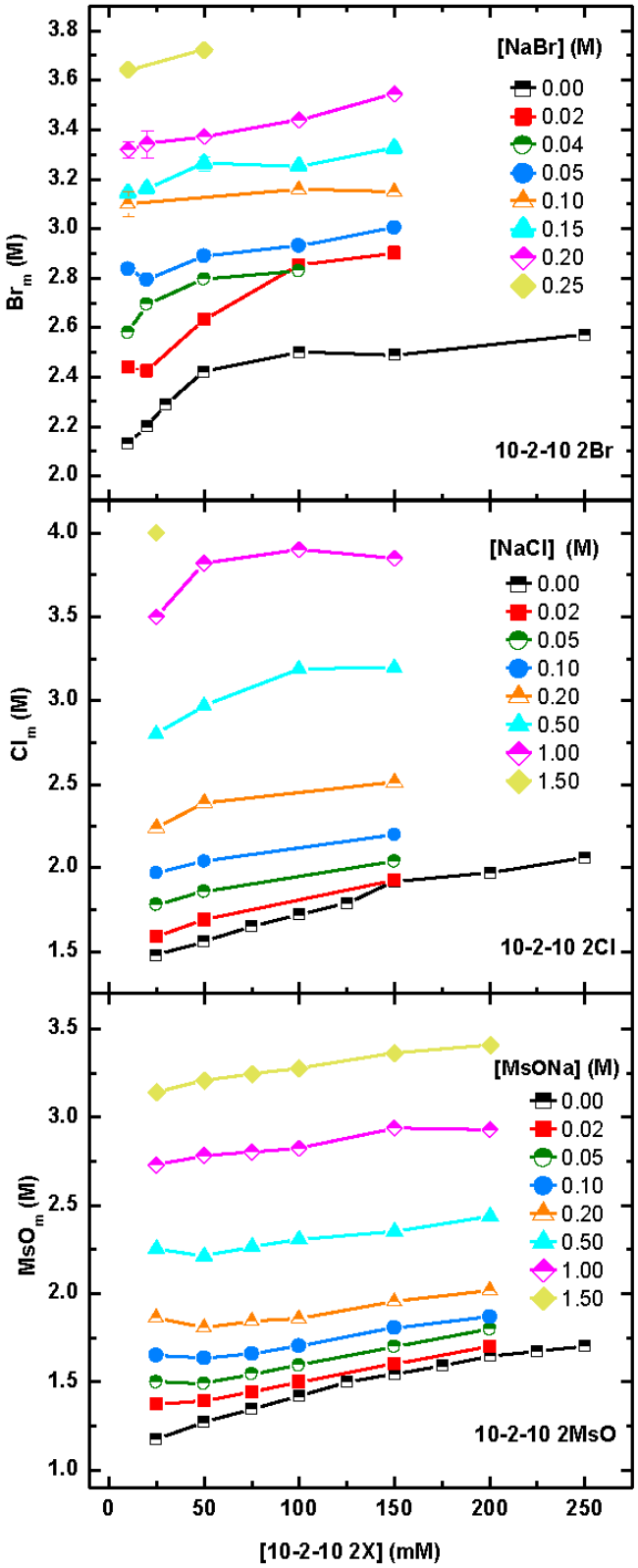

Figure 3.1: Effect of increasing stoichiometric concentration of 10-2-10 2X and NaX (X=MsO, Cl, Br) on interfacial molarities of counterions,X_m, at 25 ^{o}C. Lines are drawn to aid the eye.

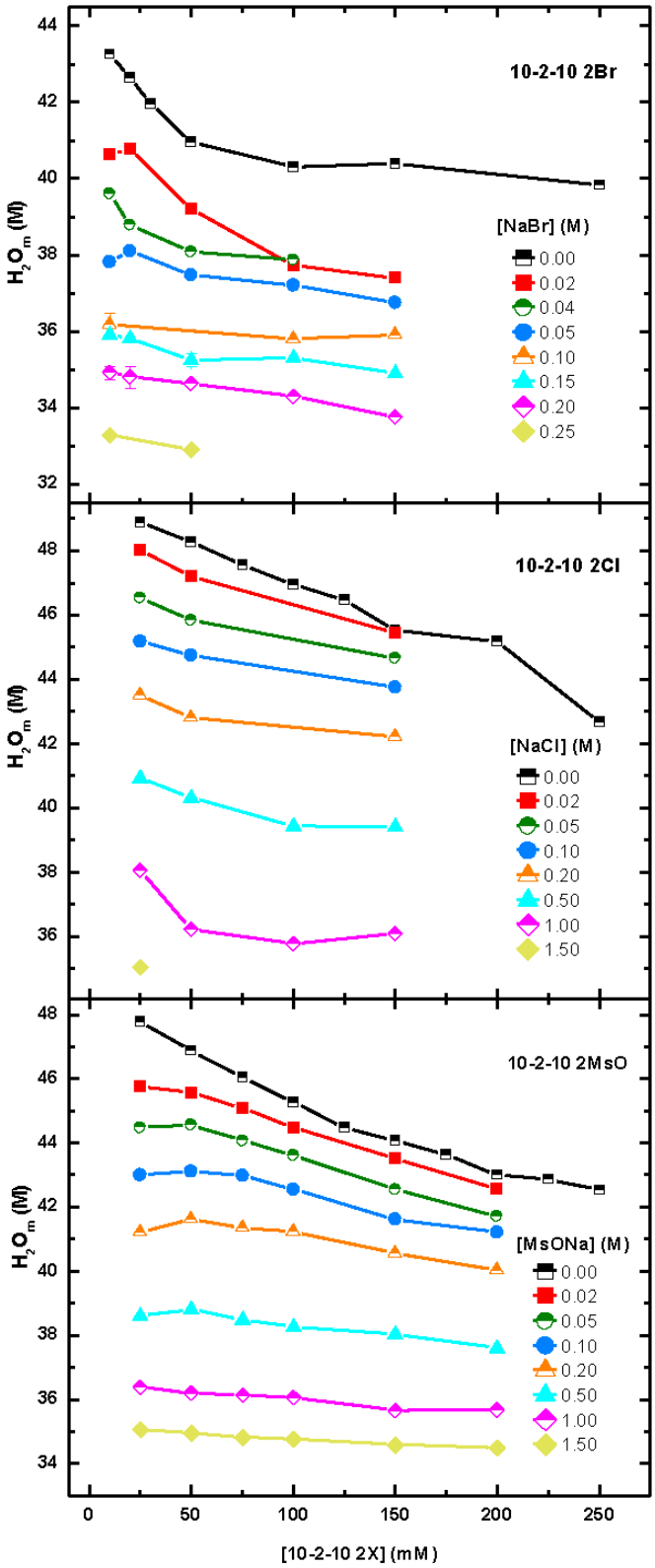

Figure 3.2: Effect of increasing stoichiometric concentration of 10-2-10 2X and NaX (X=MsO, Cl, Br) on interfacial molarities of water,H_2O_m, at 25 ^{o}C. Lines are drawn to aid the eye.

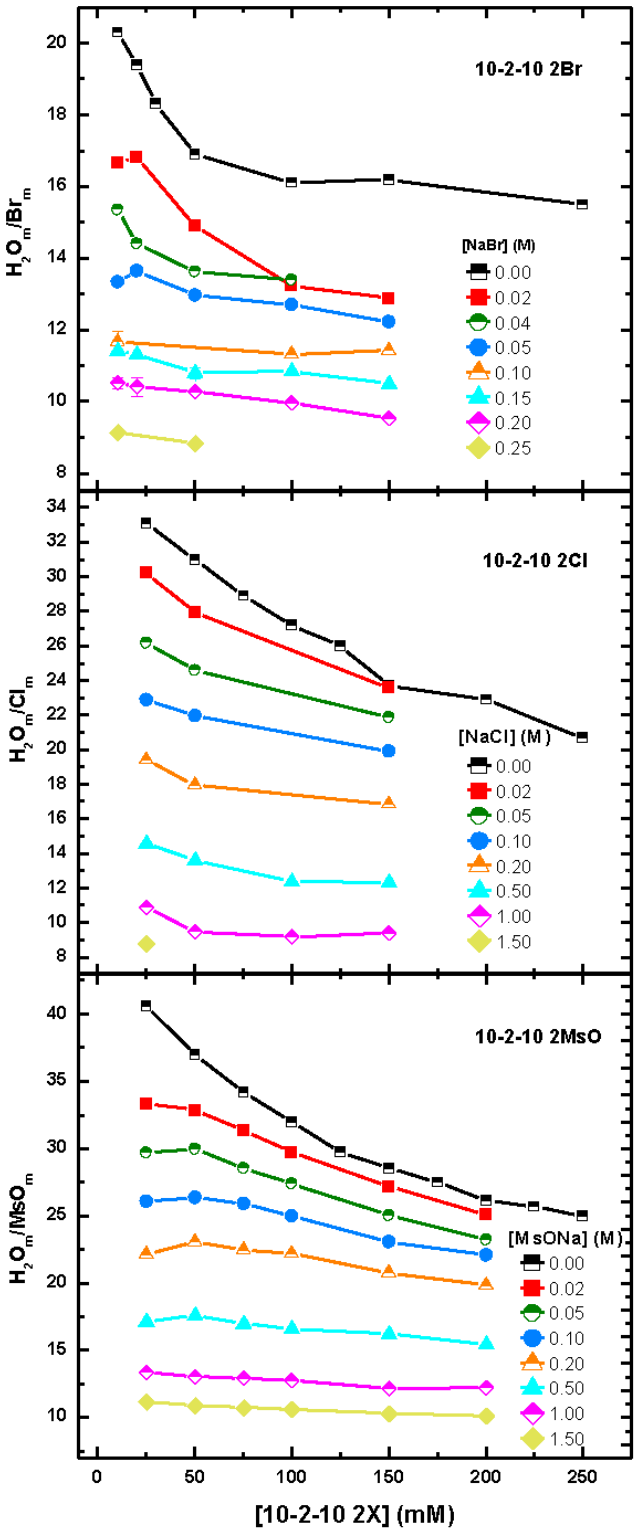

Figure 3.3: Effect of increasing stoichiometric concentration of 10-2-10 2X and NaX (X=MsO, Cl, Br) on H_2O_m/X_m, at 25 °C. Lines are drawn to aid the eye.

interfacial molarities of counterions, X_m,and water, H_2O_m, were estimated, by the same method described in Chapter 2, using the standard curves listed in Table 2.24 and chemical trapping results, listed in Tables 2.2-2.5, from reaction of 1-ArN_2^+ in 1-2-1 2X (X = MsO, Cl, Br) aqueous reference solutions. These figures clearly show: (a) X_m increases gradually as the surfactant concentration increases; (b) X_m increases with added salt; (c) the increases follow the order $Br^- > Cl^- > MsO^-$; for example, to obtain interfacial molarities of 3.5 M, the final concentration of NaBr, NaCl, and MsONa, added to the corresponding 10-2-10 2X gemini solutions were 0.2 M, 1.0 M, and 1.5M, respectively; (d) the corresponding H_2O_m (and H_2O_m/X_m) in those solutions follow the opposite order.

However, the detailed patterns for MsO^-, Cl^-, and Br^- are also completely different. For MsO^-, X_m (and H_2O_m) basically lie on a series of almost parallel lines. Increasing [MsONa] produces a nearly incremental increase in X_m and a proportional decrease in H_2O_m. The pattern for Cl^- is similar to MsO^- when [NaCl] is below 0.2 M. However, when [NaCl] is above 0.5 M, X_m (H_2O_m) deviate from the linear trends by increasing (decreasing) more rapidly. For 1.5 M added NaCl, the chemical trapping experiments could not be carried out when surfactant concentration above 25 mM because of precipitation. For Br^-, there is a rapid increase in X_m (decrease in H_2O_m) at low [NaBr] concentration ($\leq$ 0.04 M) and even in the absence of added salt. The increase in X_m (decrease in H_2O_m) slows down at relative higher [NaBr] concentration. The 10-2-10 2Br solutions were opaque with $\geq$ 0.2 M added NaBr, and stirred to prevent phase separation. Experiments could not be carried out for surfactant concentration above 50 mM when [NaBr] $>$ 0.25 M because of precipitation also. The rapid increases in X_m (decrease in H_2O_m) for 10-2-10 2Cl/NaCl and 10-2-10 2Br/NaBr may correspond to the formation of rodlike micelles. These results are consistant with the increase of viscosity in 10-2-10 2Cl solutions with 1 M added NaCl, and 150 mM 10-2-10 2Br micellar solution in the absence of added NaBr. The overlapping concentration obtained by Alla was 78 and 377 mM for 10-2-10 2Br and 10-2-10 2Cl, respectively.[92]

3.2.2 Dependence of interfacial molarities X_m and H_2O_m on the counterion concentration in the aqueous pseudophase, [X_w]: a two-site pseudophase model

Table 3.1: Values of cmc, ionization degree, α, molar volumes of anhydrous surfactant, V, for 10-2-10 2X (X = MsO, Cl, Br) surfactants

Surfactant	cmc (mM)	α^a	α^b	V (L/mol)
10-2-10 2MsO	15.3	0.23	0.2	0.589
10-2-10 2Cl	12.8	0.21	0.2	0.470
10-2-10 2Br	6.5	0.15	0.2	0.558

[a] ref [92] (Evans' method)
[b] Value of α gives the smoothest curve in Figures 3.4-3.6.

The counterion concentration in the surrounding aqueous pseudophase, [X_w], for 10-2-10 2X/NaX solutions can be calculated by using Equation 3.1:

$$[X_w] = \frac{2\alpha\{[10-2-10 \quad 2X] - cmc\} + 2 * cmc + [NaX] + [HX]}{1 - V * \{[10-2-10 \quad 2X] - cmc\})} \tag{3.1}$$

where V is the molar volume of the anhydrous surfactant in moles per liter assuming that the density of the surfactants is ca. 1.0 g/mL.[99] This term works as a volume correction because micelles occupy a significant fraction of the total solution. Values of cmc were estimated by conductivity measurements by Alla.[92] Values of α for 10-2-10 2X were estimated by treating α as a disposable parameter in Equation 3.1 and selecting the best α that gives the smoothest curves in the plots of X_m versus [X_w] (X= MsO, Cl, Br), Figures 3.4-3.6. For α values between 0.2 and 0.3, all MsO_m values fall on a smooth curve, but for larger or smaller α values the data are significantly more dispersed. $\alpha = 0.2$ was chosen as the optimal values for 10-2-10 2MsO because it is close to values obtained by conductivity measurement.[92] Similarly, we choose $\alpha = 0.2$ as the optimal values for 10-2-10 2Cl and 10-2-10 2Br, and plot the X_m versus [X_w] and H_2O_m versus [X_w] results for MsO^-, Cl^-, and Br^- in Figures 3.7, 3.8, and 2.18, respectively. Note, variation in $\alpha(\pm 0.1)$ has only a small effect on the shapes of the curves, and the interpretation is not sensitive to the precise value of α.[99] Values of cmc, α, and V are summarized in Table 3.1.

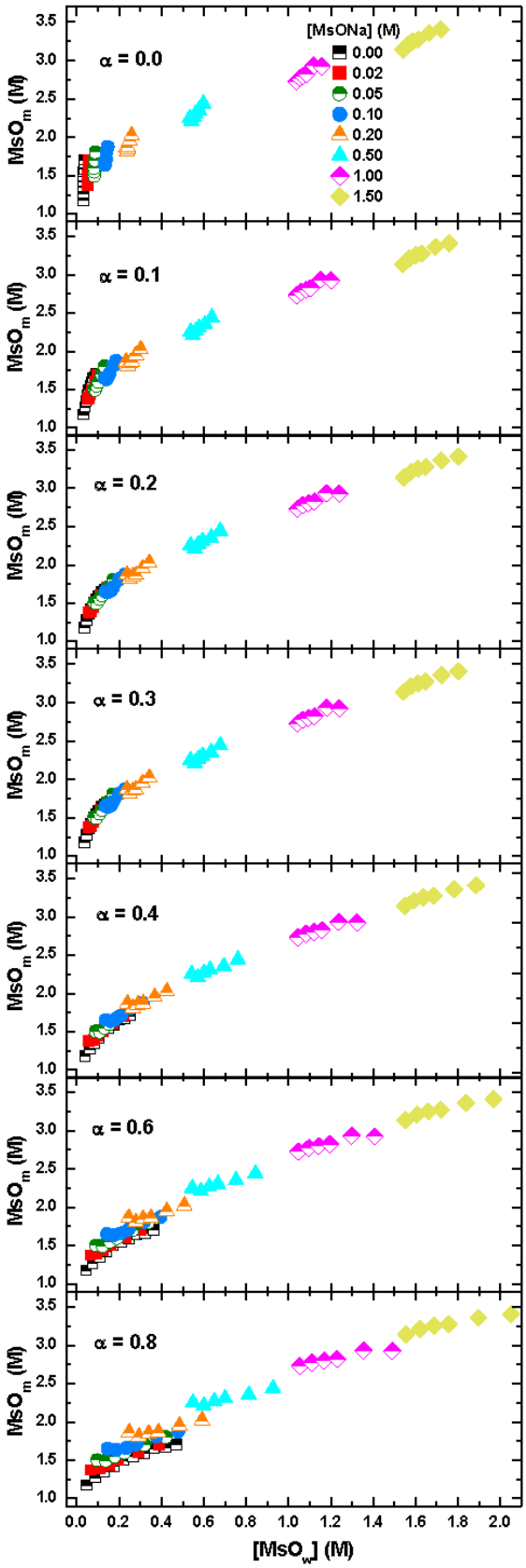

Figure 3.4: Effect of increasing the degree of ionization, α, in 10-2-10 2MsO/MsONa solutions on plots of the interfacial MsO^- concentration, MsO_m, versus the concentration of MsO^- in the aqueous pseudophase, $[MsO_w]$. $[MsO_w]$ was obtained by using Equation 3.1

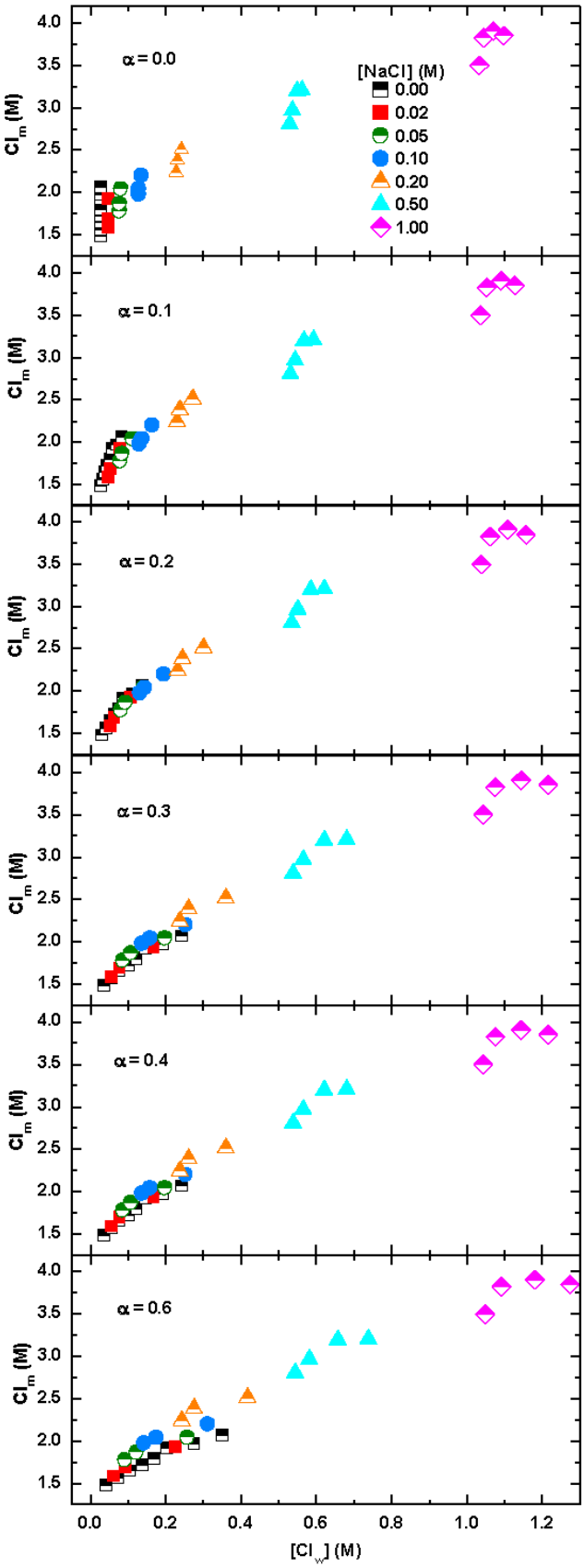

Figure 3.5: Effect of increasing the degree of ionization, α, in 10-2-10 2Cl/NaCl solutions on plots of the interfacial Cl^- concentration, Cl_m, versus the concentration of Cl^- in the aqueous pseudophase, $[Cl_w]$. $[Cl_w]$ was obtained by using Equation 3.1

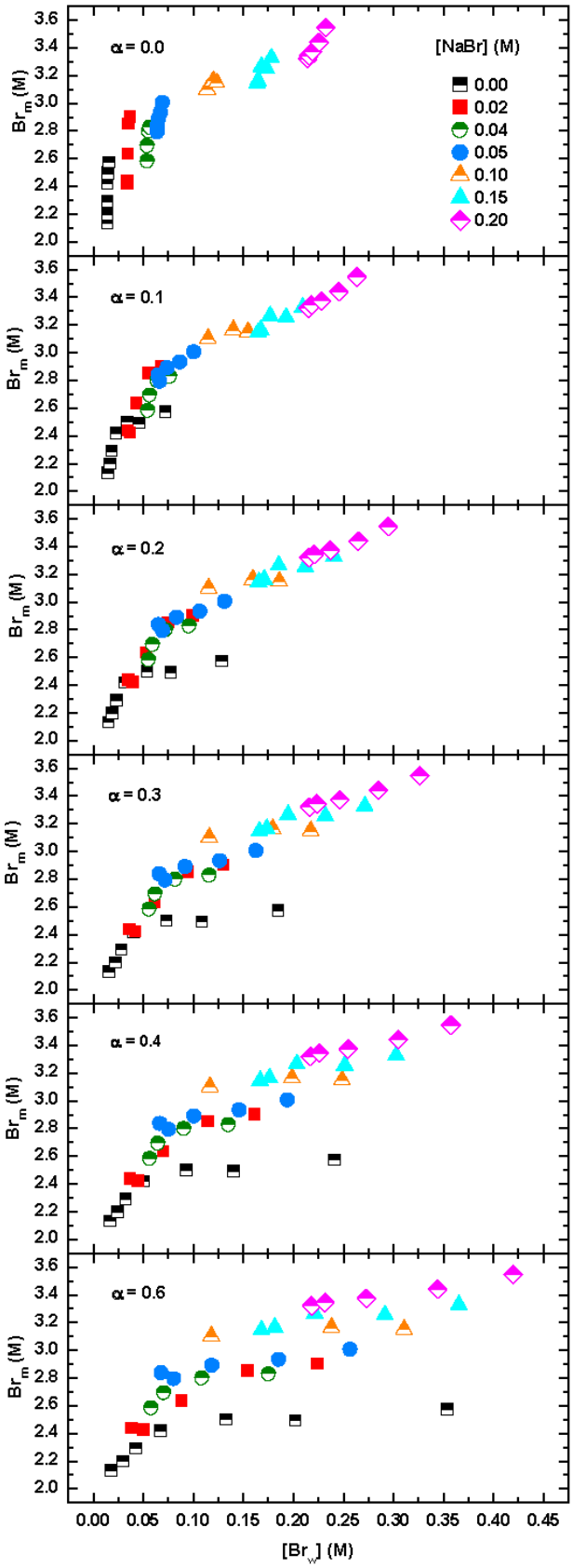

Figure 3.6: Effect of increasing the degree of ionization, α, in 10-2-10 2Br/NaBr solutions on plots of the interfacial Br^- concentration, Br_m, versus the concentration of Br^- in the aqueous pseudophase, $[Br_w]$. $[Br_w]$ was obtained by using Equation 3.1

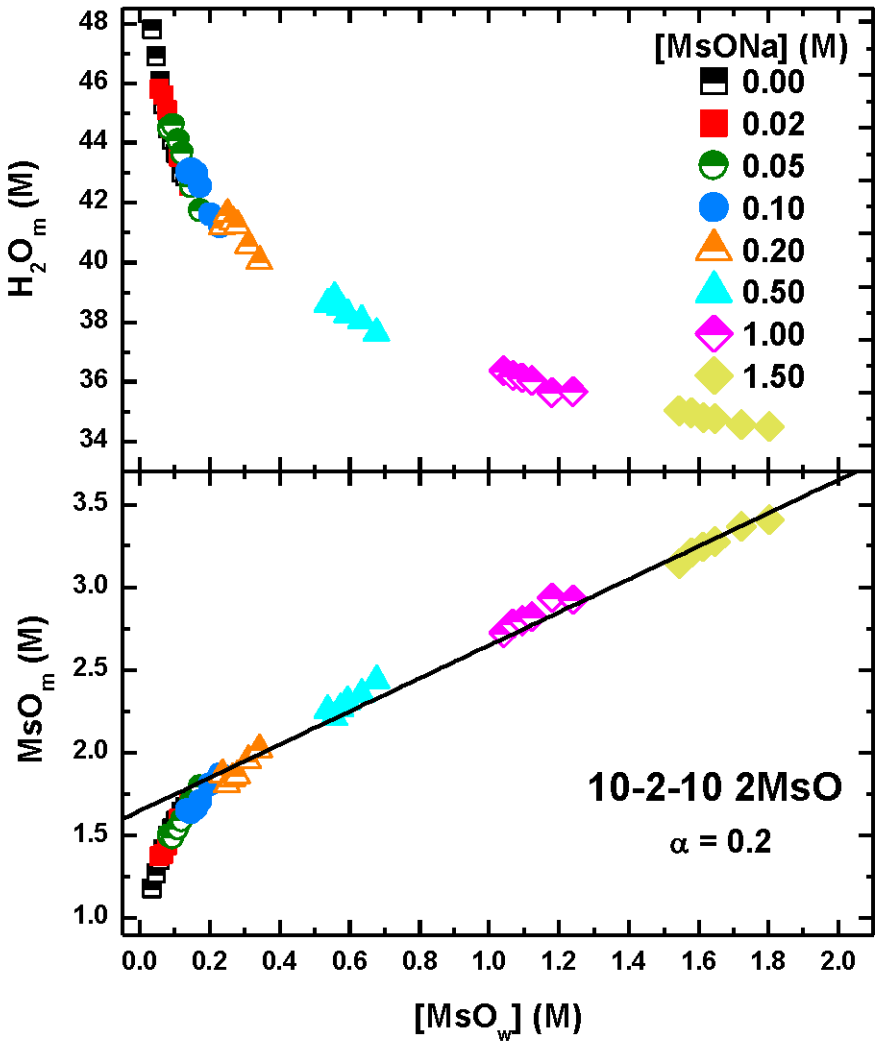

Figure 3.7: Plots of MsO_m and H_2O_m versus $[MsO_w]$ at the optimal α value (See Figure 3.4) of 0.2 for 10-2-10 2MsO/MsONa solutions. $[MsO_w]$ was obtained by using Equation 3.1. The straight line has a slope of 1 and the intercept was selective to give optimal contact with the linear portion of the curve.

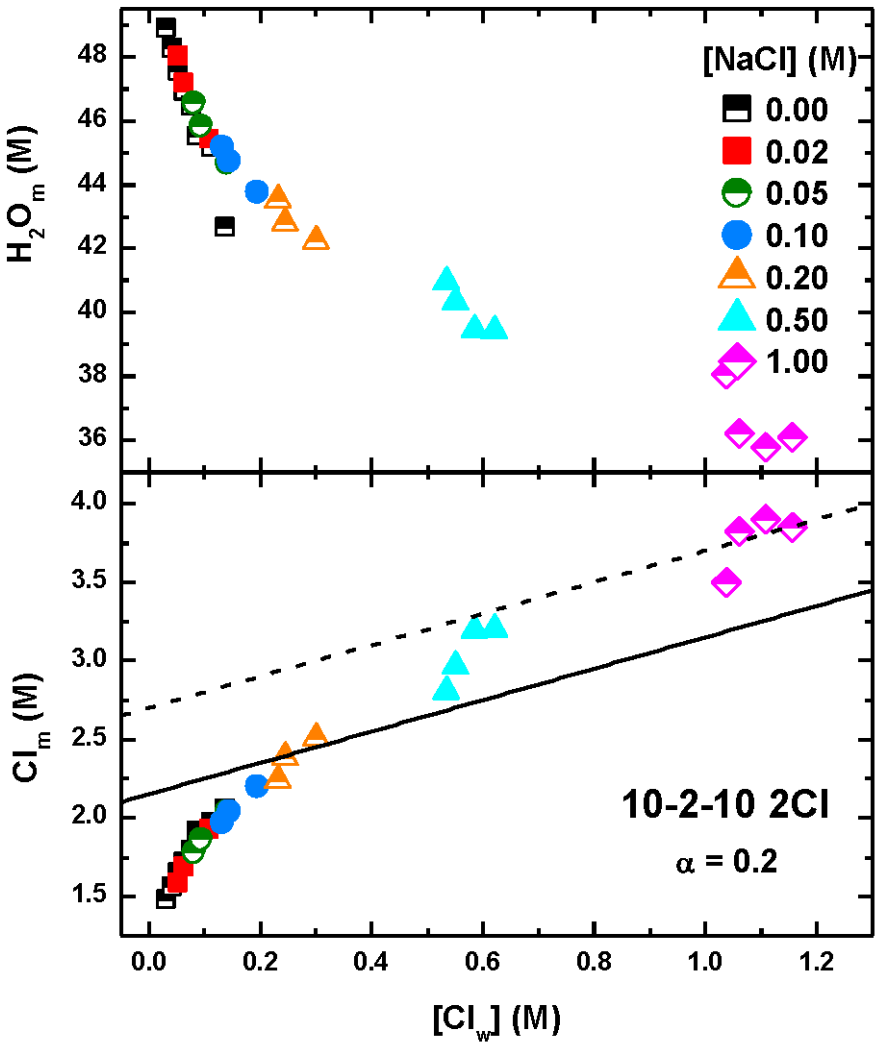

Figure 3.8: Plots of Cl_m and H_2O_m versus $[Cl_w]$ at the optimal α value (See Figure 3.5) of 0.2 for 10-2-10 2Cl/NaCl solutions. $[Cl_w]$ was obtained by using Equation 3.1. The straight line has a slope of 1 and the intercept was selective to give optimal contact with the linear portion of the curve. Note break from smooth curve above 0.5 M $[Cl_w]$.

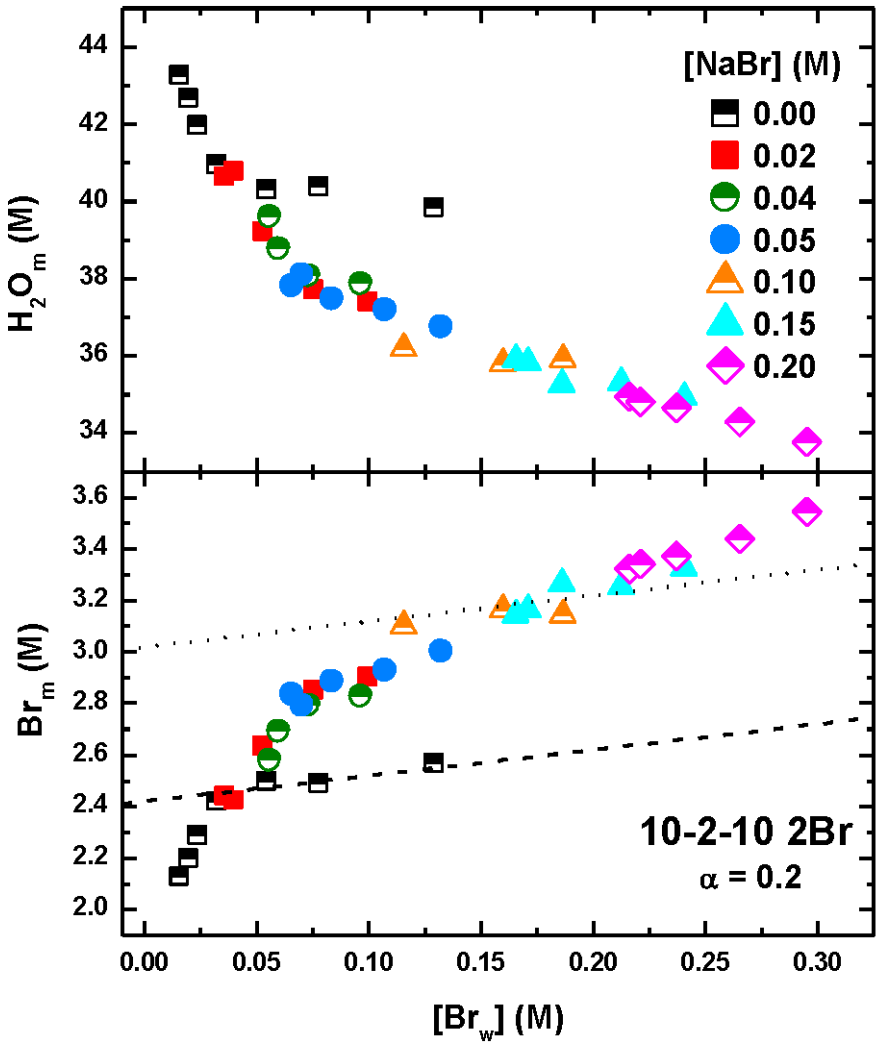

Figure 3.9: Plots of Br_m and H_2O_m versus $[Br_w]$ at the optimal α value (See Figure 3.4) of 0.2 for 10-2-10 2Br/NaBr solutions. $[Br_w]$ was obtained by using Equation 3.1. The straight line has a slope of 1 and the intercept was selective to give optimal contact with the linear portion of the curve. Note break from smooth curve above 0.04 M $[Br_w]$.

Figures 3.7-3.9 show the plots of interfacial molarities of counterions, X_m, and water, H_2O_m, against the counterion concentrations in the surrounding aqueous pseudophase, $[X_w]$ for MsO^-, Cl^-, and Br^-, respectively. Again, the results for MsO^-, Cl^-, and Br^- show different patterns. MsO_m and H_2O_m values, in Figure 3.7, fall on a single curve, whereas discontinuities shows for Cl^- and Br^- in Figures 3.8 and 3.9, respectively. Below 0.2 M $[MsO_w]$, MsO_m increase (and H_2O_m decrease) more rapidly with increasing $[MsO_w]$ than at higher $[MsO_w]$ concentration. Above 0.2 M $[MsO_w]$, MsO_m increases approximately linearly with increasing $[MsO_w]$, and interestingly the data can be fitted with a slope 1.0. For Cl^-, Cl_m and H_2O_m deviate from the smooth curve above ca. 0.5 M $[Cl_w]$, and the selection of the intercept for the fitting line with a slope of 1.0 is more arbitrary. The result is more complicated for Br^-. In the absence of added NaBr, the data above 0.04 M $[Br_w]$ can be fitted by a dashed line with slope 1.0; Whereas in the presence of added NaBr, Br_m increase (and H_2O_m decrease) rapidly with increasing $[Br_w]$ until ca. 0.1 M $[Br_w]$. A dotted line with slope 1.0 was drawn arbitrarily on the figure to be compared to the MsO^- and Cl^- results.

The results in Figures 3.7-3.9 can be interpreted by a modified two-site PIE model.[99] In the original PIE model, the interfacial counterion molarities was defined by Equation 3.2:

$$X_m = \frac{[X_m]}{[D_n]V_m} = \frac{\beta}{V_m} \tag{3.2}$$

were [ ] indicate concentration in moles per liter of total solution volume; $[X_m]$ is the molarity of counterion within the micelle; $[D_n]$, $[D_t]$ - cmc, is the molarity of micellized surfactant; V_m is the interfacial volume; and β (1- α) is the degree of counterion binding. However, in the presence of added salt, X_m can be defined, by the modified two-site PIE model, as the sum of the interfacial and aqueous counterion concentrations within the interfacial region in Equation 3.3:

$$X_m = \frac{[X_m]}{[D_n]V_m} + [X_w] = \frac{\beta}{V_m} + [X_w] \tag{3.3}$$

where an additional term, $[X_w]$ is added to Equation 3.2 assuming that the concentration of

counterions in the aqueous pseudophase extends up to the hydrocarbon core of the micelles. First, the results in Figures 3.7-3.9 shows that interfacial counterion concentration is a function of [X_w], which is consistant with Equation 3.3. Second, if we assume that both β and V_m are constant, or as least the term β/V_m is constant, the plot of X_m versus [X_w] would be a straight line with slope of 1.0 according to Equation 3.3. The linear increase of MsO_m with the increase of [MsO_w] above 0.2 M [MsO_w] in Figure 3.7 support this assumption for the higher concentration range of 10-2-10 2MsO/MsONa solutions. Above about 0.2 M [MsO_w], the primary contribution to the increase in MsO_m appears to be from added X_w. Third, a salt-induced contraction in the interfacial volume, V_m,[122, 123, 124] and a relative stable β[94, 125, 126, 127, 128] lead to the initial rapid increase in X_m in Figures 3.7-3.9. Fourth, the rapid increase in Cl_m and, therefore, deviation from the line with slope of 1.0 above ca. 0.5 M [Cl_w] in Figure 3.8 may correspond to the increase in β (or decrease in α) in sphere to rod transition.[129] Cl_m appear to approach a new line with slope 1.0 after the transition. Similarly, the rapid change in Br_m above 0.04 M [Br_w] in the present of added NaBr may be also attributed to β increase, and therefore increase in packing through other transitions.

3.3 Conclusions

The chemical trapping method was used to characterize the interfacial region of 10-2-10 2X (X = MsO, Cl, and Br) gemini surfactant solutions in the present of added counterion salts NaX (X = MsO, Cl, and Br, respectively). The interfacial counterion molarities increase with added salt, and follow the Hofmeister series: Br > Cl > MsO. The corresponding interfacial water molarities follow the opposite order. The dependence of the interfacial counterion molarities, X_m, on the estimated counterion concentration in the aqueous pseudophase, [X_w], was discussed by a two-site pseudophase model. The increase of MsO_m in higher concentration range with the increase of [MsO_w] fell on a straight line with slope of 1.0 supports the assumption that the counterion concentration in the aqueous pseudophase

extend up to the interfacial region of the micelle. The discontinuities shown in the plots of Br_m and Cl_m versus $[Br_w]$ and $[Cl_w]$, respectively, may correspond to increase in β indicating sphere-to-rod transition or other aggregate transitions.

3.4 Experimental

3.4.1 General method

HPLC measurements were performed on a Perkin-Elmer Series 200 equipped with a UV/Vis detector, a Varian Microsorb MV C18 column (length, 25 cm; particle size, 5 μm), and a computer-controlled Perkin-Elmer 600 Series Interface.

3.4.2 Materials

All aqueous solutions were prepared from water that was distilled, passed over activated carbon, an ion exchange resin and then redistilled. All solvents, MeCN, *i*-PrOH, MeOH, were of the highest commercially available reagent grade. 10-2-10 2X (X=MsO, Cl, Br) were synthesized by our collaborator, Alla Malinenko, based on the procedure developed by Manet et al for the syntheses of 14-2-14 2X.[70, 92] The chemical trapping probe salts 1-ArN_2BF_4 and 16-ArN_2BF_4 were prepared as needed by a previously developed synthetic procedure.[81] Reaction products 16-ArX, (X = MsO, Cl, Br), 16-ArOH, which were used to create needed calibration curves, were either commercially available or prepared by established procedures.[81, 90] The preparation of 16-ArOMs was described in Figure 2.18. NaX (X = MsO, Cl, Br) salts were reagent grade (Sigma-Aldrich) and used as received.

3.4.3 Chemical trapping with 16-ArN_2^+ in aqueous 10-2-10 2X/NaX (X = MsO, Cl, Br) solutions

The reaction was initiated by adding 10-20 μL freshly prepared stock solutions of 16-ArN_2BF_4 dissolved in ice-cold MeCN to 1-2 mL of the aqueous mixture of 10-2-10 2X and NaX of the needed concentration, 1 mM HX, and a final probe concentration of 1-2.5

x 10^{-4} M. The volumetric flasks were sealed and thermostated at 25 ^{o}C for 2 days. The 10-2-10 2Br/NaBr mixture were opaque in the present of $\geq$ 0.2 M NaBr, and these solutions were stirred during reaction. Otherwise, phase separation in those solutions were observed in 10 hours. Prior to HPLC analysis, some of the product mixtures were diluted 4-5 fold with MeCN because of their heterogenous property or high viscosity. Conditions for product separation on the HPLC for Br^- and Cl^- were: a 65% MeOH/35% i-PrOH (v/v) mobile phase; flow rate = 0.4 ml/min; detector = 220 nm; and the injection volume was 100 μL. For MsO^-, the mobile phase were changed to 80% MeOH/20% i-PrOH (v/v); whereas the flow rate, detector wavelengh, and the injection volume remain the same. Percent yields were obtained from average values of peak areas from triplicate or duplicate injections with the appropriate calibration curves.

3.5 Appendix

Table 3.2: HPLC Average peak areas, observed yields and normalized yields (subscript N) for reaction of 16-ArN_2^+ in 10-2-10 2MsO / MsONa solutions and estimated interfacial concentrations of MsO^-, MsO_m, water, H_2O_m at 25 ^{o}C.[$MeSO_3H$]=1 mM.[a]

[MsONa]	[10-2-10 2MsO]	Average Peak Areas[b]		Observed Yields			Normalized Yields		MsO_m	H_2O_m	$\underline{H_2O_m}$
(M)	(mM)	(10^6 μv•s)		(%)			(%)		(M)	(M)	MsO_m
		16-ArOH	16-ArOMs	16-ArOH	16-ArOMs	Total	16-ArOH_N	16-ArOMs_N			
0.00	25	11.24	1.02	85.4	11.5	96.9	88.1	11.9	1.18	47.79	40.6
0.00	50	11.32	1.10	86.0	12.4	98.4	87.4	12.6	1.27	46.88	37.0
0.00	75	11.29	1.16	85.7	13.1	98.9	86.7	13.3	1.35	46.05	34.2
0.00	100	11.27	1.22	85.6	13.8	99.4	86.1	13.9	1.42	45.29	32.0
0.00	125	11.46	1.31	87.0	14.8	102	85.5	14.5	1.50	44.49	29.7
0.00	150	11.47	1.36	87.1	15.4	102	85.0	15.0	1.54	44.06	28.6
0.00	175	11.42	1.40	86.7	15.8	102	84.6	15.4	1.59	43.64	27.5
0.00	200	11.39	1.45	86.5	16.4	103	84.1	15.9	1.65	43.01	26.1
0.00	225	11.36	1.47	86.3	16.6	103	83.9	16.1	1.67	42.87	25.7
0.00	250	11.00	1.45	83.6	16.4	100	83.7	16.3	1.70	42.54	25.0
0.02	25	22.21	2.34	84.6	13.3	97.8	86.5	13.5	1.37	45.77	33.4
0.02	50	10.36	1.10	85.8	13.6	99.4	86.4	13.6	1.39	45.58	32.9
0.02	75	9.69	1.07	83.1	13.6	96.7	85.9	14.1	1.44	45.09	31.3
0.02	100	9.91	1.14	82.2	14.1	96.2	85.4	14.6	1.50	44.49	29.7

Table 3.2 – continued from previous page

[MsONa] (M)	[10-2-10 2MsO] (mM)	Average Peak Areas[b] (10^6 μv•s)		Observed Yields (%)			Normalized Yields (%)		MsO_m (M)	H_2O_m (M)	$\frac{H_2O_m}{MsO_m}$
		16-ArOH	16-ArOMs	16-ArOH	16-ArOMs	Total	16-ArOH$_N$	16-ArOMs$_N$			
0.02	150	9.89	1.22	82.0	15.1	97.1	84.5	15.5	1.60	43.53	27.2
0.02	200	9.92	1.31	82.2	16.1	98.4	83.6	16.4	1.70	42.55	25.1
0.05	25	22.48	2.59	85.6	14.7	100	85.4	14.6	1.50	44.48	29.7
0.05	50	10.23	1.17	84.8	14.4	99.2	85.5	14.5	1.49	44.59	30.0
0.05	75	9.66	1.15	82.8	14.6	97.5	85.0	15.0	1.54	44.06	28.6
0.05	100	9.97	1.22	82.7	15.1	97.8	84.6	15.4	1.59	43.63	27.4
0.05	150	9.94	1.31	82.4	16.2	98.6	83.6	16.4	1.70	42.55	25.0
0.05	200	8.92	1.25	73.9	15.4	89.3	82.8	17.2	1.80	41.73	23.2
0.10	25	21.22	2.71	80.8	15.4	96.2	84.1	15.9	1.65	43.00	26.1
0.10	50	10.34	1.31	85.7	16.1	102	84.2	15.8	1.64	43.11	26.4
0.10	75	9.92	1.27	85.1	16.2	101	84.0	16.0	1.66	42.98	25.9
0.10	100	10.33	1.36	85.6	16.8	102	83.6	16.4	1.70	42.54	25.0
0.10	150	10.01	1.41	83.0	17.4	100	82.7	17.3	1.81	41.62	23.1
0.10	200	10.31	1.51	85.4	18.6	104	82.2	17.8	1.87	41.21	22.0
0.20	25	21.30	3.11	81.1	17.6	98.8	82.2	17.8	1.86	41.22	22.1
0.20	50	10.05	1.41	83.3	17.4	101	82.7	17.3	1.81	41.62	23.0

Table 3.2 – continued from previous page

[MsONa] (M)	[10-2-10 2MsO] (mM)	Average Peak Areas[b] (10^6 μv•s)		Observed Yields (%)			Normalized Yields (%)		MsO_m (M)	H_2O_m (M)	$\frac{H_2O_m}{MsO_m}$
		16-ArOH	16-ArOMs	16-ArOH	16-ArOMs	Total	16-ArOH$_N$	16-ArOMs$_N$			
0.20	75	9.66	1.39	82.8	17.7	101	82.4	17.6	1.84	41.36	22.4
0.20	100	9.91	1.44	82.1	17.8	100	82.2	17.8	1.86	41.23	22.2
0.20	150	9.53	1.46	79.0	18.1	97.0	81.4	18.6	1.95	40.56	20.8
0.20	200	9.78	1.56	81.1	19.2	100	80.8	19.2	2.02	40.04	19.8
0.50	25	20.93	3.79	79.7	21.5	101	78.8	21.2	2.25	38.60	17.1
0.50	50	9.36	1.66	77.6	20.4	98.0	79.2	20.8	2.21	38.81	17.6
0.50	75	9.28	1.69	79.5	21.6	101	78.7	21.3	2.26	38.48	17.0
0.50	100	9.61	1.79	79.7	22.1	102	78.3	21.7	2.31	38.27	16.6
0.50	150	9.11	1.74	75.6	21.4	97.0	77.9	22.1	2.35	38.04	16.2
0.50	200	9.35	1.86	77.5	22.9	100	77.2	22.8	2.44	37.61	15.4
1.00	25	19.95	4.56	76.0	25.9	102	74.7	25.3	2.73	36.39	13.3
1.00	50	10.57	2.47	76.2	26.6	103	74.2	25.8	2.78	36.21	13.0
1.00	75	10.20	2.41	73.6	25.9	99.5	74.0	26.0	2.80	36.13	12.9
1.00	100	10.06	2.40	72.6	25.8	98.4	73.8	26.2	2.82	36.06	12.8
1.00	150	10.25	2.58	74.0	27.7	102	72.8	27.2	2.94	35.64	12.1
1.00	200	4.67	1.17	75.7	28.2	104	72.9	27.1	2.93	35.68	12.2

Table 3.2 – continued from previous page

[MsONa] (M)	[10-2-10 2MsO] (mM)	Average Peak Areas[b] (10^6 μv•s)		Observed Yields (%)			Normalized Yields (%)		MsO_m (M)	H_2O_m (M)	$\frac{H_2O_m}{MsO_m}$
		16-ArOH	16-ArOMs	16-ArOH	16-ArOMs	Total	16-ArOH_N	16-ArOMs_N			
1.50	25	9.50	2.61	68.5	28.0	96.5	71.0	29.0	3.14	35.06	11.2
1.50	50	9.39	2.65	67.7	28.5	96.2	70.5	29.5	3.21	34.96	10.9
1.50	75	9.62	2.76	69.4	29.7	99.1	70.1	29.9	3.25	34.81	10.7
1.50	100	9.31	2.70	67.2	29.0	96.2	69.9	30.1	3.28	34.78	10.6
1.50	150	8.41	2.54	65.4	29.4	94.9	69.0	31.0	3.36	34.58	10.3
1.50	200	4.36	1.34	70.8	32.2	103	68.7	31.3	3.41	34.49	10.1

a. Reaction time ca. 48 hours to ensure that dediazoniation reaction is complete. Measured yields are based on the weighed amount of 16-ArN_2^+ which varys between 0.5 - 2 x 10^{-4} M.

b. 100 μL sample injections. Peak areas are average of triplicate injections. Eluting solvents: 80%MeOH/20%H_2O; Flow rate: 0.4 mL/min; Detector wavelength: 220 nm.

Table 3.3: HPLC Average peak areas, observed yields and normalized yields (subscript N) for reaction of 16-ArN_2^+ in 10-2-10 2Cl / NaCl solutions and estimated interfacial concentrations of Cl^-, Cl_m, water, H_2O_m at 25 ^oC.[HCl]=1 mM.[a]

[NaCl]	[10-2-10 2Cl]	Average Peak Areas[b]		Observed Yields			Normalized Yields		Cl_m	H_2O_m	$\frac{H_2O_m}{Cl_m}$
(M)	(mM)	(10^6 μv•s)		(%)			(%)		(M)	(M)	
		16-ArOH	16-ArCl	16-ArOH	16-ArCl	Total	16-ArOH_N	16-ArCl_N			
0.00	25	9.09	1.90	77.2	14.8	92.6	84.0	16.0	1.48	48.90	33.1
0.00	50	9.55	2.08	83.3	16.6	100	83.4	16.6	1.56	48.27	31.0
0.00	75	9.48	2.16	82.7	17.3	100	82.7	17.3	1.65	47.55	28.9
0.00	100	9.54	2.28	83.2	18.2	102	82.1	17.9	1.72	46.94	27.2
0.00	125	9.67	2.38	84.3	19.0	104	81.6	18.4	1.79	46.46	26.0
0.00	150	9.71	2.55	76.7	18.5	95.6	80.6	19.4	1.92	45.53	23.7
0.00	200	9.68	2.62	76.4	19.0	95.8	80.2	19.8	1.97	45.18	22.9
0.00	250	9.53	2.69	75.2	19.5	95.3	79.5	20.5	2.06	42.68	20.7
0.02	25	9.66	2.13	78.1	15.8	93.9	83.1	16.9	1.59	48.02	30.2
0.02	50	10.53	2.46	78.2	16.7	94.9	82.4	17.6	1.69	47.19	37.9
0.02	150	8.52	2.25	74.3	18.0	92.3	80.5	19.5	1.93	45.44	23.6
0.05	25	9.46	2.31	76.5	17.2	93.7	81.7	18.3	1.78	46.54	26.2
0.05	50	10.74	2.74	79.8	18.7	98.5	81.0	19.0	1.86	45.38	24.6
0.05	150	8.36	2.33	72.9	18.6	91.6	79.6	20.4	2.04	44.67	21.9

Table 3.3 – continued from previous page

0.10	25	9.04	2.44	73.1	18.1	91.2	80.2	19.8	1.97	45.17	22.9
0.10	50	10.51	2.92	78.1	19.9	98.0	79.7	20.3	2.04	44.75	21.9
0.10	150	8.19	2.46	71.5	19.7	91.1	78.4	21.6	2.20	43.76	19.9
0.20	25	8.82	2.69	71.3	20.0	91.3	78.1	21.9	2.24	43.51	19.4
0.20	50	10.23	3.33	76.0	22.7	98.7	77.0	23.0	2.39	42.81	17.9
0.20	150	8.06	2.77	70.3	22.1	92.4	76.1	23.9	2.51	42.22	16.8
0.50	25	8.35	3.24	67.5	24.0	91.6	73.8	26.2	2.80	40.94	14.6
0.50	50	11.56	4.77	85.8	32.5	118	72.5	27.5	2.97	40.32	13.6
0.50	100	9.57	4.31	71.1	29.3	100	70.8	29.2	3.19	39.44	12.3
0.50	150	7.38	3.33	64.4	26.7	91.1	70.7	29.3	3.20	39.42	12.3
1.00	25	3.67	1.85	59.6	27.5	87.1	68.4	31.6	3.50	38.05	10.9
1.00	50	4.26	2.41	63.1	32.6	95.7	65.9	34.1	3.82	36.23	9.48
1.00	100	4.27	2.48	63.2	33.6	96.7	65.3	34.7	3.90	35.78	9.17
1.00	150	3.44	1.97	65.4	34.1	99.6	65.7	34.3	3.85	36.08	9.37
1.50	25	3.57	2.51	58.1	31.9	89.9	64.6	35.4	4.00	35.06	8.77

a. Reaction time ca. 48 hours to ensure that dediazoniation reaction is complete. Measured yields are based on the weighed amount of 16-ArN_2^+ which varys between in 0.5 - 1 x 10^{-4} M.

b. 100 μL sample injections. Peak areas are average of triplicate injections. Eluting solvents: 65%MeOH/35%*i*-PrOH; Flow rate: 0.4 mL/min; Detector wavelength: 220 nm.

Table 3.4: HPLC Average peak areas, observed yields and normalized yields (subscript N) for reaction of 16-ArN_2^+ in 10-2-10 2Br / NaBr solutions and estimated interfacial concentrations of Br^-, Br_m, water, H_2O_m at 25 ^oC.[HBr]=1 mM.[a]

[NaBr]	[10-2-10 2Br]	Average Peak Areas[b]		Observed Yields			Normalized Yields		Br_m	H_2O_m	$\frac{H_2O_m}{Br_m}$
(M)	(mM)	(10^6 μv•s)		(%)			(%)		(M)	(M)	
		16-ArOH	16-ArBr	16-ArOH	16-ArBr	Total	16-$ArOH_N$	16-$ArBr_N$			
0.00	10	7.83	4.27	69.1	26.8	98.3	72.4	27.6	2.13	43.27	20.3
0.00	20	8.14	4.55	71.8	28.6	102	71.7	28.3	2.20	42.66	19.4
0.00	30	7.81	4.55	68.9	28.6	99.0	70.9	29.1	2.29	41.96	18.3
0.00	50	8.48	5.23	74.8	32.9	109	69.7	30.3	2.42	40.96	16.9
0.00	100	6.94	4.67	56.7	27.2	91.3	68.9	31.1	2.50	40.31	16.1
0.00	150	3.22	2.23	53.0	25.9	88.3	69.0	31.0	2.49	40.39	16.2
0.00	250	3.14	2.35	51.6	27.3	93.5	68.3	31.7	2.57	39.84	15.5
0.02	10	3.29	2.05	70.9	31.2	102	69.4	30.6	2.44	40.64	16.7
0.02	20	3.33	2.06	65.5	28.7	94.2	69.6	30.4	2.42	40.77	16.8
0.02	50	3.29	2.23	67.0	32.1	99.1	67.6	32.4	2.63	39.21	14.9
0.02	100	3.20	2.38	63.1	33.2	96.3	65.5	34.5	2.85	37.71	13.2
0.02	150	3.24	2.46	63.8	34.3	98.1	65.1	34.9	2.90	37.40	12.9
0.04	10	3.28	2.00	70.8	30.5	101	68.1	31.9	2.58	39.60	15.3

Table 3.4 – continued from previous page

0.04	20	3.00	2.09	64.5	31.7	96.2	67.0	33.0	2.69	38.78	14.4
0.04	50	2.98	2.17	64.0	32.9	96.9	66.1	33.9	2.80	38.09	13.6
0.04	100	2.62	1.93	56.3	29.3	85.6	65.8	34.2	2.83	37.87	13.4
0.05	10	3.30	2.44	64.9	33.9	98.9	65.7	34.3	2.84	37.81	13.3
0.05	20	3.02	2.19	61.8	31.7	93.6	66.1	33.9	2.79	38.10	13.6
0.05	50	3.14	2.37	63.9	34.1	98.0	65.2	34.8	2.89	37.48	13.0
0.05	100	2.95	2.27	60.5	32.9	93.4	64.8	35.2	2.93	37.21	12.7
0.05	150	2.92	2.31	59.8	33.5	93.3	64.1	35.9	3.00	36.75	12.2
0.10	10	3.60	3.00	64.5	38.2	103	62.8	37.2	3.14	35.95	11.4
0.10	10	2.82	2.27	58.9	33.5	92.4	63.7	36.3	3.04	36.52	12.0
0.10	10	3.01	2.49	59.3	34.7	94.1	63.1	36.9	3.12	36.09	11.6
0.10	100	3.06	2.58	60.2	36.0	96.2	62.6	37.4	3.16	35.80	11.3
0.10	150	4.94	4.12	76.7	45.5	122	62.8	37.2	3.15	35.91	11.4
0.15	10	2.83	2.38	58.0	34.4	92.4	62.8	37.2	3.15	35.91	11.4
0.15	20	2.79	2.36	57.2	34.2	91.4	62.6	37.4	3.16	35.81	11.3
0.15	50	3.00	2.62	61.2	37.7	98.8	61.9	38.1	3.24	35.37	10.9
0.15	50	2.97	2.63	58.5	36.7	95.2	61.5	38.5	3.28	35.13	10.7
0.15	100	2.80	2.46	57.5	35.6	93.0	61.8	38.2	3.25	35.31	10.8
0.15	150	2.75	2.48	56.3	35.9	92.2	61.1	38.9	3.32	34.91	10.5

Table 3.4 – continued from previous page

0.20	10	3.39	3.02	63.3	40.0	103	61.3	38.7	3.31	35.02	10.6
0.20	10	2.63	2.41	55.0	35.5	90.5	60.8	39.2	3.36	34.74	10.3
0.20	10	2.88	2.57	56.7	35.8	92.5	61.3	38.7	3.30	35.04	10.6
0.20	20	2.74	2.45	56.1	35.5	91.6	61.3	38.7	3.31	35.02	10.6
0.20	20	2.94	2.71	58.1	37.8	95.9	60.6	39.4	3.38	34.61	10.2
0.20	50	2.90	2.66	59.0	38.3	97.4	60.6	39.4	3.37	34.65	10.3
0.20	100	2.67	2.52	54.7	36.4	91.1	60.0	40.0	3.44	34.30	9.97
0.20	150	2.66	2.61	54.5	37.9	92.4	59.0	41.0	3.54	33.77	9.53
0.25	10	2.51	2.56	52.4	37.8	90.1	58.1	41.9	3.64	33.29	9.14
0.25	50	2.79	2.94	56.9	42.3	99.2	57.3	42.7	3.72	32.90	8.84

a. Reaction time ca. 48 hours to ensure that dediazoniation reaction is complete. Measured yields are based on the weighed amount of 16-ArN_2^+ which varys between 0.5 - 1 x 10^{-4} M.

b. 100 μL sample injections. Peak areas are average of triplicate injections. Eluting solvents: 65%MeOH/35%*i*-PrOH; Flow rate: 0.4 mL/min; Detector wavelength: 220 nm.

Chapter 4

Salt Induced Micelle-to-vesicle Transitions in Aqueous AOT Solutions

4.1 Introduction

Thermodynamically stable vesicles form spontaneously on mixing oppositely charged surfactants, producing catanionic aggregates, at relatively low concentrations in water. Examples include spontaneous formation of catanionic vesicles by mixing cetyl trimethylammonium tosylate (CTAT) and sodium dodecyl benzene sulfonate (SDBS),[11] dodecyltrimethylammonium bromide (DTAB) and sodium dodecyl sulfate (SDS),[42] and cetyltrimethylammonium bromide (CTAB) and sodium octyl sulfate (SOS) in well-defined ratios.[41, 130] Vesicle formation also occurs by mixing ordinary salt into bi-chained surfactant solutions[131] or salts containing hydrophobic counterions into single-chain surfactant[132, 133]. Typically, in both surfactant mixtures and salt/surfactant mixtures, a mesophase of worm-like micelles are formed between micellar and vesicular mesophases.[41, 130]

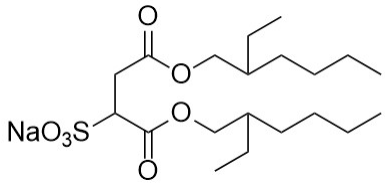

Figure 4.1: Chemical structure of AOT

Sodium bis(2-ethyl hexyl)sulfosuccinate (AOT), Figure 4.1, is an anionic double-chained surfactant. The phase diagram of AOT-NaCl-water system has been studied for more than three decades.[134, 135, 136] The kinetics of micelle-to-vesicle transition after addition of

NaCl, NaBr, KCl, and KBr in a micellar solution of AOT was also investigated.[40] Recently, the micelle-to-vesicle transition of aqueous AOT solution induced by tetraalkylammonium bromide (TAAB, where alkyl = ethyl (TEABr), propyl (TPABr) and butyl (TBABr)) and NH_4Cl was studied by Ismail's group using multiple techniques including small-angle neutro scattering (SANS) and dynamic light scattering (DLS).[137] The results show that 15 mM aqueous AOT solutions in the presence of TEABr/TPABr/TBABr/NH_4Cl undergo a transition from prolate-ellipsoid micelles, to a coexisting mixture of rodlike micelle and vesicle, to vesicles. Detailed results are summarized in Tables 4.1 and 4.2. The micelle-to-vesicle transitions of 15 mM AOT solutions in the presence of TBABr, TPABr, TEABr, and NH_4Cl begin when salt concentration reaches approximately 5, 10, 15, and 9 mM, respectively.

Table 4.1: Micellar parameters obtained by fitting the SANS data for 15 mM AOT in the presence of varying concentrations of salts using the prolate-ellipsoidal shape model.[137]

Salt	Salt concentration (mM)	Semi-major axis ($\AA$)	Semi-minor axis ($\AA$)	Aggregation number
NH_4Cl	0	29.7	12.6	30.0
	5	27.9	12.6	30.4
TEABr	1	24.4	12.6	26.5
	5	29.0	12.6	31.5
	10	39.4	12.6	42.8
TPABr	1	24.3	12.6	26.4
	3	33.9	12.6	37.0
TBABr	0.3	25.1	12.6	28.2
	0.5	31.8	12.6	34.6
	1.0	25.9	12.6	28.2

Although the micelle-to-vesicle transition have been widely characterized, the changes in the balance of forces controlling the transition of aggregate morphologies remain an unsolved problem. The critical salt concentration (CSC) for the micelle-to-vesicle transition in AOT depend on cation type, indicating an specific effect on micelle-to-vesicle transition shifting the delicated balance of forces controlled by ion-pairing and hydration interaction in the interfacial region. Evidences showing the interfacial hydration changes during the miecelle-to-vesicle transitions in the AOT/salt aqueous solutions are provided by chemical

Table 4.2: Micellar parameters obtained by fitting the SANS data for 15 mM AOT in the presence of varying concentrations of salts using different shape models.[137]

Salt	Salt concentration (mM)	Model	Thickness of vesicle ($\AA$)	Radius of rod ($\AA$)
NH_4Cl	9	Rods and ULV[a]	15.3	12.6
	15	Rods and ULV	23.8	12.6
TEABr	15	Rods and ULV	20.2	12.6
TPABr	10	ULV	15.8	-
	15	ULV	17.0	-
TBABr	5	Rods and ULV	18.0	12.6
	10	ULV	17.9	-

[a] unilamellar vesicles.

trapping method in this chapter. The reasons to choose AOT/salt system are: (a) this is a relative simple and well-studied system for micelle-to-vesicle transition as described in the last paragraph; (b) the chemical trapping reaction between probe and AOT surfactant have been studied in AOT reverse micellar solutions, and the method for the preparation of the chemical trapping products and standard curves are available;[138] and (c) specific cation effects on anionic surfactant aggregates have not been investigated by chemical trapping method. In general, specific cation effects are less pronounced than specific anion effect,[54] and, even though important, are harder to be observed and characterized.

4.2 Results and Discussion

4.2.1 The effect of added organic ammonium salts on the interfacial hydration of AOT aggregates

Tables 4.4-4.9 in the Appendix list chemical trapping results from the dediazoniation of 16-ArN_2^+ in 15 mM aqueous AOT solutions containing 0-50 mM quaternary ammonium (tetraalkylammonium bromide: TMABr, TEABr, TPABr, TBABr), tertiary ammonium (triethylammonium bromide, TriEABr), and ammonium (NH_4Br) salts, respectively, and 1 mM HBr at 28 ^oC. The micelle-to-vesicle transition occurs in the selected concentration range. The concentration range for TBABr is below 50 mM because a precipitate

forms above 30 mM. 1 mM HBr was added to control the solution acidity. Included in Tables 4.4-4.9 are the HPLC average peak areas, observed and normalized product yields, and estimated interfacial molarities of headgroups and water, denoted as AOT_m and H_2O_m respectively, and their molar ratios, H_2O_m/AOT_m. The two products identified by HPLC were from the dediazoniation reaction between probe and water, 16-ArOH, and probe and AOT headgroup, 16-ArS. No unexpected products were observed in the HPLC chromatograms. The observed yields of 16-ArOH and 16-ArS were calculated from HPLC peak areas and their calibration curves listed in Table 4.3. The standard curve used for the calculation of AOT_m was determined previously in reference solutions containing sodium dimethylsulfosuccinate, %16-ArS = 9.036AOT_m -0.103,[138], and confirmed by carrying out chemical trapping method in reference solutions containing $MeSO_3Na$, a oversimplified but convenient headgroup model for AOT. For each composition, the chemical trapping reaction were carried out twice, with stirring or not, and, delightedly, the two results were always similar. Thus, the calculated interfacial molarities are the average results from both experiments. The footnotes give the reaction condition and the HPLC conditions.

Figure 4.2 shows the changes in interfacial molarities of water, H_2O_m, headgroup, AOT_m, and their ratio, H_2O_m/AOT_m, with increasing stoichiometric concentrations of added organic salts in 15 mM AOT solutions at 28 ^oC. These figures clearly show: (a) a marked increase in AOT_m (ca. 1 to 2 M) and concomitant decrease in H_2O_m, (ca. 45 to 35 M) for TPABr/TEABr/TMABr/TriEABr/NH_4Br, but not TBABr. Note that the H_2O_m/AOT_m ratio drops from ca. 42 to 20 for these salts. (b) Added TBABr produces the same concurrent increases and decrease, respectively, of AOT_m and H_2O_m, but the changes are much greater compared to other salts. In the present of 10 mM added TBABr, AOT_m increases from ca. 1 to 1.7 M, whereas H_2O_m decreases from ca. 45 M to 38 M, and the molar ratio drops to ca. 22. Further addition of TBABr causes a dramatic decrease and increase, respectively, in H_2O_m and AOT_m to ca. 15 M and 4 M, and their molar ratio, H_2O_m/AOT_m, is only ca. 4. (c) The concurrrent dehydration of the interfacial region

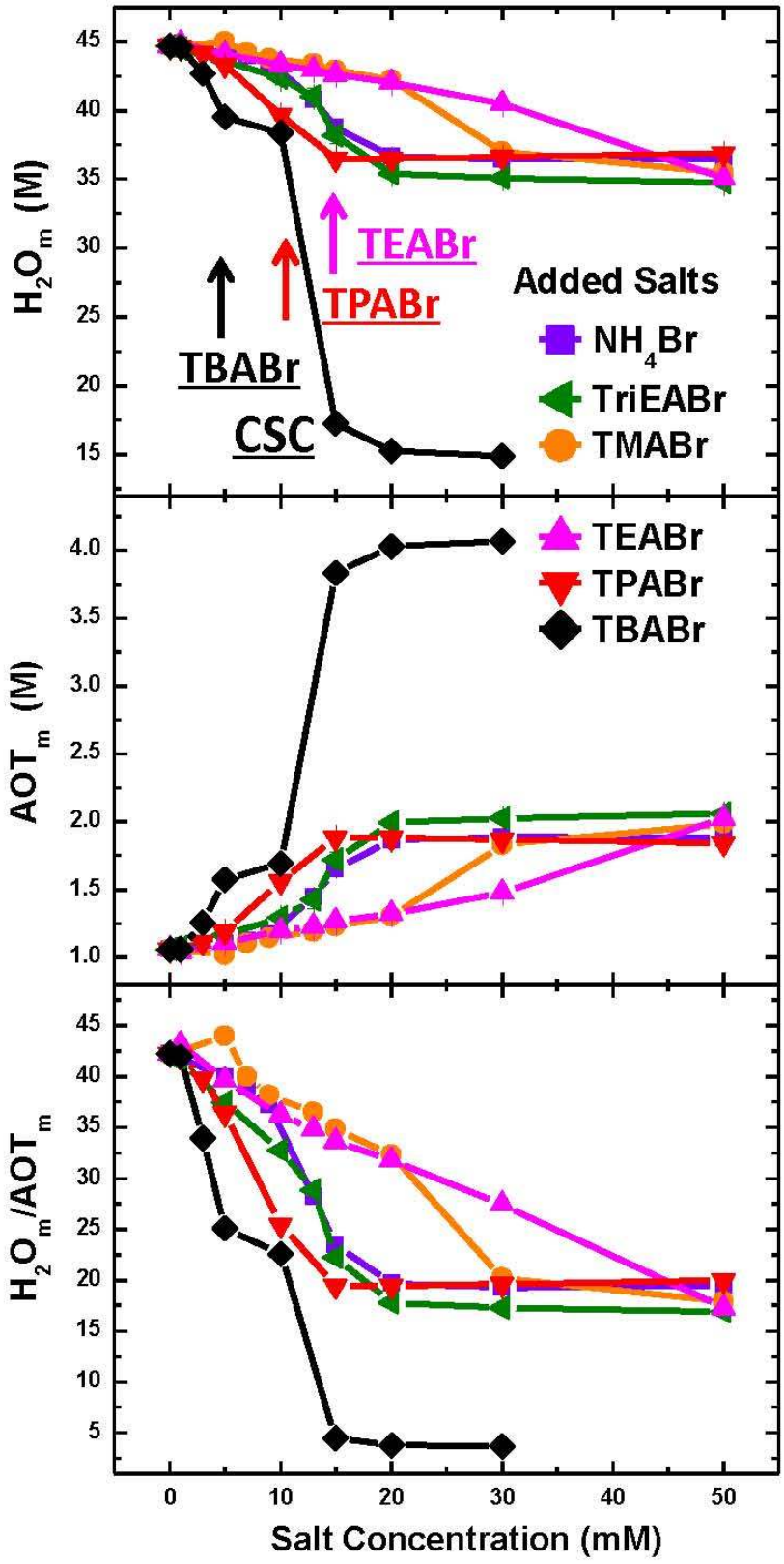

Figure 4.2: Changes in interfacial molarities of water, H_2O_m, headgroup, AOT_m, and their ratio, H_2O_m/AOT_m, with increasing stoichiometric concentrations of added organic ammonium salts in 15 mM AOT solutions at 28 ^{o}C. Lines are drawn to aid the eye.

occurs with the micelle-to-vesicle transition for each system determined by SANS.[137] For TBABr, while the first part of the dehydration occurs with the micelle-to-vesicle transition, the second part of the dehydration is consistent with its physical appearance change from bluish to white emulsion. (d) The transition from left to right follows the order: TBABr > TPABr > TriEABr $\sim$ NH_4Br > TMABr $\sim$ TEABr. The most hydrophobic cation, TBABr, induces interfacial dehydration at the lowest concentration.

The results in Figure 4.2 demonstrate that the chemical trapping method provides unique information about changes in interfacial composition during micelle-to-vesicle transition. The H_2O_m/AOT_m ratio shows that about 42 water molecules hydrate the AOT headgroups and counterions in the interfacial region of AOT micelles. However, after vesicle formation, only 17-20 water molecules hydrate the headgroups and counterions. This direct experimental evidence support the hypothesis that the added cations enter the interfacial region and form ion-pairs, which have a lower demand for hydration than free headgroups and counterions, with AOT headgroups. The micelle-to-vesicle transition occurs when the interface dehydrates sufficiently induced by added salts to shift the equilibrium to the headgroup and counterion ion-pairs. Therefore, this transition also depends on the types of the added counterions.

The tendencies of different ammonium cations to form ion-pairs with AOT headgroups are different. The AOT sulfonate headgroup is considered to be a weakly-hydrated, chaotropic, anions. Thus, weakly hydrated cations form ion-pairs with the sulfonate headgroups in the interfacial region. Our observed transition order is, to some extent, consistent with the hydrated radius of these ammonium ions, $TBA^+ > TPA^+ > TEA^+ > TMA^+ > NH_4^+$,[139] except for NH_4^+. The greatest dehydration in the interfacial region occurs with TBA^+, probably because it ion-pairs most strongly. The strong interaction by hydrophilic NH_4^+ is probably caused by hydrogen bonding with the sulfonate group. Similarly, The interaction between $TriEA^+$ and sulfonate headgroup is also caused by hydrogen bonding.

The products between probe and added co-ion, Br^-, 16-ArBr, is probably too small to

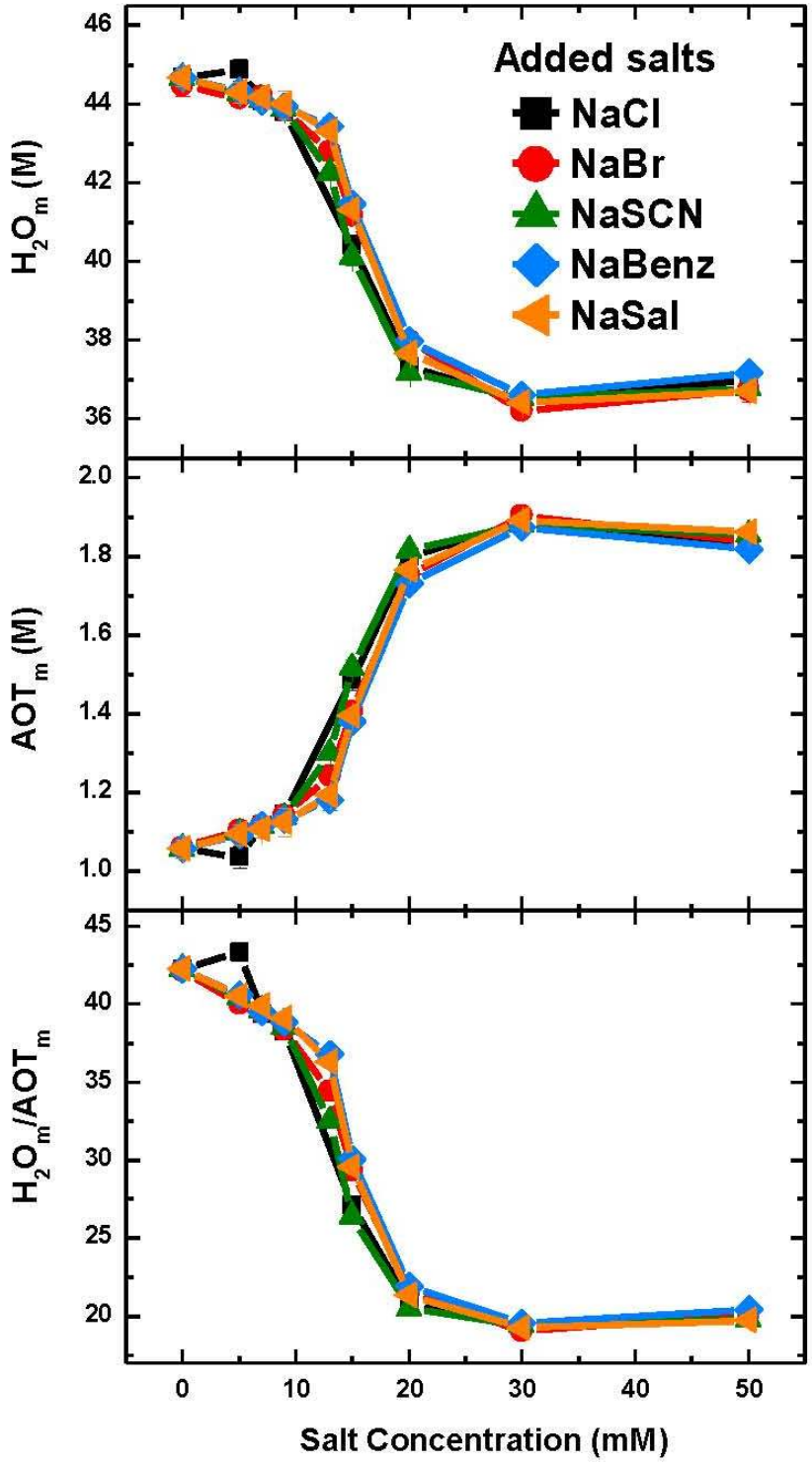

Figure 4.3: Changes in interfacial molarities of water, H_2O_m, headgroup, AOT_m, and their ratio, H_2O_m/AOT_m, with increasing stoichiometric concentrations of added added NaY (Y= Cl, Br, SCN, Benzoate, and Salicylate) in 15 mM AOT solutions at 28 ^{o}C. Lines are drawn to aid the eye.

be detected, which is reasonable because the interfacial bromide co-ion concentration, of 100 mM SDS micelles with ca. 200 mM added NaBr was only ca. 16 mM.[140] The low interfacial co-ion concentration was also demonstrated by the addition of extreme hydrophobic co-ions, including, SCN^-, benzoate, and salicylate, have no effect on the interfacial water and headgroup molarities.

Figure 4.3 shows the changes in interfacial molarities of water, H_2O_m, headgroup, AOT_m, and their ratio, H_2O_m/AOT_m, with increasing stoichiometric concentrations of added NaY (Y= Cl, Br, SCN, benzoate, and salicylate) in 15 mM AOT solutions at 28 ^oC. Again, detailed chemical trapping results are listed in Tables 4.11 and 4.19-4.22 in the Appendix. Interfacial hydration is identical for different co-ions, regardless of their size and hydrophobicity, within experimental error. This result is consistent with previous results showing that there is no specific interaction in the interfacial co-ion compartment.[140] Compared to counterions, it's unlikely for co-ions with headgroup to form ion-pairs at such extremely low concentrations.

4.2.2 The effects of added inorganic chloride salts on the interfacial hydration of AOT aggregates

Tables 4.10-4.18 in the Appendix list the analogous chemical trapping results from the dediazoniation of 16-ArN_2^+ in 15 mM aqueous AOT solutions containing 0-50 mM inorganic chloride salts, and 1 mM HCl at 28 ^oC. Added inorganic salts are either monovalent, MCl (M = Li, Na, K, Rb, Cs), divalent, MCl_2 (M = Ca, Mg, Zn), or trivalent, $AlCl_3$. The micelle-to-vesicle transition occurs in the selected concentration range. The concentration range for multivalent chloride salts are below 50 mM because these solutions precipitate after the highest listed salt concentration values. These tables are similar to Tables 4.4-4.9, and please see last section for the descriptions of these tables.

Figure 4.4 shows the changes in interfacial molarities of water, H_2O_m, headgroup, AOT_m, and their ratio, H_2O_m/AOT_m, with increasing stoichiometric concentrations of

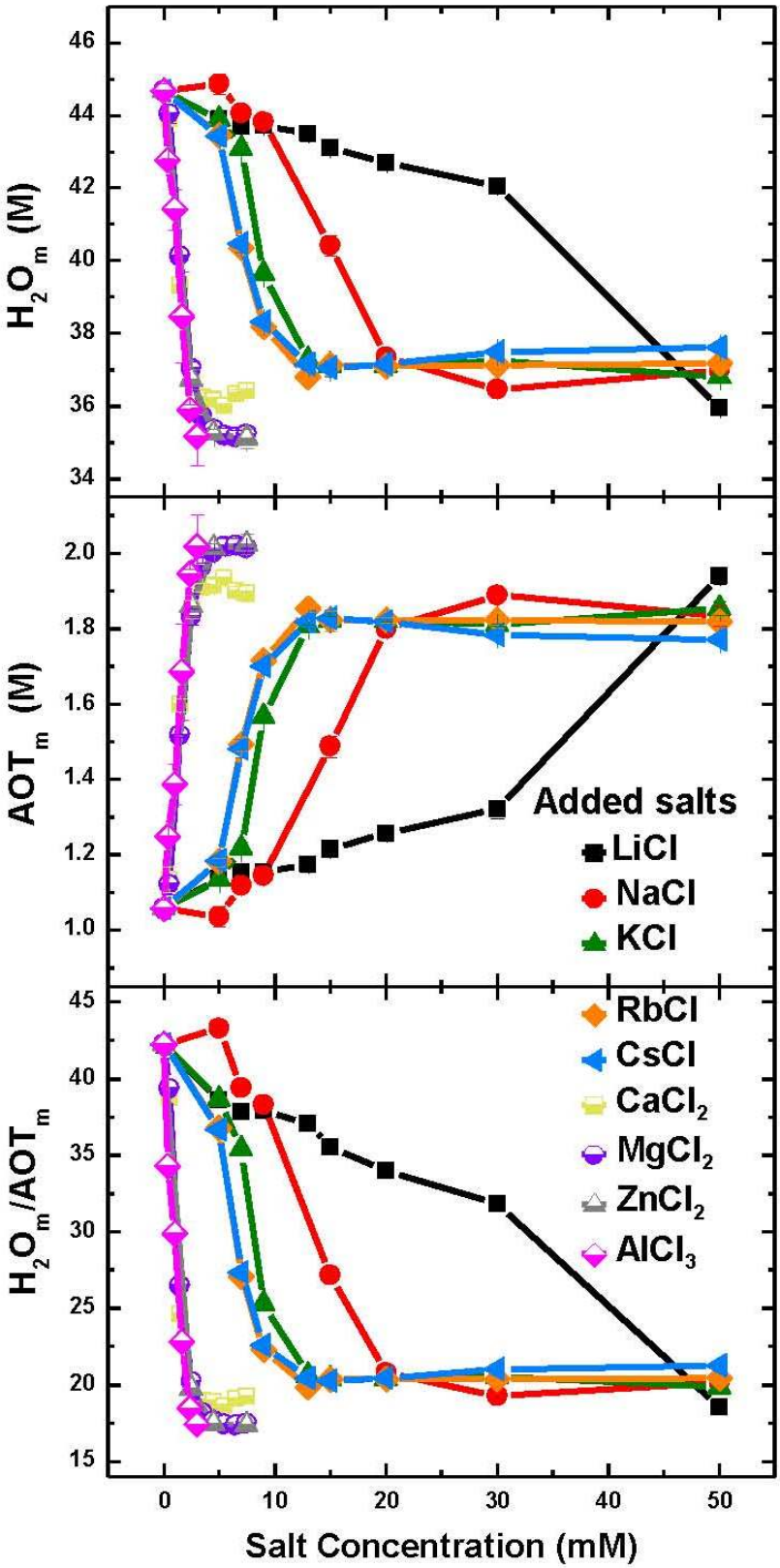

Figure 4.4: Changes in interfacial molarities of water, H_2O_m, headgroup, AOT_m, and their ratio, H_2O_m/AOT_m, with increasing stoichiometric concentrations of added inorganic salts in 15 mM AOT solutions at 28 ^{o}C. Lines are drawn to aid the eye.

added inorganic chloride salts in 15 mM AOT solutions at 28 ^{o}C. Note here: (a) Marked increase in AOT_m (ca. 1-1.9 M) and a concomitant decrease in H_2O_m, (ca. 45-36 M) for each salt. The H_2O_m/AOT_m ratio drops from ca. 42 to 20 in all cases. (b) Monovalent cations follow: $Cs^+ \sim Rb^+ > K^+ > Na^+ > Li^+$. (c) No significant difference could be found for multivalent inorganic salts(X = Ca Mg Zn Al). (d)Lower concentrations of multivalent cations are needed to induce interfacial dehydration. (e) For the dications, the dehydration in the interfacial region occurs at the same concentration range as the solutions' physical appearance changes from clear to bluish cloudy.

The hydration changes in the interfacial region shown in Figure 4.4 are similar to the results in Figure 4.2. Again, the hydration number, H_2O_m/AOT_m, decrease from 42 to 17-20 with the addition of inorganic chloride salts, consistent with ion-pairing formation between added metal cations and headgroups. In the case of monovalent cations, the observed order is consistent with Hofmeister series. It's easier for the weakly hydrated cations, Cs^+ and Rb^+, to form ion-pairs with the AOT headgroup, whereas the interaction between strongly hydrated cations, Li^+, and AOT headgroup is significantly weaker. For multivalent cations, the ion specific effects are not very significant. However, less multivalent salts are generally needed for interfacial dehydration. Probably, multivalent cations can interact with multiple headgroups simultaneously, which requires even less hydration water in the interfacial region.

4.3 Conclusions

The chemical trapping method provided estimates of interfacial molarities of headgroup anions and water through the micelle-to-vesicle transition of AOT solutions with added different salts, including both ammonium organic salts and simple metal chloride salts. In all the cases, there are marked increases in AOT_m and concomitant decreases in H_2O_m at micelle-to-vesicle transitions. Specific cation effects were observed, i.e., the molarities of added salts required induce the dehydration depend on their sizes and structures. In the

presence of organic salts, the dehydration follows: TBABr > TPABr > TriEABr ∼ NH_4Br > TMABr ∼ TEABr. The order for monovalent inorganic salts is: CsCl ∼ RbCl > KCl > NaCl > LiCl. Multivalent inorganic salts dehydrates very efficiently. These results fully support ion pair model in which vesicle formation is induced by specific ion pair formation and dehydration in the interfacial region.

4.4 Experimental

4.4.1 General method

HPLC measurements were performed on a Perkin-Elmer Series 200 equipped with a UV/Vis detector, a Varian Microsorb MV C18 column (length, 25 cm; particle size, 5 μm), and a computer-controlled Perkin-Elmer 600 Series Interface. ^{1}H NMR spectra were recorded on Varian VNMRS 500 MHz spectrometer. The temperature of the chemical trapping experiments were maintained by a Haake A10 circulation bath or a Fisher scientific microtube thermal mixer.

4.4.2 Materials

All aqueous solutions were prepared from water that was distilled, passed over activated carbon, an ion exchange resin and then redistilled. *i*-PrOH and MeOH were of the highest commercially available reagent grade. AOT (Sigma, 99%) were used as received. All additives, TMABr (Sigma, 98%), TEABr (TCI America, 98%), TPABr (TCI America, 98%), TBABr (TCI America, 98%), TriEABr (Alfa Aesar, 98%), NH_4Br (Sigma, 99%), LiCl (sigma, 99%), NaCl (Alfa Aesar, 99%), KCl (Sigma, 99%), RbCl (Sigma, 99%), CsCl (Sigma, 99.9%), $MgCl_2$ (Sigma, 98%), $CaCl_2$ (Sigma, 97%), $ZnCl_2$ (Sigma, 97%), $AlCl_3$ (Fluka, 99%), NaBr (Sigma, 99%), sodium salicylate NaSal (Alfa Aesar, 99%), sodium benzoate NaBenz (Alfa Aesar, 99%), NaSCN (Sigma, 98%) were used as received. 16-ArOH was prepared by established procedure.[81]

Synthesis of bis(2-ethylhexyl) 2-((4-hexadecyl-2,6-dimethylphenoxy)sulfonyl)succinate, 16-ArS. 16-ArS was prepared by trapping of 16-ArN_2^+ by AOT, modification of the method of Chaudhuri and Srilakshmi.[138] The dediazoniation reaction was carried out in a mixture of 15 mM AOT, 20 mM TBAB, and 1 mM HCl. 150 mL 25 mM AOT solution, 5 mL 1M TBAB, and 2.5 mL 0.1 M HCl were mixed in a 250 mL flask. 67 mg long-chain probe 16-ArN_2BF_4 was dissolved in 5 mL ice-cold MeCN, and added to the mixture. The reaction mixture was stirred for 2 days at room temperature in dark. The mixture was extracted with EtOAc (3 x 250 mL) The orgainc layer was isolated, and EtOAc layer was removed by rotatory evaporation. The crude product was purified by HPLC with a 65% MeOH/35% *i*-PrOH (v/v) mobile phase. ^{1}H NMR ($CDCl_3$) δ (PPM): 0.88 (15H, t), 1.26 (42H, m), 1.58-1.69 (4H, m), 2.34 (6H, s), 2.48 (2H, t), 3.33-3.56 (2H, 2dd), 4.08-4.25 (5H, d), 6.86 (2H, s), Figure 4.5.

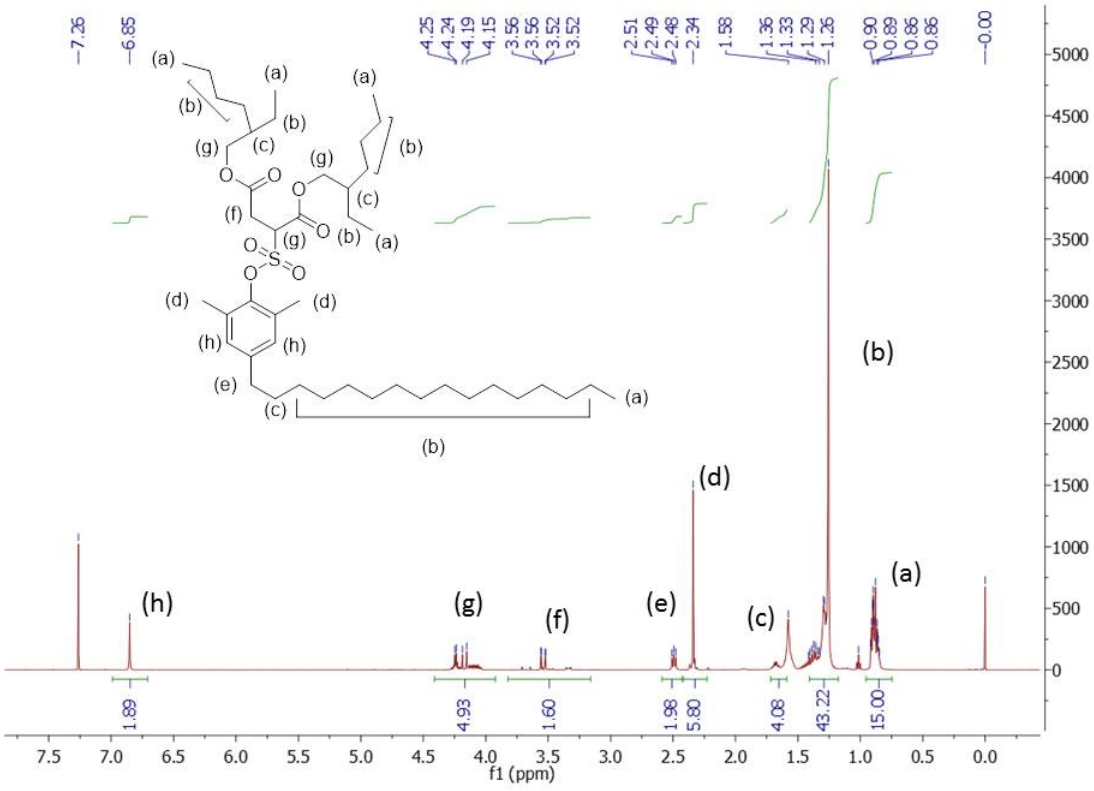

Figure 4.5: ^{1}H NMR spectrum of 16-ArS at 500 MHz in $CDCl_3$

4.4.3 Chemical trapping with 16-ArN$_2^+$ in aqueous AOT/salt solutions

The reaction was initiated by adding 50 μL freshly prepared stock solutions of 16-ArN$_2$BF$_4$ dissolved in ice-cold MeCN to 5 mL of the aqueous mixture of 15 mM AOT and added salts of the required concentrations, 1 mM HX, and a final probe concentration of 1.1-1.3 x 10^{-4} M. 1 mL of the each reaction solution was transferred to a microtube, and was shaken and thermostated at 28 ^{o}C in a Fisher scientific microtube thermal mixer for 2 days. The remaining of each solution were thermostated at 28 ^{o}C in a water bath for 2 days. Samples with a bluish appearance are designated as containing vesicles. The physical appearance of the mixtures are consistent with literature.[137] Prior to HPLC analysis, the product mixtures were mixed with an equal volume of water. Conditions for product separation on the HPLC were: a 65% MeOH/35% i-PrOH (v/v) mobile phase; flow rate = 0.4 ml/min; detector = 220 nm; and the injection volume was 100 μL. Percent yields were obtained from average values of peak areas from triplicate or duplicate injections with the appropriate calibration curves.

4.5 Appendix

Table 4.3: Linear calibration equations for 16-ArOH and 16-ArS.[a]

Reaction Products	Calibration Equations[b]	R^2
16-ArS	Y = 1.380 x 10^{11}X	1.0000
16-ArOH[c]	Y = 1.000 x 10^{11}X - 28660	0.9998

[a] HPLC Eluting solvent: 35%/65% v/v, *i*-PrOH/MeOH. Flow rate: 0.4 ml/min. Detector wavelength: 220 nm. Injection volume: 100 μL .

[b] Units: Y-peak area (in μv•s), X-concentration (in molarity), and R^2.

[c] Ref[109]

Table 4.4: HPLC Average peak areas, observed yields and normalized yields (subscript N) for dediazoniation reaction of 16-ArN_2^+ in solutions of 15 mM AOT in the present of 0-50 mM TMABr and estimated interfacial concentrations of headgroup, AOT_m, water, H_2O_m, and their molar ratio, H_2O_m/AOT_m, at 28 ^oC.[HBr] = 1 mM.

[TMABr] (mM)	Shaker[b]	Average Peak Areas[c] (10^6 μv•s)		Observed Yields (%)			Normalized Yields (%)		AOT_m [d] (M)	H_2O_m [d] (M)	$\frac{H_2O_m}{AOT_m}$ [d]
		16-ArOH	16-ArS	16-ArOH	16-ArS	Total	16-ArOH_N	16-ArS_N			
0	Yes	5.29	0.75	87.2	8.9	96.2	90.7	9.3	1.06	44.65	42.2
0	No	5.21	0.77	85.8	9.1	94.9	90.4	9.6			
1	Yes	5.24	0.73	86.4	8.7	95.1	90.8	9.2	1.02	45.01	44.0
1	No	5.42	0.76	89.3	9.0	98.3	90.9	9.1			
5	Yes	5.20	0.81	85.8	9.6	95.4	89.9	10.1	1.10	44.19	40.0
5	No	5.31	0.79	87.4	9.4	96.8	90.3	9.7			
10	Yes	5.17	0.83	85.2	9.8	95.0	89.7	10.3	1.15	43.78	38.2
10	No	5.21	0.82	85.9	9.7	95.6	89.8	10.2			
13	Yes	5.06	0.85	83.4	10.1	93.5	89.2	10.8	1.19	43.37	36.5
13	No	5.22	0.85	86.0	10.1	96.1	89.5	10.5			
15	Yes	5.07	0.89	83.5	10.5	94.1	88.8	11.2	1.23	42.93	34.8
15	No	5.14	0.87	84.6	10.3	95.0	89.1	10.9			
20	Yes	4.84	0.88	79.8	10.5	90.3	88.4	11.6	1.30	42.22	32.3
20	No	4.98	0.92	82.0	10.9	93.0	88.2	11.8			
30	Yes	4.51	1.23	74.5	14.6	89.1	83.6	16.4	1.83	37.01	20.2
30	No	4.56	1.25	75.1	14.8	90.0	83.5	16.5			
50	Yes	4.42	1.33	72.9	15.8	88.7	82.2	17.8	1.99	35.46	17.8
50	No	4.41	1.34	72.7	15.9	88.6	82.0	18.0			

a. Reaction time ca. 48 hours. Prior to HPLC analysis, the product mixture was mixed with an equal volume of water. The final concentrations of 16-ArN_2^+ were ca. 6.1 x 10^{-5} M. b. The reaction tubes were either placed in a thermostated shaker or water bath. c.100 μL sample injections. Peak areas are average of triplicate or duplicate injections. Eluting solvents: 65%MeOH/35%*i*-PrOH; Flow rate: 0.4 mL/min; Detector wavelength: 220 nm. d. The estimated AOT_m and H_2O_m values were average results calculated from both experiments carried out with or without shaker for a particular solution composition.

Table 4.5: HPLC Average peak areas, observed yields and normalized yields (subscript N) for dediazoniation reaction of 16-ArN_2^+ in solutions of 15 mM AOT in the present of 1-50 mM TEABr and estimated interfacial concentrations of headgroup, AOT_m, water, H_2O_m, and their molar ratio, H_2O_m/AOT_m, at 28 ^{o}C.[HBr] = 1 mM.

[TEABr] (mM)	Shaker[b]	Average Peak Areas[c] (10^6 μv•s)		Observed Yields (%)			Normalized Yields (%)		AOT_m [d] (M)	H_2O_m [d] (M)	$\frac{H_2O_m}{AOT_m}$ [d]
		16-ArOH	16-ArS	16-ArOH	16-ArS	Total	16-ArOH_N	16-ArS_N			
1	Yes	4.98	0.71	86.4	8.9	95.3	90.6	9.4	1.04	44.85	43.2
1	No	5.04	0.71	87.4	8.9	96.3	90.8	9.2			
5	Yes	5.02	0.78	87.0	9.7	96.7	90.0	10.0	1.11	44.10	39.6
5	No	4.95	0.76	85.8	9.4	95.2	90.1	9.9			
10	Yes	4.68	0.78	81.1	9.7	90.8	89.3	10.7	1.20	43.30	36.2
10	No	4.80	0.80	83.2	10.0	93.2	89.3	10.7			
13	Yes	4.64	0.80	80.6	10.0	90.6	88.9	11.1	1.23	42.93	34.8
13	No	4.78	0.82	82.8	10.2	93.1	89.0	11.0			
15	Yes	4.64	0.83	80.4	10.4	90.8	88.6	11.4	1.27	42.60	33.6
15	No	4.74	0.84	82.2	10.4	92.6	88.7	11.3			
20	Yes	4.55	0.86	78.9	10.7	89.6	88.0	12.0	1.32	42.07	31.8
20	No	4.69	0.86	81.3	10.7	92.0	88.3	11.7			
30	Yes	4.51	0.96	78.3	12.0	90.3	86.7	13.3	1.48	40.50	27.4
30	No	4.53	0.96	78.6	12.0	90.6	86.8	13.2			
50	Yes	4.26	1.30	73.9	16.3	90.2	81.9	18.1	2.02	35.11	17.3
50	No	4.25	1.33	73.8	16.6	90.3	81.7	18.3			

a. Reaction time ca. 48 hours. Prior to HPLC analysis, the product mixture was mixed with an equal volume of water. The final concentrations of 16-ArN_2^+ were ca. 5.8 x 10^{-5} M. b. The reaction tubes were either placed in a thermostated shaker or water bath. c.100 μL sample injections. Peak areas are average of triplicate or duplicate injections. Eluting solvents: 65%MeOH/35%*i*-PrOH; Flow rate: 0.4 mL/min; Detector wavelength: 220 nm. d. The estimated AOT_m and H_2O_m values were average results calculated from both experiments carried out with or without shaker for a particular solution composition.

Table 4.6: HPLC Average peak areas, observed yields and normalized yields (subscript N) for dediazoniation reaction of 16-ArN_2^+ in solutions of 15 mM AOT in the present of 1-50 mM TPABr and estimated interfacial concentrations of headgroup, AOT_m, water, H_2O_m, and their molar ratio, H_2O_m/AOT_m, at 28 ^oC.[HBr] = 1 mM.

[TPABr] (mM)	Shaker[b]	Average Peak Areas[c] (10^6 μv•s)		Observed Yields (%)			Normalized Yields (%)		AOT_m [d] (M)	H_2O_m [d] (M)	$\frac{H_2O_m}{AOT_m}$ [d]
		16-ArOH	16-ArS	16-ArOH	16-ArS	Total	16-$ArOH_N$	16-ArS_N			
1	Yes	4.84	0.70	83.9	8.7	92.6	90.6	9.4	1.06	44.62	42.0
1	No	4.92	0.72	85.3	9.1	94.4	90.4	9.6			
3	Yes	4.84	0.74	83.9	9.2	93.1	90.1	9.9	1.11	44.15	39.8
3	No	4.90	0.75	85.0	9.4	94.3	90.1	9.9			
5	Yes	4.68	0.77	81.1	9.6	90.7	89.4	10.6	1.19	43.34	36.4
5	No	4.77	0.80	82.7	10.0	92.7	89.2	10.8			
10	Yes	4.54	1.03	78.8	12.9	91.7	85.9	14.1	1.56	39.68	25.4
10	No	4.60	1.04	79.8	12.9	92.7	86.1	13.9			
15	Yes	4.41	1.25	76.6	15.7	92.2	83.0	17.0	1.88	36.51	19.4
15	No	4.43	1.25	76.8	15.6	92.3	83.2	16.8			
20	Yes	4.38	1.25	76.0	15.6	91.5	83.0	17.0	1.88	36.51	19.4
20	No	4.37	1.23	75.8	15.3	91.1	83.2	16.8			
30	Yes	4.40	1.24	76.4	15.5	91.9	83.1	16.9	1.87	36.62	19.6
30	No	4.40	1.23	76.4	15.4	91.7	83.2	16.8			
50	Yes	4.38	1.21	76.0	15.2	91.1	83.4	16.6	1.84	36.90	20.0
50	No	4.35	1.19	75.4	14.9	90.3	83.5	16.5			

a. Reaction time ca. 48 hours. Prior to HPLC analysis, the product mixture was mixed with an equal volume of water. The final concentrations of 16-ArN_2^+ were ca. 5.8 x 10^{-5} M. b. The reaction tubes were either placed in a thermostated shaker or water bath. c.100 μL sample injections. Peak areas are average of triplicate or duplicate injections. Eluting solvents: 65%MeOH/35%*i*-PrOH; Flow rate: 0.4 mL/min; Detector wavelength: 220 nm. d. The estimated AOT_m and H_2O_m values were average results calculated from both experiments carried out with or without shaker for a particular solution composition.

Table 4.7: HPLC Average peak areas, observed yields and normalized yields (subscript N) for dediazoniation reaction of 16-ArN_2^+ in solutions of 15 mM AOT in the present of 1-30 mM TBABr and estimated interfacial concentrations of headgroup, AOT_m, water, H_2O_m, and their molar ratio, H_2O_m/AOT_m, at 28 ^oC.[HBr] = 1 mM.

[TBABr] (mM)	Shaker[b]	Average Peak Areas[c] (10^6 μv•s)		Observed Yields (%)			Normalized Yields (%)		AOT_m [d] (M)	H_2O_m [d] (M)	$\frac{H_2O_m}{AOT_m}$ [d]
		16-ArOH	16-ArS	16-ArOH	16-ArS	Total	16-$ArOH_N$	16-ArS_N			
1	Yes	5.16	0.75	82.3	8.7	91.0	90.5	9.5	1.06	44.61	42.0
1	No	5.28	0.77	84.2	8.8	93.0	90.5	9.5			
3	Yes	5.12	0.91	81.8	10.5	92.3	88.6	11.4	1.26	42.70	34.0
3	No	5.13	0.89	81.9	10.2	92.1	88.9	11.1			
5	Yes	4.90	1.13	78.2	13.0	91.2	85.7	14.3	1.58	39.55	25.1
5	No	5.04	1.14	80.4	13.1	93.4	86.0	14.0			
10	Yes	4.96	1.26	79.2	14.5	93.7	84.5	15.5	1.69	38.37	22.6
10	No	5.04	1.23	80.4	14.1	94.5	85.1	14.9			
15	Yes	3.45	2.50	55.3	28.8	84.1	65.7	34.3	3.83	17.25	4.5
15	No	3.52	2.61	56.3	30.0	86.3	65.2	34.8			
20	Yes	3.50	2.79	56.0	32.1	88.0	63.6	36.4	4.03	15.28	3.8
20	No	2.79	2.21	44.7	25.4	70.1	63.8	36.2			
30	Yes	3.35	2.67	53.6	30.7	84.3	63.6	36.4	4.07	14.89	3.7
30	No	2.01	1.65	32.4	18.9	51.3	63.1	36.9			

a. Reaction time ca. 48 hours. Prior to HPLC analysis, the product mixture was mixed with an equal volume of water. The final concentrations of 16-ArN_2^+ were ca. 6.3 x 10^{-5} M. b. The reaction tubes were either placed in a thermostated shaker or water bath. c.100 μL sample injections. Peak areas are average of triplicate or duplicate injections. Eluting solvents: 65%MeOH/35%i-PrOH; Flow rate: 0.4 mL/min; Detector wavelength: 220 nm. d. The estimated AOT_m and H_2O_m values were average results calculated from both experiments carried out with or without shaker for a particular solution composition.

Table 4.8: HPLC Average peak areas, observed yields and normalized yields (subscript N) for dediazoniation reaction of 16-ArN_2^+ in solutions of 15 mM AOT in the present of 1-50 mM TriEABr and estimated interfacial concentrations of headgroup, AOT_m, water, H_2O_m, and their molar ratio, H_2O_m/AOT_m, at 28 ^{o}C.[HBr] = 1 mM.

[TriEABr] (mM)	Shaker[b]	Average Peak Areas[c] (10^6 μv•s)		Observed Yields (%)			Normalized Yields (%)		AOT_m [d] (M)	H_2O_m [d] (M)	$\frac{H_2O_m}{AOT_m}$ [d]
		16-ArOH	16-ArS	16-ArOH	16-ArS	Total	16-ArOH_N	16-ArS_N			
1	Yes	4.88	0.73	83.1	8.9	92.1	90.3	9.7	1.08	44.49	41.4
1	No	4.82	0.70	82.1	8.7	90.8	90.5	9.5			
5	Yes	4.80	0.78	81.9	9.5	91.4	89.6	10.4	1.17	43.60	37.4
5	No	4.83	0.78	82.3	9.6	91.9	89.6	10.4			
10	Yes	4.58	0.86	78.1	10.5	88.6	88.1	11.9	1.29	42.34	32.7
10	No	4.76	0.84	81.1	10.3	91.4	88.7	11.3			
13	Yes	4.40	0.93	75.1	11.4	86.4	86.8	13.2	1.43	41.03	28.8
13	No	4.56	0.90	77.7	11.0	88.7	87.6	12.4			
15	Yes	4.28	1.11	73.0	13.7	86.6	84.2	15.8	1.72	38.15	22.2
15	No	4.44	1.09	75.7	13.4	89.0	85.0	15.0			
20	Yes	4.24	1.29	72.4	15.8	88.2	82.1	17.9	1.99	35.43	17.8
20	No	4.25	1.29	72.5	15.8	88.3	82.1	17.9			
30	Yes	4.24	1.32	72.4	16.2	88.6	81.7	18.3	2.03	35.08	17.3
30	No	4.26	1.31	72.6	16.1	88.7	81.9	18.1			
50	Yes	4.13	1.30	70.5	16.0	86.5	81.5	18.5	2.06	34.75	16.9
50	No	4.21	1.34	71.8	16.4	88.2	81.4	18.6			

a. Reaction time ca. 48 hours. Prior to HPLC analysis, the product mixture was mixed with an equal volume of water. The final concentrations of 16-ArN_2^+ were ca. 5.9 x 10^{-5} M. b. The reaction tubes were either placed in a thermostated shaker or water bath. c.100 μL sample injections. Peak areas are average of triplicate or duplicate injections. Eluting solvents: 65%MeOH/35%*i*-PrOH; Flow rate: 0.4 mL/min; Detector wavelength: 220 nm. d. The estimated AOT_m and H_2O_m values were average results calculated from both experiments carried out with or without shaker for a particular solution composition.

Table 4.9: HPLC Average peak areas, observed yields and normalized yields (subscript N) for dediazoniation reaction of 16-ArN_2^+ in solutions of 15 mM AOT in the present of 5-50 mM NH_4Br and estimated interfacial concentrations of headgroup, AOT_m, water, H_2O_m, and their molar ratio, H_2O_m/AOT_m, at 28 ^{o}C.[HBr] = 1 mM.

[NH_4Br] (mM)	Shaker[b]	Average Peak Areas[c] (10^6 μv•s)		Observed Yields (%)			Normalized Yields (%)		AOT_m [d] (M)	H_2O_m [d] (M)	$\frac{H_2O_m}{AOT_m}$ [d]
		16-ArOH	16-ArS	16-ArOH	16-ArS	Total	16-ArOH_N	16-ArS_N			
5	Yes	4.83	0.75	81.7	9.1	90.8	89.9	10.1	1.11	44.19	40.0
5	No	4.99	0.74	84.3	9.1	93.3	90.3	9.7			
7	Yes	4.88	0.78	82.5	9.5	92.0	89.7	10.3	1.13	43.98	39.0
7	No	5.06	0.77	85.5	9.4	94.9	90.1	9.9			
9	Yes	4.85	0.80	82.0	9.8	91.8	89.3	10.7	1.17	43.54	37.2
9	No	4.95	0.79	83.7	9.6	93.3	89.7	10.3			
13	Yes	4.63	0.99	78.2	12.1	90.3	86.6	13.4	1.45	40.82	28.2
13	No	4.75	0.95	80.3	11.6	91.9	87.4	12.6			
15	Yes	4.46	1.10	75.4	13.4	88.9	84.9	15.1	1.65	38.77	23.4
15	No	4.61	1.09	77.9	13.3	91.2	85.4	14.6			
20	Yes	4.37	1.24	74.0	15.1	89.1	83.0	17.0	1.87	36.67	19.7
20	No	4.41	1.22	74.5	14.8	89.3	83.4	16.6			
30	Yes	4.35	1.26	73.5	15.4	88.9	82.7	17.3	1.89	36.46	19.3
30	No	4.36	1.21	73.7	14.7	88.3	83.4	16.6			
50	Yes	4.37	1.25	74.0	15.3	89.2	82.9	17.1	1.88	36.52	19.4
50	No	4.37	1.22	73.8	14.8	88.6	83.3	16.7			

a. Reaction time ca. 48 hours. Prior to HPLC analysis, the product mixture was mixed with an equal volume of water. The final concentrations of 16-ArN_2^+ were ca. 5.9 x 10^{-5} M. b. The reaction tubes were either placed in a thermostated shaker or water bath. c.100 μL sample injections. Peak areas are average of triplicate or duplicate injections. Eluting solvents: 65%MeOH/35%*i*-PrOH; Flow rate: 0.4 mL/min; Detector wavelength: 220 nm. d. The estimated AOT_m and H_2O_m values were average results calculated from both experiments carried out with or without shaker for a particular solution composition.

Table 4.10: HPLC Average peak areas, observed yields and normalized yields (subscript N) for dediazoniation reaction of 16-ArN_2^+ in solutions of 15 mM AOT in the present of 5-50 mM LiCl and estimated interfacial concentrations of headgroup, AOT_m, water, H_2O_m, and their molar ratio, H_2O_m/AOT_m, at 28 ^{o}C.[HCl] = 1 mM.

[LiCl] (mM)	Shaker[b]	Average Peak Areas[c] (10^6 μv•s)		Observed Yields (%)			Normalized Yields (%)		AOT_m [d] (M)	H_2O_m [d] (M)	$\frac{H_2O_m}{AOT_m}$ [d]
		16-ArOH	16-ArS	16-ArOH	16-ArS	Total	16-ArOH_N	16-ArS_N			
5	Yes	4.68	0.74	84.0	9.5	93.5	89.8	10.2	1.14	43.88	38.6
5	No	4.81	0.76	86.2	9.8	95.9	89.8	10.2			
7	Yes	4.67	0.74	83.8	9.6	93.4	89.7	10.3	1.15	43.71	37.8
7	No	4.82	0.78	86.4	10.0	96.4	89.6	10.4			
9	Yes	4.65	0.75	83.5	9.7	93.1	89.6	10.4	1.15	43.72	37.9
9	No	4.77	0.76	85.5	9.8	95.3	89.8	10.2			
13	Yes	4.67	0.77	83.8	9.9	93.7	89.4	10.6	1.17	43.51	37.1
13	No	4.72	0.76	84.6	9.8	94.4	89.6	10.4			
15	Yes	4.68	0.79	84.0	10.2	94.2	89.2	10.8	1.21	43.12	35.5
15	No	4.71	0.80	84.4	10.3	94.7	89.1	10.9			
20	Yes	4.64	0.82	83.2	10.5	93.7	88.7	11.3	1.26	42.70	34.0
20	No	4.66	0.82	83.6	10.6	94.2	88.8	11.2			
30	Yes	4.59	0.87	82.3	11.2	93.5	88.0	12.0	1.32	42.06	31.8
30	No	4.63	0.85	83.0	11.0	93.9	88.3	11.7			
50	Yes	4.14	1.22	74.2	15.8	90.0	82.5	17.5	1.94	35.95	18.5
50	No	4.22	1.23	75.6	15.8	91.5	82.7	17.3			

a. Reaction time ca. 48 hours. Prior to HPLC analysis, the product mixture was mixed with an equal volume of water. The final concentrations of 16-ArN_2^+ were ca. 5.6 x 10^{-5} M. b. The reaction tubes were either placed in a thermostated shaker or water bath. c.100 μL sample injections. Peak areas are average of triplicate or duplicate injections. Eluting solvents: 65%MeOH/35%*i*-PrOH; Flow rate: 0.4 mL/min; Detector wavelength: 220 nm. d. The estimated AOT_m and H_2O_m values were average results calculated from both experiments carried out with or without shaker for a particular solution composition.

Table 4.11: HPLC Average peak areas, observed yields and normalized yields (subscript N) for dediazoniation reaction of 16-ArN_2^+ in solutions of 15 mM AOT in the present of 5-50 mM NaCl and estimated interfacial concentrations of headgroup, AOT_m, water, H_2O_m, and their molar ratio, H_2O_m/AOT_m, at 28 ^{o}C.[HCl] = 1 mM.

[NaCl] (mM)	Shaker[b]	Average Peak Areas[c] (10^6 μv•s)		Observed Yields (%)			Normalized Yields (%)		AOT_m [d] (M)	H_2O_m [d] (M)	$\frac{H_2O_m}{AOT_m}$ [d]
		16-ArOH	16-ArS	16-ArOH	16-ArS	Total	16-ArOH_N	16-ArS_N			
5	Yes	5.09	0.74	84.0	8.8	92.7	90.6	9.4	1.04	44.88	43.3
5	No	5.17	0.72	85.2	8.5	93.7	90.9	9.1			
7	Yes	5.08	0.78	83.7	9.3	93.0	90.0	10.0	1.12	44.07	39.4
7	No	5.21	0.80	85.9	9.5	95.5	90.0	10.0			
9	Yes	5.00	0.80	82.4	9.5	91.8	89.7	10.3	1.14	43.82	38.3
9	No	5.10	0.80	84.0	9.5	93.5	89.8	10.2			
15	Yes	4.72	1.02	77.8	12.2	89.9	86.5	13.5	1.49	40.42	27.2
15	No	4.78	1.01	78.9	12.0	90.8	86.8	13.2			
20	Yes	4.55	1.23	75.0	14.6	89.6	83.7	16.3	1.80	37.35	20.8
20	No	4.72	1.25	77.8	14.8	92.7	84.0	16.0			
30	Yes	4.45	1.27	73.4	15.0	88.5	83.0	17.0	1.89	36.45	19.3
30	No	4.41	1.25	72.7	14.8	87.5	83.1	16.9			
50	Yes	4.55	1.26	75.1	15.0	90.1	83.3	16.7	1.84	36.98	20.2
50	No	4.55	1.23	75.1	14.6	89.7	83.7	16.3			

a. Reaction time ca. 48 hours. Prior to HPLC analysis, the product mixture was mixed with an equal volume of water. The final concentrations of 16-ArN_2^+ were ca. 6.1 x 10^{-5} M. b. The reaction tubes were either placed in a thermostated shaker or water bath. c.100 μL sample injections. Peak areas are average of triplicate or duplicate injections. Eluting solvents: 65%MeOH/35%i-PrOH; Flow rate: 0.4 mL/min; Detector wavelength: 220 nm. d. The estimated AOT_m and H_2O_m values were average results calculated from both experiments carried out with or without shaker for a particular solution composition.

Table 4.12: HPLC Average peak areas, observed yields and normalized yields (subscript N) for dediazoniation reaction of 16-ArN_2^+ in solutions of 15 mM AOT in the present of 5-50 mM KCl and estimated interfacial concentrations of headgroup, AOT_m, water, H_2O_m, and their molar ratio, H_2O_m/AOT_m, at 28 ^{o}C.[HCl] = 1 mM.

[KCl] (mM)	Shaker[b]	Average Peak Areas[c] (10^6 μv•s)		Observed Yields (%)			Normalized Yields (%)		AOT_m [d] (M)	H_2O_m [d] (M)	$\frac{H_2O_m}{AOT_m}$ [d]
		16-ArOH	16-ArS	16-ArOH	16-ArS	Total	16-$ArOH_N$	16-ArS_N			
5	Yes	4.49	0.71	83.0	9.4	92.4	89.8	10.2	1.14	43.90	38.7
5	No	4.57	0.72	84.5	9.5	94.1	89.9	10.1			
7	Yes	4.44	0.75	82.2	9.9	92.2	89.2	10.8	1.22	43.09	35.4
7	No	4.49	0.77	83.0	10.3	93.2	89.0	11.0			
9	Yes	4.28	0.97	79.2	12.9	92.1	86.0	14.0	1.57	39.63	25.3
9	No	4.31	0.98	79.8	13.1	92.9	85.9	14.1			
13	Yes	4.12	1.11	76.2	14.8	91.0	83.7	16.3	1.81	37.27	20.6
13	No	4.16	1.12	76.9	14.9	91.8	83.8	16.2			
15	Yes	4.08	1.12	75.6	14.9	90.5	83.6	16.4	1.82	37.11	20.4
15	No	4.09	1.11	75.7	14.7	90.4	83.7	16.3			
20	Yes	4.13	1.12	76.4	14.9	91.3	83.7	16.3	1.82	37.13	20.4
20	No	4.13	1.12	76.4	14.9	91.3	83.7	16.3			
30	Yes	4.12	1.11	76.3	14.8	91.2	83.7	16.3	1.81	37.23	20.6
30	No	4.16	1.12	77.0	14.9	91.9	83.8	16.2			
50	Yes	3.99	1.10	73.9	14.7	88.6	83.5	16.5	1.85	36.79	19.8
50	No	3.97	1.11	73.4	14.8	88.2	83.2	16.8			

a. Reaction time ca. 48 hours. Prior to HPLC analysis, the product mixture was mixed with an equal volume of water. The final concentrations of 16-ArN_2^+ were ca. 5.4 x 10^{-5} M. b. The reaction tubes were either placed in a thermostated shaker or water bath. c.100 μL sample injections. Peak areas are average of triplicate or duplicate injections. Eluting solvents: 65%MeOH/35%*i*-PrOH; Flow rate: 0.4 mL/min; Detector wavelength: 220 nm. d. The estimated AOT_m and H_2O_m values were average results calculated from both experiments carried out with or without shaker for a particular solution composition.

Table 4.13: HPLC Average peak areas, observed yields and normalized yields (subscript N) for dediazoniation reaction of 16-ArN_2^+ in solutions of 15 mM AOT in the present of 5-50 mM RbCl and estimated interfacial concentrations of headgroup, AOT_m, water, H_2O_m, and their molar ratio, H_2O_m/AOT_m, at 28 ^{o}C.[HCl] = 1 mM.

[RbCl] (mM)	Shaker[b]	Average Peak Areas[c] (10^6 μv•s)		Observed Yields (%)			Normalized Yields (%)		AOT_m [d] (M)	H_2O_m [d] (M)	$\frac{H_2O_m}{AOT_m}$ [d]
		16-ArOH	16-ArS	16-ArOH	16-ArS	Total	16-ArOH_N	16-ArS_N			
5	Yes	4.64	0.76	85.9	10.1	96.0	89.5	10.5	1.18	43.44	36.8
5	No	4.57	0.76	84.4	10.1	94.5	89.4	10.6			
7	Yes	4.45	0.95	82.3	12.6	94.9	86.7	13.3	1.49	40.36	27.0
7	No	4.34	0.94	80.2	12.5	92.7	86.5	13.5			
9	Yes	4.23	1.06	78.2	14.1	92.3	84.7	15.3	1.71	38.18	22.3
9	No	4.19	1.07	77.5	14.3	91.8	84.5	15.5			
13	Yes	4.07	1.13	75.3	15.1	90.4	83.3	16.7	1.85	36.81	19.9
13	No	4.17	1.15	77.1	15.3	92.4	83.4	16.6			
15	Yes	4.08	1.12	75.6	15.0	90.6	83.5	16.5	1.82	37.12	20.4
15	No	4.16	1.12	76.9	14.9	91.8	83.8	16.2			
20	Yes	4.12	1.12	76.2	15.0	91.2	83.6	16.4	1.82	37.11	20.4
20	No	4.06	1.10	75.2	14.7	89.8	83.7	16.3			
30	Yes	4.11	1.13	76.0	15.0	91.0	83.5	16.5	1.82	37.11	20.4
30	No	4.07	1.10	75.3	14.6	89.8	83.8	16.2			
50	Yes	4.09	1.11	75.6	14.7	90.4	83.7	16.3	1.82	37.16	20.4
50	No	4.21	1.14	77.8	15.2	93.7	83.7	16.3			

a. Reaction time ca. 48 hours. Prior to HPLC analysis, the product mixture was mixed with an equal volume of water. The final concentrations of 16-ArN_2^+ were ca. 5.4 x 10^{-5} M. b. The reaction tubes were either placed in a thermostated shaker or water bath. c.100 μL sample injections. Peak areas are average of triplicate or duplicate injections. Eluting solvents: 65%MeOH/35%*i*-PrOH; Flow rate: 0.4 mL/min; Detector wavelength: 220 nm. d. The estimated AOT_m and H_2O_m values were average results calculated from both experiments carried out with or without shaker for a particular solution composition.

Table 4.14: HPLC Average peak areas, observed yields and normalized yields (subscript N) for dediazoniation reaction of 16-ArN_2^+ in solutions of 15 mM AOT in the present of 5-50 mM CsCl and estimated interfacial concentrations of headgroup, AOT_m, water, H_2O_m, and their molar ratio, H_2O_m/AOT_m, at 28 ^{o}C.[HCl] = 1 mM.

[CsCl] (mM)	Shaker[b]	Average Peak Areas[c] (10^6 μv•s)		Observed Yields (%)			Normalized Yields (%)		AOT_m [d] (M)	H_2O_m [d] (M)	$\frac{H_2O_m}{AOT_m}$ [d]
		16-ArOH	16-ArS	16-ArOH	16-ArS	Total	16-ArOH_N	16-ArS_N			
5	Yes	4.80	0.79	86.1	10.2	96.3	89.4	10.6	1.18	43.42	36.7
5	No	4.79	0.79	85.8	10.2	96.0	89.4	10.6			
7	Yes	4.53	0.98	81.2	12.6	93.8	86.6	13.4	1.48	40.47	27.3
7	No	4.58	0.96	82.1	12.4	94.5	86.9	13.1			
9	Yes	4.48	1.12	80.4	14.5	94.9	84.7	15.3	1.70	38.32	22.6
9	No	4.48	1.12	80.3	14.4	94.7	84.8	15.2			
13	Yes	4.37	1.19	78.4	15.4	93.8	83.6	16.4	1.82	37.15	20.4
13	No	4.40	1.19	78.9	15.3	94.2	83.7	16.3			
15	Yes	4.28	1.18	76.8	15.2	92.0	83.4	16.6	1.83	37.05	20.3
15	No	4.37	1.18	78.4	15.2	93.6	83.7	16.3			
20	Yes	4.34	1.18	77.9	15.2	93.1	83.6	16.4	1.82	37.14	20.4
20	No	4.42	1.20	79.3	15.4	94.7	83.7	16.3			
30	Yes	4.36	1.16	78.2	14.9	93.2	84.0	16.0	1.78	37.49	21.0
30	No	4.33	1.15	77.7	14.8	92.5	84.0	16.0			
50	Yes	4.35	1.14	78.0	14.7	92.7	84.2	15.8	1.77	37.61	21.2
50	No	4.25	1.12	76.2	14.5	90.6	84.0	16.0			

a. Reaction time ca. 48 hours. Prior to HPLC analysis, the product mixture was mixed with an equal volume of water. The final concentrations of 16-ArN_2^+ were ca. 5.6 x 10^{-5} M. b. The reaction tubes were either placed in a thermostated shaker or water bath. c.100 μL sample injections. Peak areas are average of triplicate or duplicate injections. Eluting solvents: 65%MeOH/35%*i*-PrOH; Flow rate: 0.4 mL/min; Detector wavelength: 220 nm. d. The estimated AOT_m and H_2O_m values were average results calculated from both experiments carried out with or without shaker for a particular solution composition.

Table 4.15: HPLC Average peak areas, observed yields and normalized yields (subscript N) for dediazoniation reaction of 16-ArN_2^+ in solutions of 15 mM AOT in the present of 0.5-7.5 mM $CaCl_2$ and estimated interfacial concentrations of headgroup, AOT_m, water, H_2O_m, and their molar ratio, H_2O_m/AOT_m, at 28 ^{o}C.[HCl] = 1 mM.

2*[$CaCl_2$] (mM)	Shaker[b]	Average Peak Areas[c] (10^6 μv•s)		Observed Yields (%)			Normalized Yields (%)		AOT_m [d] (M)	H_2O_m [d] (M)	$\frac{H_2O_m}{AOT_m}$ [d]
		16-ArOH	16-ArS	16-ArOH	16-ArS	Total	16-ArOH_N	16-ArS_N			
1	Yes	4.95	0.79	83.8	9.7	93.5	89.6	10.4	1.13	43.92	38.8
1	No	5.14	0.78	86.9	9.6	96.5	90.1	9.9			
3	Yes	4.70	1.10	79.7	13.5	93.1	85.5	14.5	1.60	39.32	24.6
3	No	4.82	1.11	81.6	13.5	95.2	85.8	14.2			
5	Yes	4.40	1.23	74.5	15.0	89.5	83.2	16.8	1.85	36.83	19.9
5	No	4.49	1.23	76.1	15.0	91.1	83.5	16.5			
7	Yes	4.52	1.31	76.6	15.9	92.5	82.8	17.2	1.91	36.24	19.0
7	No	4.49	1.29	76.1	15.7	91.7	82.9	17.1			
9	Yes	4.42	1.29	74.9	15.7	90.6	82.7	17.3	1.91	36.20	18.9
9	No	4.50	1.29	76.2	15.7	91.8	82.9	17.1			
11	Yes	4.31	1.26	73.0	15.3	88.3	82.6	17.4	1.93	36.01	18.6
11	No	4.66	1.36	78.9	16.6	95.5	82.6	17.4			
13	Yes	4.48	1.29	75.8	15.7	91.5	82.9	17.1	1.90	36.33	19.1
13	No	4.43	1.26	75.1	15.4	90.4	83.0	17.0			
15	Yes	4.35	1.23	73.7	15.0	88.7	83.0	17.0	1.89	36.40	19.2
15	No	4.24	1.21	71.8	14.8	86.5	82.9	17.1			

a. Reaction time ca. 48 hours. Prior to HPLC analysis, the product mixture was mixed with an equal volume of water. The final concentrations of 16-ArN_2^+ were ca. 5.9 x 10^{-5} M. b. The reaction tubes were either placed in a thermostated shaker or water bath. c.100 μL sample injections. Peak areas are average of triplicate or duplicate injections. Eluting solvents: 65%MeOH/35%*i*-PrOH; Flow rate: 0.4 mL/min; Detector wavelength: 220 nm. d. The estimated AOT_m and H_2O_m values were average results calculated from both experiments carried out with or without shaker for a particular solution composition.

Table 4.16: HPLC Average peak areas, observed yields and normalized yields (subscript N) for dediazoniation reaction of 16-ArN_2^+ in solutions of 15 mM AOT in the present of 0.5-7.5 mM $MgCl_2$ and estimated interfacial concentrations of headgroup, AOT_m, water, H_2O_m, and their molar ratio, H_2O_m/AOT_m, at 28 ^{o}C.[HCl] = 1 mM.

2*[$MgCl_2$] (mM)	Shaker[b]	Average Peak Areas[c] (10^6 μv•s)		Observed Yields (%)			Normalized Yields (%)		AOT_m [d] (M)	H_2O_m [d] (M)	$\frac{H_2O_m}{AOT_m}$ [d]
		16-ArOH	16-ArS	16-ArOH	16-ArS	Total	16-ArOH_N	16-ArS_N			
1	Yes	5.49	0.86	79.9	9.1	89.0	89.8	10.2	1.12	44.05	39.3
1	No	5.58	0.84	81.2	8.9	90.1	90.1	9.9			
3	Yes	5.17	1.13	75.4	11.9	87.3	86.4	13.6	1.52	40.13	26.5
3	No	5.30	1.16	77.2	12.1	89.4	86.4	13.6			
5	Yes	4.97	1.37	72.4	14.4	86.8	83.4	16.6	1.83	37.02	20.2
5	No	5.05	1.37	73.5	14.3	87.9	83.7	16.3			
7	Yes	5.01	1.50	73.0	15.7	88.7	82.3	17.7	1.96	35.70	18.2
7	No	5.00	1.48	72.9	15.5	88.4	82.4	17.6			
9	Yes	4.95	1.51	72.1	15.9	88.0	82.0	18.0	2.00	35.35	17.7
9	No	5.10	1.55	74.3	16.2	90.6	82.1	17.9			
11	Yes	4.93	1.53	71.9	16.1	88.0	81.7	18.3	2.02	35.18	17.4
11	No	5.71	1.74	83.1	18.2	101	82.0	18.0			
13	Yes	4.92	1.53	71.7	16.0	87.7	81.7	18.3	2.02	35.14	17.4
13	No	5.49	1.68	79.9	17.6	97.5	82.0	18.0			
15	Yes	4.94	1.52	72.0	15.9	87.9	81.9	18.1	2.01	35.21	17.5
15	No	5.41	1.66	78.7	17.4	96.1	81.9	18.1			

a. Reaction time ca. 48 hours. Prior to HPLC analysis, the product mixture was mixed with an equal volume of water. The final concentrations of 16-ArN_2^+ were ca. 6.9 x 10^{-5} M. b. The reaction tubes were either placed in a thermostated shaker or water bath. c.100 μL sample injections. Peak areas are average of triplicate or duplicate injections. Eluting solvents: 65%MeOH/35%*i*-PrOH; Flow rate: 0.4 mL/min; Detector wavelength: 220 nm. d. The estimated AOT_m and H_2O_m values were average results calculated from both experiments carried out with or without shaker for a particular solution composition.

Table 4.17: HPLC Average peak areas, observed yields and normalized yields (subscript N) for dediazoniation reaction of 16-ArN_2^+ in solutions of 15 mM AOT in the present of 2.5-7.5 mM $ZnCl_2$ and estimated interfacial concentrations of headgroup, AOT_m, water, H_2O_m, and their molar ratio, H_2O_m/AOT_m, at 28 ^oC.[HCl] = 1 mM.

2*[$ZnCl_2$] (mM)	Shaker[b]	Average Peak Areas[c] (10^6 μv•s)		Observed Yields (%)			Normalized Yields (%)		AOT_m [d] (M)	H_2O_m [d] (M)	$\frac{H_2O_m}{AOT_m}$ [d]
		16-ArOH	16-ArS	16-ArOH	16-ArS	Total	16-$ArOH_N$	16-ArS_N			
5	Yes	4.64	1.31	71.9	14.6	86.5	83.1	16.9	1.86	36.73	19.7
5	No	4.68	1.29	72.4	14.3	86.7	83.5	16.5			
9	Yes	4.56	1.41	70.6	15.7	86.3	81.8	18.2	2.01	35.23	17.5
9	No	4.66	1.42	72.1	15.8	88.0	82.0	18.0			
15	Yes	4.52	1.41	69.9	15.7	85.6	81.6	18.4	2.02	35.12	17.4
15	No	5.53	1.38	70.1	15.4	85.4	82.0	18.0			

a. Reaction time ca. 48 hours. Prior to HPLC analysis, the product mixture was mixed with an equal volume of water. The final concentrations of 16-ArN_2^+ were ca. 6.5 x 10^{-5} M. b. The reaction tubes were either placed in a thermostated shaker or water bath. c.100 μL sample injections. Peak areas are average of triplicate or duplicate injections. Eluting solvents: 65%MeOH/35%i-PrOH; Flow rate: 0.4 mL/min; Detector wavelength: 220 nm. d. The estimated AOT_m and H_2O_m values were average results calculated from both experiments carried out with or without shaker for a particular solution composition.

Table 4.18: HPLC Average peak areas, observed yields and normalized yields (subscript N) for dediazoniation reaction of 16-ArN_2^+ in solutions of 15 mM AOT in the present of 0.33-3 mM $AlCl_3$ and estimated interfacial concentrations of headgroup, AOT_m, water, H_2O_m, and their molar ratio, H_2O_m/AOT_m, at 28 ^{o}C.[HCl] = 1 mM.

3*[$AlCl_3$] (mM)	Shaker[b]	Average Peak Areas[c] (10^6 μv•s)		Observed Yields (%)			Normalized Yields (%)		AOT_m [d] (M)	H_2O_m [d] (M)	$\frac{H_2O_m}{AOT_m}$ [d]
		16-ArOH	16-ArS	16-ArOH	16-ArS	Total	16-$ArOH_N$	16-ArS_N			
1	Yes	4.87	0.85	82.5	10.4	92.9	88.8	11.2	1.25	42.78	34.3
1	No	5.03	0.88	85.1	10.7	95.8	88.9	11.1			
3	Yes	5.54	1.13	85.7	12.6	98.3	87.2	12.8	1.39	41.41	29.9
3	No	5.96	1.14	92.1	12.7	105	87.9	12.1			
5	Yes	4.71	1.24	79.7	15.1	94.8	84.1	15.9	1.69	38.45	22.8
5	No	5.37	1.25	90.9	15.2	106	85.7	14.3			
7	Yes	4.41	1.31	74.8	15.9	90.7	82.4	17.6	1.95	35.89	18.4
7	No	4.38	1.28	74.2	15.6	89.8	82.6	17.4			
9	Yes	4.04	1.29	68.6	15.7	84.3	81.3	18.7	2.02	35.16	17.4
9	No	4.36	1.30	73.9	15.8	89.7	82.4	17.6			

a. Reaction time ca. 48 hours. Prior to HPLC analysis, the product mixture was mixed with an equal volume of water. The final concentrations of 16-ArN_2^+ were ca. 5.9 x 10^{-5} M. b. The reaction tubes were either placed in a thermostated shaker or water bath. c.100 μL sample injections. Peak areas are average of triplicate or duplicate injections. Eluting solvents: 65%MeOH/35%*i*-PrOH; Flow rate: 0.4 mL/min; Detector wavelength: 220 nm. d. The estimated AOT_m and H_2O_m values were average results calculated from both experiments carried out with or without shaker for a particular solution composition.

Table 4.19: HPLC Average peak areas, observed yields and normalized yields (subscript N) for dediazoniation reaction of 16-ArN_2^+ in solutions of 15 mM AOT in the present of 5-50 mM NaBr and estimated interfacial concentrations of headgroup, AOT_m, water, H_2O_m, and their molar ratio, H_2O_m/AOT_m, at 28 ^oC.[HBr] = 1 mM.

[NaBr] (mM)	Shaker[b]	Average Peak Areas[c] (10^6 μv•s)		Observed Yields (%)			Normalized Yields (%)		AOT_m [d] (M)	H_2O_m [d] (M)	$\frac{H_2O_m}{AOT_m}$ [d]
		16-ArOH	16-ArS	16-ArOH	16-ArS	Total	16-ArOH_N	16-ArS_N			
5	Yes	5.04	0.76	86.0	9.4	95.3	90.2	9.8	1.10	44.21	40.0
5	No	5.04	0.77	85.9	9.5	95.4	90.1	9.9			
7	Yes	5.00	0.78	85.3	9.6	94.9	89.9	10.1	1.12	44.08	39.5
7	No	5.03	0.76	85.7	9.4	95.0	90.1	9.9			
9	Yes	4.94	0.78	84.3	9.6	93.9	89.8	10.2	1.14	43.82	38.3
9	No	5.01	0.79	85.4	9.7	95.1	89.8	10.2			
13	Yes	4.79	0.83	81.7	10.2	91.9	88.9	11.1	1.24	42.83	34.4
13	No	4.90	0.86	83.5	10.5	94.0	88.8	11.2			
15	Yes	4.65	0.93	79.2	11.4	90.6	87.4	12.6	1.41	41.22	29.3
15	No	4.73	0.95	80.6	11.7	92.2	87.4	12.6			
20	Yes	4.47	1.17	76.2	14.4	90.6	84.1	15.9	1.75	37.82	21.6
20	No	4.53	1.16	77.3	14.2	91.5	84.4	15.6			
30	Yes	4.29	1.22	73.2	15.0	88.2	83.0	17.0	1.90	36.30	19.1
30	No	4.32	1.25	73.7	15.3	89.0	82.8	17.2			
50	Yes	4.42	1.20	75.5	14.7	90.2	83.7	16.3	1.84	36.95	20.1
50	No	4.47	1.25	76.2	15.3	91.5	83.3	16.7			

a. Reaction time ca. 48 hours. Prior to HPLC analysis, the product mixture was mixed with an equal volume of water. The final concentrations of 16-ArN_2^+ were ca. 5.9 x 10^{-5} M. b. The reaction tubes were either placed in a thermostated shaker or water bath. c.100 μL sample injections. Peak areas are average of triplicate or duplicate injections. Eluting solvents: 65%MeOH/35%*i*-PrOH; Flow rate: 0.4 mL/min; Detector wavelength: 220 nm. d. The estimated AOT_m and H_2O_m values were average results calculated from both experiments carried out with or without shaker for a particular solution composition.

Table 4.20: HPLC Average peak areas, observed yields and normalized yields (subscript N) for dediazoniation reaction of 16-ArN_2^+ in solutions of 15 mM AOT in the present of 5-50 mM NaSCN and estimated interfacial concentrations of headgroup, AOT_m, water, H_2O_m, and their molar ratio, H_2O_m/AOT_m, at 28 ^{o}C.[HBr] = 1 mM.

[NaSCN] (mM)	Shaker[b]	Average Peak Areas[c] (10^6 μv•s)		Observed Yields (%)			Normalized Yields (%)		AOT_m [d] (M)	H_2O_m [d] (M)	$\frac{H_2O_m}{AOT_m}$ [d]
		16-ArOH	16-ArS	16-ArOH	16-ArS	Total	16-ArOH_N	16-ArS_N			
5	Yes	5.35	0.82	85.6	9.5	95.1	90.1	9.9	1.10	44.28	40.4
5	No	5.44	0.81	87.0	9.3	96.3	90.3	9.7			
7	Yes	5.30	0.82	84.8	9.5	94.3	89.9	10.1	1.11	44.11	39.6
7	No	5.40	0.82	86.5	9.5	96.0	90.1	9.9			
9	Yes	5.26	0.83	84.3	9.6	93.8	89.8	10.2	1.14	43.87	38.5
9	No	5.31	0.83	85.1	9.6	94.7	89.8	10.2			
13	Yes	5.05	0.93	80.8	10.7	91.5	88.3	11.7	1.30	42.27	32.5
13	No	5.19	0.95	83.2	10.9	94.1	88.4	11.6			
15	Yes	4.96	1.10	79.4	12.7	92.1	86.3	13.7	1.52	40.12	26.4
15	No	5.10	1.10	81.7	12.7	94.4	86.5	13.5			
20	Yes	4.74	1.29	75.9	14.8	90.7	83.6	16.4	1.82	37.17	20.5
20	No	4.81	1.30	77.1	15.0	92.1	83.7	16.3			
30	Yes	4.63	1.32	74.2	15.2	89.5	83.0	17.0	1.88	36.53	19.4
30	No	4.76	1.33	76.2	15.3	91.5	83.2	16.8			
50	Yes	4.75	1.32	76.0	15.2	91.2	83.3	16.7	1.86	36.78	19.8
50	No	4.75	1.32	76.1	15.2	91.3	83.3	16.7			

a. Reaction time ca. 48 hours. Prior to HPLC analysis, the product mixture was mixed with an equal volume of water. The final concentrations of 16-ArN_2^+ were ca. 6.3 x 10^{-5} M. b. The reaction tubes were either placed in a thermostated shaker or water bath. c.100 μL sample injections. Peak areas are average of triplicate or duplicate injections. Eluting solvents: 65%MeOH/35%*i*-PrOH; Flow rate: 0.4 mL/min; Detector wavelength: 220 nm. d. The estimated AOT_m and H_2O_m values were average results calculated from both experiments carried out with or without shaker for a particular solution composition.

Table 4.21: HPLC Average peak areas, observed yields and normalized yields (subscript N) for dediazoniation reaction of 16-ArN_2^+ in solutions of 15 mM AOT in the present of 5-50 mM sodium benzoate NaBenz and estimated interfacial concentrations of headgroup, AOT_m, water, H_2O_m, and their molar ratio, H_2O_m/AOT_m, at 28 ^{o}C.[HBr] = 1 mM.

[NaBenz] (mM)	Shaker[b]	Average Peak Areas[c] (10^6 μv•s)		Observed Yields (%)			Normalized Yields (%)		AOT_m [d] (M)	H_2O_m [d] (M)	$\frac{H_2O_m}{AOT_m}$ [d]
		16-ArOH	16-ArS	16-ArOH	16-ArS	Total	16-ArOH_N	16-ArS_N			
5	Yes	5.06	0.76	82.3	9.0	91.3	90.2	9.8	1.09	44.32	40.6
5	No	5.25	0.78	85.3	9.2	94.5	90.3	9.7			
7	Yes	4.99	0.77	81.2	9.0	90.2	90.0	10.0	1.12	44.09	39.5
7	No	5.19	0.80	84.4	9.3	93.7	90.0	10.0			
9	Yes	4.94	0.78	80.5	9.1	89.6	89.8	10.2	1.13	43.94	38.8
9	No	5.15	0.80	83.7	9.4	93.1	89.9	10.1			
13	Yes	4.90	0.82	79.8	9.6	89.3	89.3	10.7	1.18	43.45	36.8
13	No	5.12	0.82	83.2	9.7	92.9	89.6	10.4			
15	Yes	4.71	0.92	76.6	10.7	87.4	87.7	12.3	1.38	41.48	30.1
15	No	4.90	0.96	79.7	11.3	91.0	87.6	12.4			
20	Yes	4.47	1.14	72.8	13.3	86.2	84.5	15.5	1.73	38.00	21.9
20	No	4.59	1.18	74.7	13.8	88.5	84.4	15.6			
30	Yes	4.46	1.26	72.6	14.7	87.4	83.1	16.9	1.87	36.60	19.5
30	No	4.52	1.27	73.5	14.8	88.4	83.2	16.8			
50	Yes	4.52	1.22	73.7	14.3	88.0	83.7	16.3	1.82	37.16	20.5
50	No	4.58	1.24	74.5	14.5	89.0	83.7	16.3			

a. Reaction time ca. 48 hours. Prior to HPLC analysis, the product mixture was mixed with an equal volume of water. The final concentrations of 16-ArN_2^+ were ca. 6.2 x 10^{-5} M. b. The reaction tubes were either placed in a thermostated shaker or water bath. c.100 μL sample injections. Peak areas are average of triplicate or duplicate injections. Eluting solvents: 65%MeOH/35%*i*-PrOH; Flow rate: 0.4 mL/min; Detector wavelength: 220 nm. d. The estimated AOT_m and H_2O_m values were average results calculated from both experiments carried out with or without shaker for a particular solution composition.

Table 4.22: HPLC Average peak areas, observed yields and normalized yields (subscript N) for dediazoniation reaction of 16-ArN_2^+ in solutions of 15 mM AOT in the present of 5-50 mM sodium salicylate NaSal and estimated interfacial concentrations of headgroup, AOT_m, water, H_2O_m, and their molar ratio, H_2O_m/AOT_m, at 28 ^{o}C.[HBr] = 1 mM.

[NaSal] (mM)	Shaker[b]	Average Peak Areas[c] (10^6 μv•s)		Observed Yields (%)			Normalized Yields (%)		AOT_m [d] (M)	H_2O_m [d] (M)	$\frac{H_2O_m}{AOT_m}$ [d]
		16-ArOH	16-ArS	16-ArOH	16-ArS	Total	16-ArOH_N	16-ArS_N			
5	Yes	4.36	0.67	79.9	8.8	88.7	90.0	10.0	1.09	44.31	40.5
5	No	4.51	0.67	82.6	8.8	91.4	90.4	9.6			
7	Yes	4.02	0.62	73.7	8.2	81.9	90.0	10.0	1.11	44.18	39.9
7	No	4.47	0.67	81.9	8.9	90.7	90.2	9.8			
9	Yes	4.22	0.67	77.2	8.9	86.1	89.7	10.3	1.13	44.00	39.1
9	No	4.42	0.67	80.9	8.8	89.8	90.2	9.8			
13	Yes	4.20	0.70	76.9	9.3	86.2	89.2	10.8	1.19	43.33	36.3
13	No	4.35	0.72	79.6	9.4	89.1	89.4	10.6			
15	Yes	4.12	0.82	75.5	10.8	86.2	87.5	12.5	1.40	41.31	29.6
15	No	4.21	0.84	77.0	11.1	88.1	87.4	12.6			
20	Yes	3.88	1.02	71.1	13.5	84.6	84.1	15.9	1.77	37.67	21.3
20	No	4.01	1.04	73.4	13.7	87.2	84.2	15.8			
30	Yes	3.76	1.08	68.9	14.2	83.1	82.9	17.1	1.89	36.42	19.2
30	No	3.80	1.08	69.6	14.2	83.8	83.1	16.9			
50	Yes	3.86	1.08	70.6	14.2	84.9	83.2	16.8	1.86	36.71	19.7
50	No	3.81	1.06	69.7	14.0	83.7	83.3	16.7			

a. Reaction time ca. 48 hours. Prior to HPLC analysis, the product mixture was mixed with an equal volume of water. The final concentrations of 16-ArN_2^+ were ca. 5.5 x 10^{-5} M. b. The reaction tubes were either placed in a thermostated shaker or water bath. c.100 μL sample injections. Peak areas are average of triplicate or duplicate injections. Eluting solvents: 65%MeOH/35%*i*-PrOH; Flow rate: 0.4 mL/min; Detector wavelength: 220 nm. d. The estimated AOT_m and H_2O_m values were average results calculated from both experiments carried out with or without shaker for a particular solution composition.

References

[1] L. S. Romsted, "Introduction to surfactant self-assembly," *Supramolecular Chemistry: From Molecules to Nanomaterials*, 2012.

[2] B. Jonsson, *Surfactants and polymers in aqueous solution.* John Wiley & Sons, 1998.

[3] Z. Weiszhár, J. Czúcz, C. Révész, L. Rosivall, J. Szebeni, and Z. Rozsnyay, "Complement activation by polyethoxylated pharmaceutical surfactants: Cremophor-el, tween-80 and tween-20," *European Journal of Pharmaceutical Sciences*, vol. 45, no. 4, pp. 492–498, 2012.

[4] R. Nelson, "Application of surfactants in the petroleum industry," *Journal of the American Oil Chemists Society*, vol. 59, no. 10, pp. 823A–826A, 1982.

[5] D. Guzey and D. J. McClements, "Formation, stability and properties of multilayer emulsions for application in the food industry," *Advances in Colloid and Interface Science*, vol. 128, pp. 227–248, 2006.

[6] Y. Matsumoto, K. Yoshida, and M. Ishida, "A novel deposition technique for fluorocarbon films and its applications for bulk-and surface-micromachined devices," *Sensors and Actuators A: Physical*, vol. 66, no. 1, pp. 308–314, 1998.

[7] F. M. Menger, "Amphiphiles i have known," *Comptes Rendus Chimie*, vol. 12, no. 1, pp. 54–60, 2009.

[8] L. S. Romsted, *Surfactant Science and Technology: Retrospects and Prospects*. CRC Press, 2014.

[9] A. Czajka, G. Hazell, and J. Eastoe, "Surfactants at the design limit," *Langmuir*, 2015.

[10] C. A. Bunton, F. Nome, F. H. Quina, and L. S. Romsted, "Ion binding and reactivity at charged aqueous interfaces," *Accounts of chemical research*, vol. 24, no. 12, pp. 357–364, 1991.

[11] E. W. Kaler, A. K. Murthy, B. E. Rodriguez, and J. Zasadzinski, "Spontaneous vesicle formation in aqueous mixtures of single-tailed surfactants," *Science*, vol. 245, no. 4924, pp. 1371–1374, 1989.

[12] Z. Chu, C. A. Dreiss, and Y. Feng, "Smart wormlike micelles," *Chemical Society Reviews*, vol. 42, no. 17, pp. 7174–7203, 2013.

[13] J. N. Israelachvili, *Intermolecular and surface forces: revised third edition*. Academic press, 2011.

[14] J. H. Fendler, *Membrane mimetic chemistry: characterizations and applications of micelles, microemulsions, monolayers, bilayers, vesicles, host-guest systems, and polyions*. Wiley New York, 1982.

[15] M. J. Rosen, "Micelle formation by surfactants," *Surfactants and Interfacial Phenomena, Third Edition*, pp. 105–177, 2004.

[16] R. Zana, "Aqueous surfactant-alcohol systems: a review," *Advances in Colloid and Interface Science*, vol. 57, pp. 1–64, 1995.

[17] R. Williams, J. Phillips, and K. Mysels, "The critical micelle concentration of sodium lauryl sulphate at 25 c," *Transactions of the Faraday Society*, vol. 51, pp. 728–737, 1955.

[18] F. M. Menger and S. A. Rizvi, "Relationship between surface tension and surface coverage," *Langmuir*, vol. 27, no. 23, pp. 13975–13977, 2011.

[19] P. Carpena, J. Aguiar, P. Bernaola-Galván, and C. Carnero Ruiz, "Problems associated with the treatment of conductivity-concentration data in surfactant solutions: simulations and experiments," *Langmuir*, vol. 18, no. 16, pp. 6054–6058, 2002.

[20] G. Porte, Y. Poggi, J. Appell, and G. Maret, "Large micelles in concentrated solutions. the second critical micellar concentration," *The Journal of Physical Chemistry*, vol. 88, no. 23, pp. 5713–5720, 1984.

[21] R. Zana and E. W. Kaler, *Giant micelles: properties and applications*, vol. 140. CRC Press, 2007.

[22] T. Shikata, H. Hirata, and T. Kotaka, "Micelle formation of detergent molecules in aqueous media: viscoelastic properties of aqueous cetyltrimethylammonium bromide solutions," *Langmuir*, vol. 3, no. 6, pp. 1081–1086, 1987.

[23] T. Shikata, H. Hirata, and T. Kotaka, "Micelle formation of detergent molecules in aqueous media. 2. role of free salicylate ions on viscoelastic properties of aqueous cetyltrimethylammonium bromide-sodium salicylate solutions," *Langmuir*, vol. 4, no. 2, pp. 354–359, 1988.

[24] F. Kern, R. Zana, and S. Candau, "Rheological properties of semidilute and concentrated aqueous solutions of cetyltrimethylammonium chloride in the presence of

sodium salicylate and sodium chloride," *Langmuir*, vol. 7, no. 7, pp. 1344–1351, 1991.

[25] F. Kern, P. Lemarechal, S. Candau, and M. Cates, "Rheological properties of semidilute and concentrated aqueous solutions of cetyltrimethylammonium bromide in the presence of potassium bromide," *Langmuir*, vol. 8, no. 2, pp. 437–440, 1992.

[26] T. Shikata, H. Hirata, and T. Kotaka, "Micelle formation of detergent molecules in aqueous media. 3. viscoelastic properties of aqueous cetyltrimethylammonium bromide-salicylic acid solutions," *Langmuir*, vol. 5, no. 2, pp. 398–405, 1989.

[27] B. A. Schubert, E. W. Kaler, and N. J. Wagner, "The microstructure and rheology of mixed cationic/anionic wormlike micelles," *Langmuir*, vol. 19, no. 10, pp. 4079–4089, 2003.

[28] M. Cates and S. Candau, "Statics and dynamics of worm-like surfactant micelles," *Journal of Physics: Condensed Matter*, vol. 2, no. 33, p. 6869, 1990.

[29] J. H. Fendler, "Membrane mimetic chemistry," tech. rep., Syracuse Univ., NY (USA). Dept. of Chemistry, 1986.

[30] F. Szoka Jr and D. Papahadjopoulos, "Comparative properties and methods of preparation of lipid vesicles (liposomes)," *Annual review of biophysics and bioengineering*, vol. 9, no. 1, pp. 467–508, 1980.

[31] K. Kurihara, M. Tamura, K.-i. Shohda, T. Toyota, K. Suzuki, and T. Sugawara, "Self-reproduction of supramolecular giant vesicles combined with the amplification of encapsulated dna," *Nature chemistry*, vol. 3, no. 10, pp. 775–781, 2011.

[32] K. Kurihara, Y. Okura, M. Matsuo, T. Toyota, K. Suzuki, and T. Sugawara, "A recursive vesicle-based model protocell with a primitive model cell cycle," *Nature*

communications, vol. 6, 2015.

[33] Y. Elani, R. V. Law, and O. Ces, "Vesicle-based artificial cells as chemical microreactors with spatially segregated reaction pathways," *Nature communications*, vol. 5, 2014.

[34] G. Cevc, "Lipid vesicles and other colloids as drug carriers on the skin," *Advanced drug delivery reviews*, vol. 56, no. 5, pp. 675–711, 2004.

[35] M. L. Immordino, F. Dosio, and L. Cattel, "Stealth liposomes: review of the basic science, rationale, and clinical applications, existing and potential," *International journal of nanomedicine*, vol. 1, no. 3, p. 297, 2006.

[36] D. F. Evans and H. Wennerström, "The colloidal domain: where physics," *Chemistry, Biology, and Technology Meet*, vol. 2, pp. 193–197, 1999.

[37] M. I. Viseu, K. Edwards, C. S. Campos, and S. M. Costa, "Spontaneous vesicles formed in aqueous mixtures of two cationic amphiphiles," *Langmuir*, vol. 16, no. 5, pp. 2105–2114, 2000.

[38] K. Edwards and M. Almgren, "Surfactant-induced leakage and structural change of lecithin vesicles: effect of surfactant headgroup size," *Langmuir*, vol. 8, no. 3, pp. 824–832, 1992.

[39] M. Bergström and J. C. Eriksson, "The energetics of forming equilibrated bilayer vesicles," *Langmuir*, vol. 12, no. 3, pp. 624–635, 1996.

[40] I. Grillo, E. Kats, and A. Muratov, "Formation and growth of anionic vesicles followed by small-angle neutron scattering," *Langmuir*, vol. 19, no. 11, pp. 4573–4581, 2003.

[41] M. T. Yatcilla, K. L. Herrington, L. L. Brasher, E. W. Kaler, S. Chiruvolu, and J. A. Zasadzinski, "Phase behavior of aqueous mixtures of cetyltrimethylammonium bromide (ctab) and sodium octyl sulfate (sos)," *The Journal of Physical Chemistry*, vol. 100, no. 14, pp. 5874–5879, 1996.

[42] K. L. Herrington, E. W. Kaler, D. D. Miller, J. A. Zasadzinski, and S. Chiruvolu, "Phase behavior of aqueous mixtures of dodecyltrimethylammonium bromide (dtab) and sodium dodecyl sulfate (sds)," *The Journal of Physical Chemistry*, vol. 97, no. 51, pp. 13792–13802, 1993.

[43] R. Zana and J. Xia, *Gemini surfactants: synthesis, interfacial and solution-phase behavior, and applications*, vol. 117. CRC Press, 2003.

[44] F. M. Menger and J. S. Keiper, "Gemini surfactants," *Angewandte Chemie International Edition*, vol. 39, no. 11, pp. 1906–1920, 2000.

[45] M. J. Rosen and D. J. Tracy, "Gemini surfactants," *Journal of Surfactants and Detergents*, vol. 1, no. 4, pp. 547–554, 1998.

[46] T. Dam, J. Engberts, J. Karthäuser, S. Karaborni, and N. Van Os, "Synthesis, surface properties and oil solubilisation capacity of cationic gemini surfactants," *Colloids and Surfaces A: Physicochemical and Engineering Aspects*, vol. 118, no. 1, pp. 41–49, 1996.

[47] E. Alami, G. Beinert, P. Marie, and R. Zana, "Alkanediyl-. alpha.,. omega.-bis (dimethylalkylammonium bromide) surfactants. 3. behavior at the air-water interface," *Langmuir*, vol. 9, no. 6, pp. 1465–1467, 1993.

[48] J. Zhao, S. D. Christian, and B. Fung, "Mixtures of monomeric and dimeric cationic surfactants," *The Journal of Physical Chemistry B*, vol. 102, no. 39, pp. 7613–7618,

1998.

[49] Y.-p. Zhu, A. Masuyama, and M. Okahara, "Preparation and surface active properties of amphipathic compounds with two sulfate groups and two lipophilic alkyl chains," *Journal of the American Oil Chemists? Society*, vol. 67, no. 7, pp. 459–463, 1990.

[50] T.-S. Kim, T. Kida, Y. Nakatsuji, T. Hirao, and I. Ikeda, "Surface-active properties of novel cationic surfactants with two alkyl chains and two ammonio groups," *Journal of the American Oil Chemists? Society*, vol. 73, no. 7, pp. 907–911, 1996.

[51] M. J. Rosen and L. Liu, "Surface activity and premicellar aggregation of some novel diquaternary gemini surfactants," *Journal of the American Oil Chemists? Society*, vol. 73, no. 7, pp. 885–890, 1996.

[52] M. J. Rosen, "Geminis: A new generation of surfactants: These materials have better properties than conventional ionic surfactants as well as positive synergistic effects with non-ionics," *Chemtech*, vol. 23, no. 3, pp. 30–33, 1993.

[53] F. Hofmeister, "Zur lehre von der wirkung der salze," *Archiv für experimentelle Pathologie und Pharmakologie*, vol. 25, no. 1, pp. 1–30, 1888.

[54] W. Kunz, "Specific ion effects in colloidal and biological systems," *Current Opinion in Colloid & Interface Science*, vol. 15, no. 1, pp. 34–39, 2010.

[55] J. L. M. Poiseuille, *Recherches expérimentales sur le mouvement des liquides de nature différente dans les tubes de très petits diamètres.* Bachelier, 1847.

[56] G. Jones and M. Dole, "The viscosity of aqueous solutions of strong electrolytes with special reference to barium chloride," *Journal of the American Chemical Society*, vol. 51, no. 10, pp. 2950–2964, 1929.

[57] W. Cox and J. Wolfenden, "The viscosity of strong electrolytes measured by a differential method," *Proceedings of the Royal Society of London. Series A, Containing Papers of a Mathematical and Physical Character*, pp. 475–488, 1934.

[58] K. D. Collins, "Ions from the hofmeister series and osmolytes: effects on proteins in solution and in the crystallization process," *Methods*, vol. 34, no. 3, pp. 300–311, 2004.

[59] K. D. Collins, G. W. Neilson, and J. E. Enderby, "Ions in water: characterizing the forces that control chemical processes and biological structure," *Biophysical chemistry*, vol. 128, no. 2, pp. 95–104, 2007.

[60] N. Skipper and G. Neilson, "X-ray and neutron diffraction studies on concentrated aqueous solutions of sodium nitrate and silver nitrate," *Journal of Physics: Condensed Matter*, vol. 1, no. 26, p. 4141, 1989.

[61] J. G. Davis, B. M. Rankin, K. P. Gierszal, and D. Ben-Amotz, "On the cooperative formation of non-hydrogen-bonded water at molecular hydrophobic interfaces," *Nature chemistry*, vol. 5, no. 9, pp. 796–802, 2013.

[62] V. Buch, A. Milet, R. Vácha, P. Jungwirth, and J. P. Devlin, "Water surface is acidic," *Proceedings of the National Academy of Sciences*, vol. 104, no. 18, pp. 7342–7347, 2007.

[63] N. Schwierz, D. Horinek, and R. R. Netz, "Reversed anionic hofmeister series: the interplay of surface charge and surface polarity," *Langmuir*, vol. 26, no. 10, pp. 7370–7379, 2010.

[64] P. Jungwirth and D. J. Tobias, "Specific ion effects at the air/water interface," *Chemical reviews*, vol. 106, no. 4, pp. 1259–1281, 2006.

[65] L. X. Dang and T.-M. Chang, "Molecular mechanism of ion binding to the liquid/vapor interface of water," *The Journal of Physical Chemistry B*, vol. 106, no. 2, pp. 235–238, 2002.

[66] M. Lund, R. Vácha, and P. Jungwirth, "Specific ion binding to macromolecules: Effects of hydrophobicity and ion pairing," *Langmuir*, vol. 24, no. 7, pp. 3387–3391, 2008.

[67] P. E. Mason, C. E. Dempsey, L. Vrbka, J. Heyda, J. W. Brady, and P. Jungwirth, "Specificity of ion- protein interactions: Complementary and competitive effects of tetrapropylammonium, guanidinium, sulfate, and chloride ions," *The Journal of Physical Chemistry B*, vol. 113, no. 10, pp. 3227–3234, 2009.

[68] D. Horinek, S. I. Mamatkulov, and R. R. Netz, "Rational design of ion force fields based on thermodynamic solvation properties," *The Journal of chemical physics*, vol. 130, no. 12, p. 124507, 2009.

[69] A. W. Omta, M. F. Kropman, S. Woutersen, and H. J. Bakker, "Negligible effect of ions on the hydrogen-bond structure in liquid water," *Science*, vol. 301, no. 5631, pp. 347–349, 2003.

[70] S. Manet, Y. Karpichev, D. Bassani, R. Kiagus-Ahmad, and R. Oda, "Counteranion effect on micellization of cationic gemini surfactants 14-2-14: Hofmeister and other counterions," *Langmuir*, vol. 26, no. 13, pp. 10645–10656, 2010.

[71] E. V. Anslyn and D. A. Dougherty, *Modern physical organic chemistry*. University Science Books, 2006.

[72] S. Solutions, "New methods of investigation," 1986.

[73] L. Novaki and O. El Seoud, "Ber bunsenges phys chem 101: 105;(b) novaki lp," *El Seoud OA (1997) Ber Bunsenges Phys Chem*, vol. 101, p. 902, 1997.

[74] C. Tanford, *The Hydrophobic Effect: Formation of Micelles and Biological Membranes 2d Ed.* J. Wiley., 1980.

[75] D. Leckband and J. Israelachvili, "Intermolecular forces in biology," *Quarterly reviews of biophysics*, vol. 34, no. 02, pp. 105–267, 2001.

[76] S. Patai, *The chemistry of diazonium and diazo groups*, vol. 58. Wiley New York, 1978.

[77] H. Zollinger, *Azo and diazo chemistry: aliphatic and aromatic compounds*. Interscience Publishers, 1961.

[78] I. M. Cuccovia, M. A. da Silva, H. M. Ferraz, J. R. Pliego Jr, J. M. Riveros, and H. Chaimovich, "Revisiting the reactions of nucleophiles with arenediazonium ions: dediazoniation of arenediazonium salts in aqueous and micellar solutions containing alkyl sulfates and alkanesulfonates and an ab initio analysis of the reaction pathway," *Journal of the Chemical Society, Perkin Transactions 2*, no. 9, pp. 1896–1907, 2000.

[79] J. Scaiano and N. Kim-Thuan, "Diazonium salts in photochemistry iii: Attempts to characterize aryl cations," *Journal of photochemistry*, vol. 23, no. 2, pp. 269–276, 1983.

[80] S. M. Gasper, C. Devadoss, and G. B. Schuster, "Photolysis of substituted benzenediazonium salts: spin-selective reactivity of aryl cations," *Journal of the American Chemical Society*, vol. 117, no. 19, pp. 5206–5211, 1995.

[81] A. Chaudhuri, J. A. Loughlin, L. S. Romsted, and J. Yao, "Arenediazonium salts: New probes of the interfacial compositions of association colloids. 1. basic approach, methods, and illustrative applications," *Journal of the American Chemical Society*, vol. 115, no. 18, pp. 8351–8361, 1993.

[82] W. A. Waters, "50. decomposition reactions of the aromatic diazo-compounds. part x. mechanism of the sandmeyer reaction," *Journal of the Chemical Society (Resumed)*, pp. 266–270, 1942.

[83] H. Zollinger, "Nitrogen as leaving group: dediazoniations of aromatic diazonium ions," *Angewandte Chemie International Edition in English*, vol. 17, no. 3, pp. 141–150, 1978.

[84] Y. Hashida, R. G. Landells, G. E. Lewis, I. Szele, and H. Zollinger, "Dediazoniation of arenediazonium ions in homogeneous solution. 11. evidence for two intermediates in the reaction of the 2, 4, 6-trimethylbenzenediazonium ion in 2, 2, 2-trifluoroethanol," *Journal of the American Chemical Society*, vol. 100, no. 9, pp. 2816–2823, 1978.

[85] C. G. Swain, J. E. Sheats, and K. G. Harbison, "Evidence for phenyl cation as an intermediated in reactions of benzenediazonium salts in solution," *Journal of the American Chemical Society*, vol. 97, no. 4, pp. 783–790, 1975.

[86] I. Szele and H. Zollinger, "Dediazoniation of arenediazonium ions in homogeneous solution. 10. solvent effects on the reactions of benzene-and 2, 4, 6-trimethylbenzenediazonium ion. evidence for two intermediates," *Journal of the American Chemical Society*, vol. 100, no. 9, pp. 2811–2815, 1978.

[87] E. S. Lewis and W. H. Hinds, "The bimolecular displacement of nitrogen from p-nitrobenzenediazonium ion1," *Journal of the American Chemical Society*, vol. 74, no. 2, pp. 304–308, 1952.

[88] E. S. Lewis, L. D. Hartung, and B. M. McKay, "Reaction of diazonium salts with nucleophiles. xiii. identity of the rate-and product-determining steps," *Journal of the American Chemical Society*, vol. 91, no. 2, pp. 419–425, 1969.

[89] H. Zollinger, "Diazo chemistry, vol. 1," *VCH, New York, 1994á SearchåPubMed á*, 1994.

[90] L. S. R. Rutgers, "Interfacial compositions of surfactant assemblies by chemical trapping with arenediazonium ions: method and applications," *Reactions and Synthesis in Surfactant Systems*, p. 265, 2001.

[91] L. S. Romsted, "Do amphiphile aggregate morphologies and interfacial compositions depend primarily on interfacial hydration and ion-specific interactions? the evidence from chemical trapping," *Langmuir*, vol. 23, no. 2, pp. 414–424, 2007.

[92] A. Malinenko, *Ion Specific Effects on the Self-Assembly of Cationic Surfactants: Experimental and Computational Approaches*. PhD thesis, University of Bordeaux, 2015.

[93] M. N. Jones and D. Chapman, "Micelles, monolayers, and biomembranes," 1995.

[94] L. Romsted, K. Mittal, and B. Lindman, "Surfactants in solution," *Vol. 2Plenum, New York*, p. 1015, 1984.

[95] N. T. Southall, K. A. Dill, and A. Haymet, "A view of the hydrophobic effect," *The Journal of Physical Chemistry B*, vol. 106, no. 3, pp. 521–533, 2002.

[96] C. Tanford, "Micellar solutions and lipid vesicles," *Pure and Applied Chemistry*, vol. 54, no. 12, pp. 2349–2358, 1982.

[97] D. Case, T. Darden, T. E. Cheatham III, C. Simmerling, J. Wang, R. Duke, R. Luo, R. Walker, W. Zhang, K. Merz, *et al.*, "Amber 12," *University of California, San Francisco*, vol. 1, no. 3, 2012.

[98] W. Humphrey, A. Dalke, and K. Schulten, "Vmd: visual molecular dynamics," *Journal of molecular graphics*, vol. 14, no. 1, pp. 33–38, 1996.

[99] V. Soldi, J. Keiper, L. S. Romsted, I. M. Cuccovia, and H. Chaimovich, "Arenediazonium salts: New probes of the interfacial compositions of association colloids. 6. relationships between interfacial counterion and water concentrations and surfactant headgroup size, sphere-to-rod transitions, and chemical reactivity in cationic micelles," *Langmuir*, vol. 16, no. 1, pp. 59–71, 2000.

[100] Y. Geng and L. S. Romsted, "Ion pair formation in water. association constants of bolaform, bisquaternary ammonium, electrolytes by chemical trapping," *The Journal of Physical Chemistry B*, vol. 109, no. 49, pp. 23629–23637, 2005.

[101] Y. Geng, L. S. Romsted, and F. Menger, "Specific ion pairing and interfacial hydration as controlling factors in gemini micelle morphology. chemical trapping studies," *Journal of the American Chemical Society*, vol. 128, no. 2, pp. 492–501, 2006.

[102] R. Gentleman, R. Ihaka, D. Bates, *et al.*, "The r project for statistical computing," *URL: http://www. r-project. org/254*, 2009.

[103] Y. Marcus and G. Hefter, "Ion pairing," *Chemical reviews*, vol. 106, no. 11, pp. 4585–4621, 2006.

[104] H. Evans, "117. alkyl sulphates. part i. critical micelle concentrations of the sodium salts," *Journal of the Chemical Society (Resumed)*, pp. 579–586, 1956.

[105] L. Pegado, O. Marsalek, P. Jungwirth, and E. Wernersson, "Solvation and ion-pairing properties of the aqueous sulfate anion: explicit versus effective electronic polarization," *Physical Chemistry Chemical Physics*, vol. 14, no. 29, pp. 10248–10257, 2012.

[106] G. S. Manning, "The critical onset of counterion condensation: A survey of its experimental and theoretical basis," *Berichte der Bunsengesellschaft für physikalische Chemie*, vol. 100, no. 6, pp. 909–922, 1996.

[107] B. A. McKernan, G. S. Manning, and L. S. Romsted, "Estimating concentrations of condensed counterions around a polyelectrolyte by chemical trapping," in *ACS Symposium Series*, vol. 832, pp. 184–202, Washington, DC; American Chemical Society; 1999, 2003.

[108] C. D Bravo-Díaz, "Diazohydroxides, diazoethers and related species," *Patai's Chemistry of Functional Groups*, 2011.

[109] Y. Zhang, L. S. Romsted, L. Zhuang, and S. de Jong, "Simultaneous determination of interfacial molarities of amide bonds, carboxylate groups, and water by chemical trapping in micelles of amphiphiles containing peptide bond models," *Langmuir*, vol. 29, no. 2, pp. 534–544, 2012.

[110] D. Gruen, "The standard picture of ionic micelles," in *Surfactants, Adsorption, Surface Spectroscopy and Disperse Systems*, pp. 6–16, Springer, 1985.

[111] Y. Nakae, I. Kusaki, and T. Sato, "Lithium perchlorate catalyzed acetylation of alcohols under mild reaction conditions," *Synlett*, vol. 2001, no. 10, pp. 1584–1586,

2001.

[112] D. A. Wilson, C. J. Wilson, C. Moldoveanu, A.-M. Resmerita, P. Corcoran, L. M. Hoang, B. M. Rosen, and V. Percec, "Neopentylglycolborylation of aryl mesylates and tosylates catalyzed by ni-based mixed-ligand systems activated with zn," *Journal of the American Chemical Society*, vol. 132, no. 6, pp. 1800–1801, 2010.

[113] J. B. Klauda, R. M. Venable, J. A. Freites, J. W. OConnor, D. J. Tobias, C. Mondragon-Ramirez, I. Vorobyov, A. D. MacKerell Jr, and R. W. Pastor, "Update of the charmm all-atom additive force field for lipids: validation on six lipid types," *The journal of physical chemistry B*, vol. 114, no. 23, pp. 7830–7843, 2010.

[114] K. P. Jensen and W. L. Jorgensen, "Halide, ammonium, and alkali metal ion parameters for modeling aqueous solutions," *Journal of Chemical Theory and Computation*, vol. 2, no. 6, pp. 1499–1509, 2006.

[115] I. S. Joung and T. E. Cheatham III, "Determination of alkali and halide monovalent ion parameters for use in explicitly solvated biomolecular simulations," *The journal of physical chemistry B*, vol. 112, no. 30, pp. 9020–9041, 2008.

[116] W. L. Jorgensen, D. S. Maxwell, and J. Tirado-Rives, "Development and testing of the opls all-atom force field on conformational energetics and properties of organic liquids," *Journal of the American Chemical Society*, vol. 118, no. 45, pp. 11225–11236, 1996.

[117] L. Martínez, R. Andrade, E. G. Birgin, and J. M. Martínez, "Packmol: a package for building initial configurations for molecular dynamics simulations," *Journal of computational chemistry*, vol. 30, no. 13, pp. 2157–2164, 2009.

[118] K. Vanommeslaeghe, E. Hatcher, C. Acharya, S. Kundu, S. Zhong, J. Shim, E. Darian, O. Guvench, P. Lopes, I. Vorobyov, *et al.*, "Charmm general force field: A force field for drug-like molecules compatible with the charmm all-atom additive biological force fields," *Journal of computational chemistry*, vol. 31, no. 4, pp. 671–690, 2010.

[119] B. Hess, C. Kutzner, D. Van Der Spoel, and E. Lindahl, "Gromacs 4: algorithms for highly efficient, load-balanced, and scalable molecular simulation," *Journal of chemical theory and computation*, vol. 4, no. 3, pp. 435–447, 2008.

[120] C. G. Mayne, J. Saam, K. Schulten, E. Tajkhorshid, and J. C. Gumbart, "Rapid parameterization of small molecules using the force field toolkit," *Journal of computational chemistry*, vol. 34, no. 32, pp. 2757–2770, 2013.

[121] W. L. Jorgensen, J. Chandrasekhar, J. D. Madura, R. W. Impey, and M. L. Klein, "Comparison of simple potential functions for simulating liquid water," *The Journal of chemical physics*, vol. 79, no. 2, pp. 926–935, 1983.

[122] G. E. Aniansson, "Dynamics and structure of micelles and other amphiphile structures," *The Journal of Physical Chemistry*, vol. 82, no. 26, pp. 2805–2808, 1978.

[123] C. A. Bunton and J. R. Moffatt, "A quantitative treatment of micellar effects in moderately concentrated hydroxide ion," *Langmuir*, vol. 8, no. 9, pp. 2130–2134, 1992.

[124] J. Boecker, J. Brickmann, and P. Bopp, "Molecular dynamics simulation study of an n-decyltrimethylammonium chloride micelle in water," *The Journal of Physical Chemistry*, vol. 98, no. 2, pp. 712–717, 1994.

[125] L. Scriven and K. Mittal, "Micellization, solubilization and microemulsions," *Micellization, solubilization and microemulsions*, 1977.

[126] D. Stigter, "On the invariance of the charge of electrical double layers under dilution of the equilibrium electrolyte solution," in *Progress in Colloid & Polymer Science*, pp. 45–52, Springer, 1978.

[127] G. Gunnarsson and H. Gustavsson, "Ion binding to polyelectrolytes as described by the poisson–boltzmann equation. comparison with 23 na nuclear magnetic resonance relaxation experiments," *Journal of the Chemical Society, Faraday Transactions 1: Physical Chemistry in Condensed Phases*, vol. 78, no. 10, pp. 2901–2910, 1982.

[128] P. Linse, G. Gunnarsson, and B. Joensson, "Electrostatic interactions in micellar solutions. a comparison between monte carlo simulations and solutions of the poisson-boltzmann equation," *The Journal of Physical Chemistry*, vol. 86, no. 3, pp. 413–421, 1982.

[129] J. Beunen and E. Ruckenstein, "A model for counterion binding to ionic micellar aggregates," *Journal of colloid and interface science*, vol. 96, no. 2, pp. 469–487, 1983.

[130] Y. Xia, I. Goldmints, P. W. Johnson, T. A. Hatton, and A. Bose, "Temporal evolution of microstructures in aqueous ctab/sos and ctab/hdbs solutions," *Langmuir*, vol. 18, no. 10, pp. 3822–3828, 2002.

[131] K. D. Farquhar, M. Misran, B. H. Robinson, D. C. Steytler, P. Morini, P. R. Garrett, and J. F. Holzwarth, "The kinetics and mechanism of micelle-vesicle transitions in aqueous solution," *Journal of Physics: Condensed Matter*, vol. 8, no. 47, p. 9397,

1996.

[132] K. Horbaschek, H. Hoffmann, and C. Thunig, "Formation and properties of lamellar phases in systems of cationic surfactants and hydroxy-naphthoate," *Journal of colloid and interface science*, vol. 206, no. 2, pp. 439–456, 1998.

[133] H. Kawasaki, R. Imahayashi, and H. Maeda, "Effects of hydrophobic counterions on the phase behavior of tetradecyldimethylhydroxylammonium chloride in aqueous solutions," *Langmuir*, vol. 18, no. 22, pp. 8358–8363, 2002.

[134] K. Fontell, "The structure of the lamellar liquid crystalline phase in aerosol otwater system," *Journal of Colloid and Interface Science*, vol. 44, no. 2, pp. 318–329, 1973.

[135] M. Skouri, J. Marignan, and R. May, "X-ray and neutron-scattering study of the lamellar and l3 phases of the system aerosol-ot-water: effect of nacl and decane," *Colloid and Polymer Science*, vol. 269, no. 9, pp. 929–937, 1991.

[136] B. Balinov, U. Olsson, and O. Soederman, "Structural similarities between the l3 and bicontinuous cubic phases in the aot-brine system," *The Journal of Physical Chemistry*, vol. 95, no. 15, pp. 5931–5936, 1991.

[137] U. Thapa, J. Dey, S. Kumar, P. Hassan, V. Aswal, and K. Ismail, "Tetraalkylammonium ion induced micelle-to-vesicle transition in aqueous sodium dioctylsulfosuccinate solutions," *Soft Matter*, vol. 9, no. 47, pp. 11225–11232, 2013.

[138] G. V. Srilakshmi and A. Chaudhuri, "snap-shooting the interface of aot reverse micelles: Use of chemical trapping," *Chemistry-A European Journal*, vol. 6, no. 15, pp. 2847–2853, 2000.

[139] E. Nightingale Jr, "Phenomenological theory of ion solvation. effective radii of hydrated ions," *The Journal of Physical Chemistry*, vol. 63, no. 9, pp. 1381–1387, 1959.

[140] I. M. Cuccovia, A. Agostinho-Neto, C. M. Wendel, H. Chaimovich, and L. S. Romsted, "Determination of interfacial co-ion concentration in ionic micelles by chemical trapping: Halide concentration at the interface of sodium dodecyl sulfate micelles," *Langmuir*, vol. 13, no. 19, pp. 5032–5035, 1997.